COMBINED FORCED AND FREE CONVECTION IN STRATIFIED AND UNSTRATIFIED FLOWS

Thesis by

Grant Earl Robertson

In Partial Fulfillment of the Requirements

for the Degree of

Doctor of Philosophy

California Institute of Technology

Pasadena, California

1975

(Submitted February 14, 1975)

To Bonnie

ACKNOWLEDGMENTS

First of all, I thank my advisors, Professor L. G. Leal and Professor J. H. Seinfeld, for suggesting this research topic and providing continued support and interest, especially in the final stages of the preparation of this dissertaion. I appreciate the graduate teaching and research assistantships made available to me, as well as the opportunity to study at the California Institute of Technology. The numerical computations were performed at the C.I.T. Computing Center, whose programming assistants and operators advised me excellently. My many discussions, both technical and esoteric, with various friends have provided me with lasting stimulation.

Special thanks go to Erdinc Zana, Loren Schreiber, Phil Wood, Rich Goldberg, Tom McMillen, Willy Lennard, Bosco Ho, and Don Cormack. Finally, the most important part of my life has been my wife, Bonnie, whose continued encouragement, patience, and understanding have been invaluable, and to whom this thesis is sincerely dedicated with love.

A little learning is a dang'rous thing;

Drink deep, or taste not the Pierian spring

Alexander Pope
"An Essay on Criticism"

ABSTRACT

The laminar, steady, horizontal flow past a hot or cold two-dimensional body is examined; the fluid is unbounded, diffusive, and viscous. The presence of significant ambient stable temperature (or density) stratification, or significant buoyancy-induced convection, or both, is considered. A detailed understanding of the fundamental structure of such flows is obtained by developing effective analytical and numerical solution procedures.

Chapter 2: This chapter considers the general problem of stably stratified, Oseen flow at large distances upstream and downstream of a body which is represented as a line sink of horizontal or vertical momentum, or as a line heat source or heat dipole. The analysis is focused on the general properties of the horizontal velocity component, as well as on explicit calculation of the horizontal velocity profiles and disturbance streamfunction fields for varying degrees of stratification. For stable stratifications, the flow fields for all four types of singularities exhibit the common feature of multiple recirculating rotors of finite thicknesses, which leads to an alternating jet structure both upstream and downstream for the horizontal velocity component and to lee-waves in the overall flow. Self-similar formulae for the velocity, temperature, and pressure at very large distances upstream and downstream are also derived and compared with the Oseen solutions

Chapter 3: The simultaneous forced and free convection flow of a neutrally- or stably-stratified fluid past a hot or cold horizontal flat plate is investigated by numerically solving the full equations of motion and thermal energy subject only to the Boussinesq approximation.

The solutions span the parameter ranges $10 \leqslant Re \leqslant 100$, $0.1 \leqslant Pr \leqslant 10$, $-2.215 \leqslant Gr/Re^{5/2} \leqslant +2.215$, and $0 \leqslant Ri \leqslant 6.325$, where Re, Pr, Gr, and Ri are based on the overall plate length ℓ and the ambient free stream fluid properties evaluated at the plate level. For all degrees of stratification a hot plate causes an acceleration of the boundary flow near the plate surface relative to the corresponding forced convection flow, thereby increasing both the local skin friction and heat transfer coefficients. On the other hand, the boundary flow adjacent to a cold plate is decelerated and the local skin friction and heat transfer rate are decreased. This deceleration effect is enhanced by either further cooling or increasing the amount of ambient stratification, Ri, leading to boundary-layer separation in some cases. When the effect of the ambient stratification dominates that of local heating or cooling, the boundary-layer displacement increases for decreasing Ri, due to the buoyancy restoring force lessening, thus diminishing the drag. The dimunition in the drag, for the same decrease in Ri, lessens (increases) by slightly heating (cooling) the plate. When the effect of local heating or cooling dominates that of the ambient stratification, the drag is diminished by increasing Ri. A wave-structure exists only for stably-stratified fluids, with the amplitudes and wavelengths of the waves being decreased for increasing Ri.

TABLE OF CONTENTS

Chapter 1. The Physical Problem

The effects of ambient stable temperature (or density) stratification and/or local buoyancy-induced convection are important to a wide variety of natural and man-related geophysical phenomena occurring in the ocean and atmosphere. Examples of such phenomena in the ocean are the intrusion of salt wedges into estuaries, and the behaviors of sediment-laden currents and the dispersion of molecular contaminants or heat. In the atmosphere, typical phenomena are the stagnation of air in the neighborhood of a mountain range whenever there is a strong inversion, the formation of atmospheric waves in the lee of mountains, the "sea-breeze" at the interface of a large body of water and land, the characteristics of the flow over an "urban heat island", the behavior of the dispersion of pollutants and heat, and the "mushroom" shaped smoke patterns above fires. Although geophysical flow situations are usually turbulent, we have considered only laminar flows. Physically, we expect the resulting phenomena in both laminar and turbulent flows to be qualitatively similar. Without introducing additional complexities through a choice of a turbulence model, we derive, for the better-defined laminar case, accurate solution procedures that enable us to understand the fundamental flow structure. The same methods may also be useful in either obtaining the solutions or illustrating potential difficulties for turbulent flow problems. In order to explain in detail some of the physical phenomena which can result due to ambient stable stratification and/or buoyancy-induced convection, analytical and numerical techniques are

developed to calculate velocity and temperature distributions for stratified laminar flows.

We consider the laminar, steady, horizontal flow past a hot or cold two-dimensional body of characteristic diameter ℓ . The incompressible, Newtonian fluid is unbounded, diffusive, and viscous. A typical flow system, including the horizontal and vertical dimensional coordinates x' and y' respectively, is shown in Figure 1. As $x' \to -\infty$, we assume that the disturbance associated with the body can be neglected, and thus we can specify the free stream velocity and temperature (density) distributions at this upstream position. We assume the free stream horizontal velocity at this upstream position to be uniform and denoted by U_∞ . The corresponding free stream temperature distribution T_s is assumed to increase linearly with vertical position; i.e.,

$$T_s = T_\infty(1 + \gamma' y') \quad , \quad \gamma' \geq 0 \tag{1}$$

where T_∞ is constant, the subscript ∞ represents the free stream value at $y' = 0$, and γ' is the constant stratification parameter. Thus, the ambient fluid is either neutrally-stratified (i.e., $\gamma' = 0$; also referred to as unstratified) or stably-stratified (i.e., $\gamma' > 0$). We invoke the usual Boussinesq approximation (Boussinesq, 1903; Spiegel and Veronis, 1960; Mihaljan, 1962): the density ρ is considered constant at ρ_∞ , except in the gravitational body force term where it is related to the temperature T through the thermodynamic state equation:

$$\rho = \rho_\infty[1 - \beta(T - T_\infty)] \quad . \tag{2}$$

Here, β is the constant coefficient of thermal expansion. In general, we shall assume that the body experiences a total drag force per unit width, D, in the $+x'$ direction, a total lift force per unit width, L, in the $+y'$ direction, and, in addition, acts either as a heat source of strength Q per unit width per unit time (corresponding to a uniform surface temperature $T_\infty + \Delta T$, where $\Delta T > 0$ and $\Delta T < 0$ for hot and cold bodies respectively), or as a heat dipole (doublet). As pointed out by Redekopp (1970), the Boussinesq approximation produces a viscosity, thermal conductivity, and heat capacity which are all constant at values $\mu_\infty (= \rho_\infty \nu_\infty)$, k_∞, and C_{p_∞} respectively, and is valid for $\Delta T/T_\infty = \Delta << 1$ and $\gamma' \ell = \gamma << 1$. As pointed out by Janowitz (1968) and List (1971), the linear free stream temperature stratification (1) cannot apply over <u>extreme</u> ranges of y' values, but it is an approximation over a large enough distance that solutions can be obtained representing, for example, the fluid flow in the center of a hyperbolic tangent temperature profile.

It is convenient to consider separately two aspects of the full problem: the "near-field" region in which one is concerned with the effects of ambient stratification and locally produced buoyancy contributions on the velocity and temperature fields very close to the hot or cold body; and the "far-field" region in which the body appears as a line singularity for both momentum and thermal energy (heat). The near-field solution depends on the precise body geometry and surface temperature distribution. To date, the majority of the near-field solutions have been concerned with the case in which a significant component of the buoyancy-induced body force is either

parallel or antiparallel with the direction of the undisturbed fluid motion (compare the work of Acrivos (1966), Merkin (1969), and others on the combined forced and free convection past a vertical flat plate); in this work we consider the flow past a horizontal flat plate of finite length ℓ and constant surface temperature. The far-field problem may be considered simultaneously for the whole class of two-dimensional bodies since the specific shape enters only indirectly through the magnitude and direction of the line drag and lift forces, and the magnitude of the line heat source. In Chapter 2, the far-field solutions for $\gamma' > 0$ are obtained by linear analysis. Chapter 3 is devoted to the near-field numerical solution (for $\gamma' \geq 0$) of the full governing nonlinear partial differential equations representing the momentum, mass, and thermal energy balances. In the near-field numerical solutions, accurate outer boundary conditions are critical in obtaining correct results; the far-field solutions of Chapter 2 are found to provide these proper conditions.

References

Acrivos, A. 1966 "On the Combined Effect of Forced and Free Convection Heat Transfer in Laminar Boundary Layer Flows". Chem. Eng. Sci. 21, 343.

Boussinesq, J. 1903 Theorie Analytique de la Chaleur, Vol. 2. Gathier-Villars, Paris.

Janowitz, G. S. 1968 "On wakes in stratified fluids". J. Fluid Mech. 33, 417.

List, E. J. 1971 "Laminar momentum jets in a stratified fluid". J. Fluid Mech. 45, 561.

Merkin, J. H. 1969 "The Effect of Buoyancy Forces on the Boundary-Layer Flow over a Semi-Infinite Vertical Flat Plate in a Uniform Stream". J. Fluid Mech. 35, 439.

Mihaljan, J. M. 1962 "A rigorous exposition of the Boussinesq approximations". Astrophys. J. 136, 1126.

Redekopp, L. G. 1970 "The development of horizontal boundary layers in stratified flows. Part 2. Diffusive Flow". J. Fluid Mech. 42, 513.

Spiegel, E. A. and Veronis, G. 1960 "On the Boussinesq Approximation for a Compressible Fluid". Astrophys. J. 131, 442.

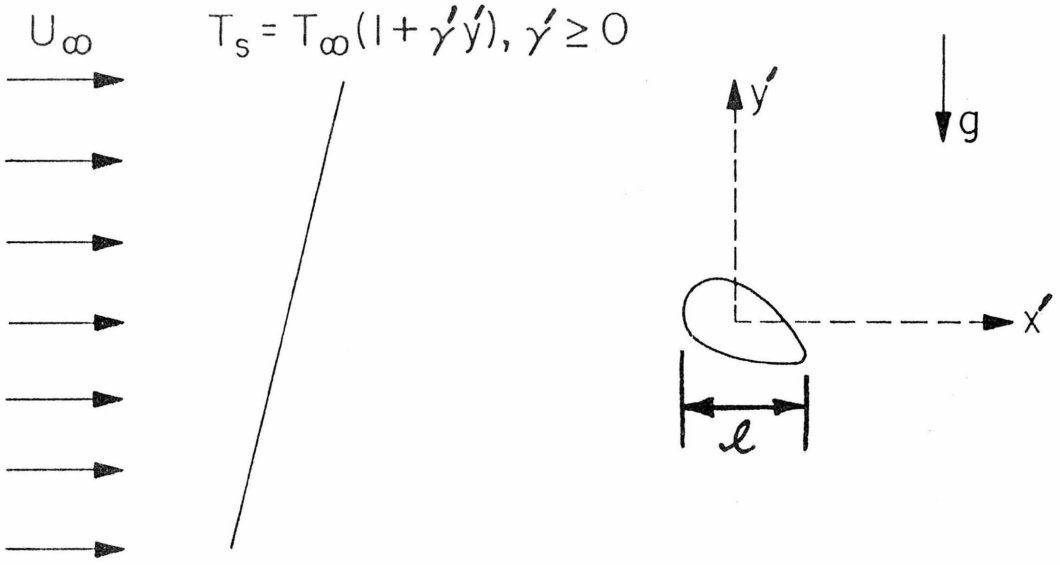

Figure 1: The Physical System

Chapter 2. The Far-Field Solution: Wakes in Stratified Flow Past a Hot or Cold Two-Dimensional Body

This chapter consists of an article submitted for publication (with co-authors Dr. L. G. Leal and Dr. J. H. Seinfeld) to the Journal of Fluid Mechanics. The tables and figures omitted in the article for brevity are given in Appendix 2-A.

This paper considers the general problem of laminar, steady, horizontal, Oseen flow at large distances upstream and downstream of a two-dimensional body which is represented as a line sink of horizontal or vertical momentum, or as a line heat source or heat dipole. The fluid is assumed to be incompressible, diffusive, viscous, and stably stratified. The analysis is focused on the general properties of the horizontal velocity component, as well as on explicit calculation of the horizontal velocity profiles and disturbance streamfunction fields for varying degrees of stratification. For stable stratifications, the flow fields for all four types of singularities exhibit the common feature of multiple recirculating rotors of finite thicknesses, which leads to an alternating jet structure both upstream and downstream for the horizontal velocity component and to lee-waves downstream in the overall flow. The self-similar formulae for the velocity, temperature, and pressure at very large distances upstream and downstream are also derived and compared with the Oseen solutions.

1. INTRODUCTION

The fluid-mechanical interactions of ambient temperature (or density) stratification and buoyancy-induced convection are important to a wide variety of natural and man-related phenomena in the oceans and atmosphere. The present paper is concerned with the horizontal motion of a stably-stratified fluid past a heated (or cooled) two-dimensional body. The disturbance motion induced in this case is fundamentally different from that which would be observed under equivalent conditions in a homogeneous fluid. The difference is primarily a result of an additional mechanism for vorticity production in the stratified case, leading to internal waves which are responsible for standing lee-wave patterns downstream and the possibility of a greatly enhanced effect on the flow upstream, when the free stream velocity is subcritical with respect to the horizontal phase velocity of the waves.

A large number of studies, both theoretical and experimental, have been reported for the stably-stratified flow past thermally inert bodies of different shapes. Near the body where the body geometry has a direct influence on flow structure, the flow has been examined theoretically for a vertical flat plate in the non-diffusive (Janowitz, 1971) and diffusive cases (Freund and Meyer, 1972), and for a circular cylinder in the non-diffusive case, both theoretically (Graebel, 1969) and experimentally (Browand and Winant, 1972).

Far from the body, the detailed body geometry may be considered unimportant so that the body can be treated as a line source of horizontal and vertical momentum and heat. Janowitz (1967, 1968) discussed the upstream and downstream wake structure for a horizontal momentum source

(i.e. the disturbance motion induced by a body which is only experiencing drag) in an unbounded viscous, diffusive or non-diffusive stratified fluid with the inertia effects approximated using an Oseen-type linearization. A closely related analysis by List (1971) considered creeping flows induced by horizontal and vertical momentum jets in a diffusive fluid.† Very far upstream and downstream of the singularity, the disturbance motion becomes self-similar, with the dynamics dominated by viscous effects due to the vertical gradients of horizontal velocity and by buoyancy due to the free stream ambient stratification. In the non-diffusive case, Long (1959) calculated a similarity solution, which has been verified experimentally (Pao, 1968; Laws and Stevenson, 1972) for the horizontal flow far upstream of a body which is experiencing only drag. Long (1959) could not obtain a corresponding disturbance flow downstream. However, when density diffusion was retained, Long (1962) found a new similarity solution which is valid both upstream and downstream of the body.

In the present study, we use the methods of Janowitz (1967) to consider the two-dimensional Oseen and self-similar solutions for a line source of vertical momentum, a line source of heat, and a vertically oriented heat dipole.‡ In addition, for comparison purposes we also repeat portions of Janowitz' (1967) analysis for the line source of horizontal momentum. We consider both the horizontal component of the velocity (with which Janowitz and most other investigators have dealt

† Note that far from the body the disturbance motion induced by a body considered as a point source is analogous to that created by a point jet.

‡ The motivation for our interest in the vertical heat dipole configuration will be considered in the next section.

exclusively) and the disturbance streamfunction fields which afford additional physical insight into the alternating jet structure and other interesting features of the horizontal velocity profiles. The similarities and differences in the flow structure resulting from the various types of singularities will be discussed.

2. PHYSICAL PROBLEM AND BASIC EQUATIONS

We consider the steady, horizontal motion of an unbounded, incompressible, Newtonian fluid past an arbitrary two-dimensional body of finite cross-section. The flow is assumed to be laminar and, at large distances from the body, uniform with magnitude U_∞. In addition, the corresponding temperature distribution far from the body, T_s, is assumed to increase linearly with vertical position, i.e. $T_s = T_\infty(1 + \gamma' y')$ with $\gamma' > 0$, so that the ambient fluid is stably stratified. Here, y' is the dimensional vertical coordinate measured from the center of the body. The corresponding downstream horizontal coordinate will be denoted as x'. The body itself is assumed to have a uniform surface temperature, $T_\infty + \Delta T$, and density diffusion (i.e. thermal conduction) is explicitly included in the analysis.

The present work is specifically concerned with the velocity and temperature fields at distances from the body which are sufficiently large that the body-induced disturbance velocity components are small in magnitude compared with the free stream speed U_∞. In this regime, the Oseen-linearization of the convective operator is applicable, and the effects of the body on the disturbance field are dominated by appropriate force and heat singularities which are concentrated at the origin, $x' = y' = 0$. For concreteness, we consider a body which is held fixed and is thus subjected to a finite lift and/or drag force. In this case, the dominant disturbance velocity fields are induced by horizontal and vertical momentum sources. If, in addition, there is a net heat transfer to (or from) the body (i.e. $\Delta T \neq 0$), both a point heat source and higher order heat singularities must also be included. Among

these higher order singularities, the dominant contribution to the disturbance velocity and temperature fields will be due to the vertically oriented heat dipole. Indeed, if the body is symmetric about $y' = 0$, and $\Delta T = 0$ so that the net heat flux from the body is zero, the only relevant heat singularity is the vertically oriented heat dipole. We thus concentrate here on the vertical momentum source, the heat source, and the vertically oriented heat dipole, following the earlier analysis of Janowitz (1967, 1968) who considered the horizontal momentum source.

The governing equations for the disturbance velocity, pressure and temperature fields are the Oseen-linearized form of the Navier-Stokes and thermal energy equations. Invoking the usual Boussinesq approximation and nondimensionalizing these equations using the ambient fluid properties evaluated at $T = T_\infty$ (i.e. $y' = 0$), the free stream velocity U_∞, and the appropriate characteristic length scale (Janowitz, 1967, 1968)

$$\lambda = (U_\infty \mu_\infty / \beta g \rho_\infty T_\infty \gamma')^{1/3}$$

where β is the coefficient of thermal expansion, we finally obtain

$$\frac{\partial u}{\partial x} = -\frac{\partial p}{\partial x} + \frac{1}{Re}\left(\frac{\partial^2 u}{\partial x^2} + \frac{\partial^2 u}{\partial y^2}\right) - K_1 \delta(x)\delta(y) \tag{1}$$

$$\frac{\partial v}{\partial x} = -\frac{\partial p}{\partial y} + \frac{1}{Re}\left(\frac{\partial^2 v}{\partial x^2} + \frac{\partial^2 v}{\partial y^2}\right) + \frac{1}{Re}\bar{\theta} - K_3 \delta(x)\delta(y) \tag{2}$$

$$\frac{\partial u}{\partial x} + \frac{\partial v}{\partial y} = 0 \tag{3}$$

$$\frac{\partial \bar{\theta}}{\partial x} + v = \frac{1}{Pe}\left(\frac{\partial^2 \bar{\theta}}{\partial x^2} + \frac{\partial^2 \bar{\theta}}{\partial y^2}\right) + K_{2_s} \delta(x)\delta(y) \tag{4}$$

Here, u and v denote the disturbance velocity components in the x and y (horizontal and vertical) directions, $\bar{\theta} = (T - T_s)/\gamma' \lambda T_\infty$, and $p = (p_d -$

$p_{d_\infty})/\rho_\infty U_\infty^2$ where p_d represents the dynamic pressure. The two dimensionless parameters which appear are the Reynolds number,

$$Re \equiv \rho_\infty U_\infty \lambda/\mu_\infty = \left(\rho_\infty^2 U_\infty^4/\mu_\infty^2 \beta g T_\infty \gamma'\right)^{1/3}$$

which is a measure of the relative magnitude of inertia compared with viscous and buoyancy (due to the ambient stratification) forces and the Peclet number,

$$Pe = PrRe \quad \text{with} \quad Pr \equiv C_{p_\infty} \mu_\infty / k_\infty \ .$$

For convenience, we have incorporated the momentum and heat source contributions directly into the governing equations (cf. Janowitz, 1967, 1968). The coefficients K_i can be related to the drag, lift and net heat flux from the body, but here we shall consider only the fundamental solutions associated with $K_i = 1$. Since the equations are linear, disturbance motions corresponding to each singularity type may be considered separately by simply decomposing the overall solutions u, v, p and $\bar{\theta}$ in the form

$$u = K_1 u_1 + K_{2_s} \frac{1}{Re} u_{2_s} + K_3 u_3 \tag{5a}$$

$$v = K_1 v_1 + K_{2_s} \frac{1}{Re} v_{2_s} + K_3 v_3 \tag{5b}$$

$$p = K_1 p_1 + K_{2_s} \frac{1}{Re} p_{2_s} + K_3 p_3 \tag{5c}$$

$$\bar{\theta} = K_1 \theta_1 + K_{2_s} \theta_{2_s} + K_3 \theta_3 \tag{5d}$$

Although the vertically oriented heat dipole could have also been explicitly included in equation (4), a more convenient method of obtaining the corresponding disturbance fields is by simply differentiating the source solutions with respect to y (Carslaw and Jaeger, 1959); e.g.

$\theta_{2_d} = -\partial\theta_{2_s}/\partial y$, where the subscripts s and d will be used to denote heat source and dipole solutions. Finally, it may be noted that $\gamma' \to 0$, $(\lambda, Re, Pe, \bar{\theta}) \to \infty$ for a homogeneous fluid; hence, in this case, the governing equations must be nondimensionalized using a different characteristic length, $\phi = \mu_\infty/U_\infty\rho_\infty$, and temperature scaling, $\theta = (T - T_s)/\Delta T$.

In the following sections, we describe solutions of equations (1) - (4), subject to the free-stream conditions

$$u \to 0, \quad v \to 0, \quad p \to 0, \quad \bar{\theta} \to 0 \text{ as } (x^2 + y^2)^{1/2} \to \infty .$$

For purposes of comparison, we include not only the vertical momentum source, heat source, and heat dipole results, but also the solution for a horizontal momentum source (i.e. $K_1 = 1$, $K_2 = K_3 = 0$) which was previously obtained by Janowitz (1967). In view of our interest in the relationships between flow structure and the degree of stratification in a "diffusive" fluid, the explicit numerical computations which we will describe were carried out for fixed Pr = 0.7 and various values of Re.

3. SOLUTION PROCEDURE

The governing equations for each of the three fundamental problems which are produced by the linear decompositions (5a-d) of equations (1) - (4) are most conveniently solved using the standard methods of Fourier transforms, as outlined in detail by Janowitz (1967, 1968) and List (1971). A most interesting feature of this analysis in the present case is the fact that both the solution form and a number of its general features are precisely the same for all four singularity types. Thus, denoting a typical unknown as ζ (e.g. any of u_1, u_{2_s}, u_3, v_1, ...), it may be shown that

$$\zeta(x,y) = \frac{1}{\pi}\int_0^\infty [I_\zeta(k_2;\ x;\ Re,\ Pe)/2\pi]J_\zeta(k_2;\ y)dk_2 \tag{6}$$

where

$$I_\zeta(k_2;\ x;\ Re,\ Pe) = i\int_{-\infty}^{\infty} [K_\zeta(k_1,\ k_2;\ Re,\ Pe)/q_1(k_1,\ k_2;\ Re,\ Pe)] \exp(ik_1x)dk_1 \tag{7}$$

and

$$q_1(k_1,\ k_2;\ Re,\ Pe) = -i\left(k_1^2 + k_2^2\right)\left(ik_1 + \frac{k_1^2 + k_2^2}{Re}\right)\left(ik_1 + \frac{k_1^2 + k_2^2}{Pe}\right) - i\,\frac{k_1^2}{Re} \tag{8}$$

The subscript ζ on I_ζ, J_ζ and K_ζ is intended to indicate that the corresponding functional forms depend on the specific variable ζ.† Explicit evaluation of equations (6) - (8) for a specific ζ is straightforward. For each k_2, the function I_ζ is evaluated by residue theory, after first determining its poles by solving for the roots of $q_1 = 0$,

† The functions J_ζ and K_ζ are tabulated by Robertson (1975). References to Robertson (1975) in Chapter 2 are found in Appendix 2-A.

i.e. the roots of the sixth-degree polynomial

$$\xi^6 + (Pe + Re)\xi^5 + (PeRe - 3k_2^2)\xi^4 - (Pe + Re)2k_2^2\xi^3$$
$$+ (3k_2^4 + Pe - PeRek_2^2)\xi^2 + (Pe + Re)k_2^4\xi - k_2^6 = 0 \qquad (9)$$

The physical space quantity ζ is then determined by a numerical integration over k_2.

The resultant solution clearly depends in detail upon the singularity type and on the variable in question. This is in accord with expectations. In every case, however, the x-dependence of the solution is completely contained in I_ζ and the y-dependence in J_ζ. Furthermore, and of greatest significance, the function q_1 and its roots are independent of ζ. Janowitz (1967) has shown, for the case of a horizontal momentum source, that the general behavior of u_1 can be deduced from a knowledge of the characteristics of the poles of I_ζ, without actually carrying out the detailed integration of equation (6). Since the present analysis has shown q_1 to be independent of the singularity type, the general far-field characteristics deduced by Janowitz are also relevant for a vertical momentum source, heat source or heat dipole at the origin. In view of the fundamental differences in the disturbance fields induced near the body, this universality of solutions in the Oseen-region is both surprising and of considerable interest.

Since q_1 is a sixth-degree polynomial, its roots (and the poles of I_ζ) must be determined numerically for each set of values of k_2, Re and Pe. Janowitz (1967) has described the general features of these roots, which were also verified in the present work. Three roots, s_1, s_2, and s_3, have positive real parts with $0 < s_{1_R} < s_{2_R} \leq s_{3_R}$ for $k_2 > 0$,†

† s_{n_R} and s_{n_I} denote the real and imaginary parts of s_n.

while the remaining three roots, s_4, s_5 and s_6, have negative real parts with $0 > s_{4_R} >> s_{5_R} \geq s_{6_R}$ for $k_2 > 0$. For all $k_2 \geq 0$, s_1 is real, whereas s_2 and s_3 are real for $k_2 \geq k_2^*$ (Re, Pe) and complex conjugates, $s_2 = s_{2_R} + is_{2_I}$, $s_3 = s_{2_R} - is_{2_I}$, with $s_{2_I} > 0$, for $0 \leq k_2 < k_2^*$; the critical wave number k_2^* increases for increasing amounts of stratification (i.e. decreasing Re). For all $k_2 \geq 0$, s_4 is real, whereas s_5 and s_6 may be real or complex conjugates, depending on the values of Re and Pe. Finally, s_1 and s_{2_R} increase with increasing $k_2 \geq 0$, while s_{2_I} decreases; s_{2_R} and s_{2_I} increase for decreasing Re and $s_1 \sim k_2^3/Pe^{1/2}$ for k_2 near zero. In contrast, the real parts of all three roots s_4, s_5 and s_6 decrease for increasing $k_2 \geq 0$, with $s_4 \sim -k_2^3/Pe^{1/2}$ for k_2 near 0. The function I_ζ for $x > 0$ (downstream of the body) is evaluated using the poles with $s_{n_R} > 0$, while the region $x < 0$ requires the poles with $s_{n_R} < 0$.

In the following discussion, we shall focus attention on the horizontal velocity components u_1, u_{2_s}, u_{2_d} and u_3. Taking account of the nature of the poles s_1, s_2, ..., s_6, the general expression (7) for I_ζ, with $\zeta = u_1$, u_{2_s}, u_{2_d}, or u_3, may be written in the more specific forms

$$\frac{1}{2\pi} I_\zeta = A_\zeta \mathrm{Re}\, \exp(-s_1 x) \Big/ \Big\{ |s_2 - s_1|^2 (s_1 - s_4)(s_1 - s_5)(s_1 - s_6) \Big\}$$

$$+ \mathrm{Re}\, \exp(-s_{2_R} x) \sum_{n=0}^{3} B_{n_\zeta} \sin(s_{2_I} x + \theta_1 + \theta_4 + \theta_5 + \theta_6 - n\theta_2) \Big/$$

$$\Big\{ s_{2_I} |s_2 - s_1||s_2 - s_4||s_2 - s_5||s_2 - s_6| \Big\};$$

$$\text{for } x > 0 \text{ and } 0 \leq k_2 < k_2^* \qquad (10a)$$

$$\frac{1}{2\pi} I_\zeta = C_\zeta \mathrm{Re}\ \exp(-s_1 x)/\left\{(s_1 - s_2)(s_1 - s_3)(s_1 - s_4)(s_1 - s_5)(s_1 - s_6)\right\}$$

$$+ D_\zeta \mathrm{Re}\ \exp(-s_2 x)/\left\{(s_2 - s_1)(s_2 - s_3)(s_2 - s_4)(s_2 - s_5)(s_2 - s_6)\right\}$$

$$+ E_\zeta \mathrm{Re}\ \exp(-s_3 x)/\left\{(s_3 - s_1)(s_3 - s_2)(s_3 - s_4)(s_3 - s_5)(s_3 - s_6)\right\};$$

for $x > 0$ and $k_2 \gtrless k_2^*$ (10b)

$$\frac{1}{2\pi} I_\zeta = F_\zeta \mathrm{Re}\ \exp(-s_4 x)/\left\{(s_4 - s_1)|s_2 - s_4|^2(s_4 - s_5)(s_4 - s_6)\right\}$$

$$+ G_\zeta \mathrm{Re}\ \exp(-s_5 x)/\left\{(s_5 - s_1)|s_2 - s_5|^2(s_5 - s_4)(s_5 - s_6)\right\}$$

$$+ L_\zeta \mathrm{Re}\ \exp(-s_6 x)/\left\{(s_6 - s_1)|s_2 - s_6|^2(s_6 - s_4)(s_6 - s_5)\right\};$$

for $x < 0$ and $0 < k_2 < k_2^*$ (11a)

$$\frac{1}{2\pi} I_\zeta = M_\zeta \mathrm{Re}\ \exp(-s_4 x)/\left\{(s_4 - s_1)(s_4 - s_2)(s_4 - s_3)(s_4 - s_5)(s_4 - s_6)\right\}$$

$$+ N_\zeta \mathrm{Re}\ \exp(-s_5 x)/\left\{(s_5 - s_1)(s_5 - s_2)(s_5 - s_3)(s_5 - s_4)(s_5 - s_6)\right\}$$

$$+ P_\zeta \mathrm{Re}\ \exp(-s_6 x)/\left\{(s_6 - s_1)(s_6 - s_2)(s_6 - s_3)(s_6 - s_4)(s_6 - s_5)\right\};$$

for $x < 0$ and $k_2 \gtrless k_2^*$ (11b)

where $|s_2 - s_i| = \left[\left[s_{2_R} - s_i\right]^2 + s_{2_I}^2\right]^{1/2}$; $i = 1, 4, 5, 6$

$$|s_2| = \left(s_{2_R}^2 + s_{2_I}^2\right)^{1/2}.$$

$$\theta_2 = \tan^{-1}\left(s_{2_I}/s_{2_R}\right)$$

$$\theta_i = \tan^{-1}\left[s_{2_I}/\left(s_{2_R} - s_i\right)\right], \quad i = 1, 4, 5, 6$$

The coefficients A_ζ, B_{o_ζ}, B_{1_ζ}, B_{2_ζ}, B_{3_ζ}, C_ζ, D_ζ, E_ζ, F_ζ, G_ζ, L_ζ, M_ζ, N_ζ and P_ζ, which are functions of ζ, k_2, s_1, s_2, s_3, s_4, s_5, s_6 and Pe, but not of x, are tabulated by Robertson (1975). For additional physical insight, we also calculate the disturbance streamfunction fields ψ_i (i = 1, 2_s, 2_d, 3) where:

$$\tilde{\psi} = y + K_1\psi_1 + K_{2_s}\frac{1}{Re}\psi_{2_s} + K_3\psi_3 \tag{12}$$

$$\tilde{u} = \partial\tilde{\psi}/\partial y,\ \tilde{v} = -\partial\tilde{\psi}/\partial x \tag{13a}$$

$$u_i = \partial\psi_i/\partial y,\ v_i = -\partial\psi_i/\partial x;\ i = 1, 2_s, 2_d, 3 \tag{13b}$$

4. SOLUTIONS

a. Self-Similar Solutions

Very far downstream and upstream of each singularity type, the integrand for ζ is non-negligible only near $k_2 = 0$; for example, expressions (10) and (11) for I_{u_i}, $i = 1, 2_s, 2_d, 3$, are dominated by the first terms of equations (10a) and (11a) respectively, evaluated near $k_2 = 0$. For $k_2 \equiv 0$, $s_1 \equiv s_4 \equiv 0$ and equation (9) yields $|s_2|^2 s_5 s_6 = Pe$. Since $A_{u_1} \approx -k_2^2$ near $k_2 = 0$ and $J_{u_1} = k_2^2 \cos k_2 y$ (Robertson, 1975), the expression for u_1 very far downstream becomes

$$u_1(x,y) = \frac{-Re}{2\pi Pe^{1/2}} \int_0^\infty k_2 \cos k_2 y \exp\left(-k_2^3 x/Pe^{1/2}\right) dk_2$$

As Janowitz has noted, this solution is identical to Long's (1962) similarity solution for the far-wake motion generated by a source of horizontal momentum in a diffusive, stratified fluid. Indeed this is simply shown by substituting s^3 for $k_2^3 x/Pe^{1/2}$ in the above exponential to yield

$$u_1 = -\frac{Re}{2\pi Pe^{1/6}|x|^{2/3}} \int_0^\infty s \cos \eta s \exp(-s^3) ds; \quad \eta = Pe^{1/6} y/|x|^{1/3} \qquad (14)$$

One can analagously obtain self-similar solutions for all of the other physical variables and singularity types, ζ, and these are listed in Table 1. The presence of two signs in some of the expressions corresponds to $x > 0$ (upper sign) and $x < 0$ (lower sign). The self-similar solutions for u_1, v_1, p_1, and θ_1 were previously calculated by Janowitz (1967) and Long (1962), and have been included here for comparison purposes. Plots of the self-similar solutions for u_1, u_{2_s}, u_{2_d}, and u_3 are presented here in Figures 1-8; a complete set of plots of the

similarity functions may be found in Robertson (1975).

It is significant that for each singularity type, the self-similar regime is dominated by the same physical processes. Indeed, one can easily show that the self-similar profiles, which were obtained as approximations of the Oseen solutions at very large distances, are also exact solutions of the equations

$$\begin{aligned} \frac{\partial p}{\partial x} &= \frac{1}{Re}\frac{\partial^2 u}{\partial y^2} - K_1\delta(x)\delta(y) \\ \frac{\partial p}{\partial y} &= \frac{1}{Re}\bar{\theta} - K_3\delta(x)\delta(y) \\ \frac{\partial u}{\partial x} &+ \frac{\partial v}{\partial y} = 0 \\ v &= \frac{1}{Pe}\frac{\partial^2\bar{\theta}}{\partial y^2} + K_{2_s}\delta(x)\delta(y) \end{aligned} \tag{15}$$

which were solved originally by Long (1962) for $K_{2_s} = K_3 = 0$, $K_1 \neq 0$. Note that, in all cases, inertia effects are unimportant in this far-wake self-similar region, although significant in the Oseen regime which lies closer to the singularity (i.e. the body).†

In spite of the fact that the basic physics relating u, v, p, and $\bar{\theta}$ is similar in all cases, the detailed differences in the flows induced nearer the body by the various types of singularities are still rather strongly reflected in the solutions as far away as the self-similar regime. This is true not only in the detailed profiles, but particularly in the dependence on the parameters Re and Pe, and in the rates of decrease of the magnitudes of the velocity, pressure and temperature profiles with increasing distances $|x|$. In the case of the horizontal

† Criteria, in terms of the required distances from the body, for the validity of the Oseen and self-similar solutions are presented in Appendix A.

momentum source, the main velocity peaks in the similarity profiles upstream and downstream result directly from the horizontal flow induced at the origin (for $K_1 > 0$, this flow is from right to left). Not surprisingly, the horizontal velocity component u_1 is dominant over the vertical component v_1. In the cases of the vertical momentum source and the heat source, the flow induced at the body is dominantly vertical, upward for $K_{2_s} > 0$ and downward for $K_3 > 0$. However, as we shall see more clearly in the next section, the vertical near-body motions are constrained by the ambient density stratification, and converted efficiently into strong horizontal motions which are antisymmetric about the x-axis ($y = 0$). As in the previous case, the magnitude of the horizontal velocity component is larger than that of the vertical component by $O(|x|^{+2/3})$ in this distant self-similar regime. The antisymmetry and sign of the induced horizontal motions in the far-wake are easily understood. For example, considering u_3, the ambient stratification causes the downward vertical motions near the body to be turned into both upstream and downstream jet-like motions. Below the plane $y = 0$ these motions will be outward, whereas above they must be inward in order to satisfy the entrainment requirements for the near-body flow. One surprising feature, from the physical point of view, is the precise upstream-downstream symmetry in the self-similar regime. Mathematically, however, it is obvious from the equations (15), in which inertia effects are neglected, that the solutions must exhibit this feature. Nearer the body, however, where convective inertia effects cannot be neglected for finite Re, the velocity and temperature fields would be expected to show some degree of upstream-downstream asymmetry, and this

will become apparent in the full Oseen solutions which we will discuss next. Finally, the horizontal velocity profile for a heat dipole appears qualitatively similar in shape to the profile for a horizontal momentum source. For a sufficiently simple body geometry, such as the horizontal flat plate (cf. Robertson, Seinfeld and Leal, 1973), this similarity appears quite natural since the local density gradients induced by the body acting as a heat dipole produce an effective horizontal pressure gradient at the body surface which acts to accelerate the fluid in the horizontal direction. The buoyancy effects which act to produce vertical motions locally produce no net vertical motion for the heat dipole. Thus, for a simple body geometry, the heat dipole appears as an effective source of horizontal momentum. Generalization of these simple ideas to more complicated body geometries is, however, not obvious although it is clear from the far-field similarity profile that, in an averaged sense, the situation is unchanged. As might be expected qualitatively, the far-wake self-similar disturbance flows are strongest for the horizontal momentum and heat sources $\left(O(|x|^{-2/3})\right)$ and weakest for the vertical momentum source $\left(O(|x|^{-4/3})\right)$ with the heat dipole falling in between.

b. Oseen Solutions

From equations (10) and (11) for the functions I_{u_i}, $i = 1, 2_s, 2_d, 3$, we can ascertain the general behavior of the horizontal velocity components in the Oseen solution regime using the characteristics of the poles $s_1, s_2, \ldots, s_6$, as indicated earlier. The case of a horizontal momentum source was discussed by Janowitz (1967). However, the general features of the horizontal velocity profiles are clearly common to all four of the singularity types which we have considered, since the

general solution forms are similar and the behavior of the poles is independent of the singularity type.

Downstream, in all four cases, I_{u_i} displays terms which are both wavelike in x due to the complex conjugate poles s_2 and s_3 for $0 \leq k_2 < k^*$, and exponential due to the real poles s_1 for $k_2 \geqslant 0$ and s_2 and s_3 for $k_2 \geqslant k_2^*$. For moderate distances downstream, all terms are significant in general, indicating the presence of lee-waves in the overall velocity field. Since the real and imaginary parts of s_2 both increase with decreasing Re, equation (10a) indicates that increasing the degree of ambient stratification will cause a decrease in the amplitude and wavelength of these lee-waves. Both the pure exponential and wave-like terms decrease in magnitude with increasing downstream distances. However, since $s_1 < s_{2_R}$, very far downstream the first term of equation (10a) dominates I_{u_i} yielding the diffusive self-similar wake solutions which were discussed in the preceding section.

Upstream, I_{u_i} is dominated for each singularity type by the term containing the real root s_4. Thus, upstream the horizontal velocity distributions do not exhibit any appreciable wave-like character with respect to x. However, as we shall see from the evaluation of the full solutions, they do exhibit an alternating jet structure with y which merges very far upstream with the diffusive self-similar wake solutions.

Finally, when the fluid is homogeneous, a similar analysis yields all real poles for $k_2 \geqslant 0$, thus indicating a complete absence of wave-like terms in the horizontal velocity components.

In spite of these general features, which are common to all four singularity types, substantial detailed differences do exist in the Oseen region due to the contrasts in the flows which are induced nearer

the body. Of course, we have seen differences even further out in the self-similar regime which we considered in the last section, and it is inconceivable that this intermediate region would not at least yield differences of comparable severity. The horizontal velocity component profiles, which we shall examine first, were calculated by integrating equation (6) for $\zeta = u_i$, $i = 1, 2_s, 2_d, 3$.

We begin by considering the variations in the upstream and downstream profiles with varying horizontal distance from the body (i.e. the origin), and a constant degree of ambient stratification. Profiles for the four singularity types are shown in Figures 1-4, together with the self-similar profiles which we discussed earlier. For each singularity type, the Oseen and self-similar profiles both exhibit the characteristic alternating jet structure which has been previously noted for u_1 by Long (1962) in the self-similar regime, and by Janowitz (1967) for the Oseen region. These profiles broaden vertically and weaken for increasing distances from the disturbances because of the influence of viscosity. Furthermore, as expected qualitatively, the deviations of the full Oseen solutions from the corresponding self-similar profiles decrease with increasing distances from the singularities. Comparison of the Oseen and self-similar profiles for a specific value of $|x|$ shows that the former are more spread out vertically and have magnitudes which are smaller upstream and larger downstream than would be the case if the flow development were everywhere self-similar (i.e. with negligible inertia). Comparing the Oseen profiles for the four singularity types shows differences in the magnitudes and symmetry about $y = 0$ which are similar to those exhibited by the similarity solutions. Thus, disturbance flows symmetric about $y = 0$ are created

by both the horizontal momentum source and the vertically oriented heat dipole. Conversely, antisymmetric disturbance flows are created by both the vertical momentum source, and the heat source as the vertically induced motion near the body is converted by the ambient density stratification into horizontal motions. Upstream, the profiles are qualitatively similar at all stations (though spread out and weakened as described before). However downstream, one striking feature of the horizontal velocity profiles is the apparent fact that they may be completely reversed in sign from one streamwise position to the next.

The effect of varying the degree of ambient stratification on the horizontal velocity component for fixed streamwise position ($\bar{x} = \pm 2.5$) is shown in Figures 5-8. As suggested by the qualitative arguments at the beginning of this section, the velocity profiles for all cases, both upstream and downstream, are decreased in magnitude and strongly compressed vertically, as the degree of stratification is increased. In contrast to the self-similar profiles which are qualitatively similar for all Re, the Oseen profiles downstream can again vary strongly with Re, sometimes showing a complete reversal of sign. Finally, by comparing Figures 1-4 for Re = 11.68 and Figures 5-8 for Re = 6.325, it can be seen that the deviations of the Oseen solutions from their self-similar forms, at a fixed streamwise position, are decreased with decreasing Re. This feature is expected qualitatively and simply reflects the decreased importance of fluid inertia for lower values of Re.

To date, nearly all of the theoretical work on the motion of bodies through a stratified fluid has concentrated on the horizontal velocity component (cf. Long 1962, Janowitz 1967, 1968). In order to

gain additional physical insight into the alternating jet structure and other interesting features of the horizontal velocity profiles, we also carried out explicit calculations of the disturbance streamfunction fields for the four types of singularities. Typical results are illustrated in Figures 9-12 for various degrees of ambient stratification. The length scale (both horizontal and vertical) in each case is indicated by marking the points $\bar{x} = 0$ and $\bar{x} = 3$ for $\bar{y} = 0$ in part (a) of the Figure, with the origin being denoted on all plots as a large dot. The disturbance flow consists of a pattern of rotors of finite vertical thicknesses for stratified fluids ($\gamma' > 0$) and an open streamline pattern for homogeneous fluids ($\gamma' = 0$). As explained by List (1971) for creeping flows, the rotor structure for stratified fluids is a simple consequence of the fact that the induced flows (and associated return flows) are constrained by the ambient stratification to regions of finite vertical extent.

Both upstream and downstream of each singularity type, the alternating jet structure of the horizontal velocity profiles for $\gamma' > 0$ (and its absence for $\gamma' = 0$) may now be associated with the existence for $\gamma' > 0$ (and absence for $\gamma' = 0$) of closed streamline rotor flows, with each rotor being of finite vertical extent and rotating in the opposite direction from its nearest neighbors. For each singularity type, the rotors increase in number and decrease in strength and size for increasing amounts of stratification; this is reflected in the decreasing magnitude and vertical wavelength of the alternating jet profiles for the horizontal velocity components. Finally, the disturbance flow downstream can also exhibit a series of alternating, closed streamline flow patterns with increasing x, whereas upstream, the alterations

in the sense of rotation are confined to the vertical direction. Hence, the occurrence in some cases of changes in shape (e.g. the reversal in sign of u_3, u_{2_d}, and u_{2_s}) of the alternating jet structure with increasing downstream distances (or increasing $\gamma' > 0$) and the contrasting similarity in all of the upstream profile shapes may again be ascribed to the existence of rotors of horizontally finite and semi-infinite extent, respectively, in the disturbance flows.

Our Oseen solutions for the horizontal and vertical momentum sources can be compared with the Stokes flow calculations of List (1971) for $\gamma' > 0$. List found the rotors to be symmetric (or antisymmetric) upstream and downstream. In contrast, the inclusion of the Oseen-type convection term results in a skewing of the rotors towards the downstream direction, as observed experimentally by Long (1959). Our solutions also show the existence of a whole family of rotors, thus allowing reversals in the flow direction as one moves either in the vertical or horizontal (downstream) directions. Thus, we obtain jets for the horizontal velocity profiles whose number depends on Re and x, as found in Pao's experiments (1968), and which may change drastically in shape between different downstream positions or different Reynolds numbers. On the other hand, for $y > 0$ and $\gamma' > 0$, List found only one rotor for ψ_1 (corresponding to only two jets for u_1) and a system of three rotors for ψ_3 which change rotation directions vertically, but not horizontally. Thus the creeping flow solutions could not account for the changes in shape of the downstream alternating jet structure or for other differences between the upstream and downstream profiles.

Finally, the total streamline plots, created by adding the disturbance flow streamlines associated with a particular singularity to

the ambient uniform flow streamlines $\tilde{\psi} = y$, have been obtained by Robertson (1975) and confirm the qualitative interpretation of the presence of a periodic structure in u_i, $i = 1, 2_s, 2_d, 3$, with respect to x for $\gamma' > 0$ as indicative of lee-waves. The presence for $\gamma' > 0$ (and absence for $\gamma' = 0$) of the wave-like structure downstream is associated with the corresponding presence for $\gamma' > 0$ (and absence for $\gamma' = 0$) of a series of alternating rotors with increasing downstream distances in the disturbance streamfunction fields.

Appendix A: Distance Requirements for Valid Solutions

Having discussed in detail both the self-similar and Oseen solutions, we would also like to estimate *a priori* the distances from each type of singularity required for the two solutions to be valid. For the Oseen solution regime, we have considered distances so large that the Oseen linearization of the convective operator is applicable; i.e. $|u| << 1$ or

$$|u| \leq 0.1 \qquad \text{(A1)}$$

where ≤ 0.1 corresponds, for numerical purposes, to $<< 1$; qualitatively, similar results would be obtained if a number other than 0.1 were chosen. Since we do not have closed form Oseen solutions for the horizontal velocity components, as they have to be evaluated by a numerical integration, we cannot calculate *a priori* explicit expressions for the distances required from the relation (A1). However, explicit expressions which provide a conservative estimate of these distances can be obtained by substituting the closed form self-similar expressions into the Oseen condition (A1), thereby yielding the distance requirements:

$|x| \geq 0.61\ Re^{5/4}Pr^{-1/4}$ for a horizontal momentum source,

$|x| \geq 0.53\ Re^{1/2}Pr^{-1/4}$ for a vertical momentum source,

and $|x| \geq 0.50\ Re^{1/2}Pr^{1/2}$ for a heat source or vertically oriented heat dipole,

when $K_1 = K_2 = K_3 = 1$. Figure A1 illustrates the estimates of the regimes of validity for the Oseen solutions due to each singularity type for Pr = 0.7. For the horizontal momentum source, these estimates are seen to approximate well the actual regimes of validity obtained *a posteriori* by calculating the Oseen solution at various values of $|x|$ to find the value of $|x|$ which must be exceeded for the Oseen

condition (A1) to apply.

The behavior of the similarity solution regime is governed by equations (15); hence, as well as by the relation (A1), additional distance restrictions on the self-similar solutions are imposed by the conditions $|\partial u/\partial x| \ll |\partial p/\partial x|$, $|\partial^2 u/\partial x^2| \ll |\partial^2 u/\partial y^2|$, $|\partial v/\partial x| \ll |\partial p/\partial y|$, $|Re^{-1}\partial^2 v/\partial y^2| \ll |\partial p/\partial y|$, $|Re^{-1}\partial^2 v/\partial x^2| \ll |\partial p/\partial y|$, $|\partial \bar{\theta}/\partial x| \ll |v|$, and $|\partial^2 \bar{\theta}/\partial x^2| \ll |\partial^2 \bar{\theta}/\partial y^2|$. The most restrictive distance requirement determined from all the above conditions is[†]

$$|x| \gg Re^2 Pr^{-1}$$

for each singularity type and Pr = 0.7, resulting in each case from the condition $|\partial u/\partial x| \ll |\partial p/\partial x|$. For the self-similar solutions, the regime of validity, which is further from each singularity than the corresponding Oseen solution regime as expected, is illustrated in Figure 13. As expected, for decreasing Re, the region in which the Oseen solution is valid but the self-similar solution is not, decreases in size.

[†] In the large stratification (low Re) limit, Freund and Meyer (1972) also derived this distance requirement for the validity of the similarity solution in which the detailed body geometry is unimportant.

References

Browand, F. K. and Winant, C. D. 1972 Blocking Ahead of a Cylinder Moving in a Stratified Fluid: An Experiment. Geophysical Fluid Dynamics 4, 29.

Carslaw, H. S. and Jaeger, J. C. 1959 Conduction of Heat in Solids, p. 271. Oxford University Press, London.

Freund, D. D. and Meyer, R. E. 1972 On the Mechanism of Blocking in a Stratified Fluid. J. Fluid Mech. 54, 719

Graebel, W. P. 1969 On the Slow Motion of Bodies in Stratified and Rotating Fluids. Q. J. Mech. Appl. Math. 22, 39.

Janowitz, G. S. 1967 On Wakes in Stratified Fluids. Tech. Rept. No. 22 (ONR Series), Nonr-4010(01), Dept. of Mech., The Johns Hopkins Univ., Baltimore, Maryland.

Janowitz, G. S. 1968 On Wakes in Stratified Fluids. J. Fluid Mech. 33, 417.

Janowitz, G. S. 1971 The Slow Transverse Motion of a Flat Plate through a Non-diffusive Stratified Fluid. J. Fluid Mech. 47, 171.

Laws, P. and Stevenson, T. N. 1972 Measurements of a Laminar Wake in a Confined Stratified Fluid. J. Fluid Mech. 54, 745.

List, E. J. 1971 Laminar Momentum Jets in a Stratified Fluid. J. Fluid Mech. 45, 561.

Long, R. R. 1959 The Motions of Fluids with Density Stratification. J. Geophysical Research 64, 2151.

Long, R. R. 1962 Velocity Concentrations in Stratified Fluids. J. Hydraulics Div. A.S.C.E. 88, 9.

Pao, Y.-H. 1968 Laminar Flow of a Stably Stratified Fluid Past a Flat Plate. J. Fluid Mech. 34, 795.

Robertson, G. E., Seinfeld, J. H. and Leal, L. G. 1973 Combined Forced and Free Convection Flow Past a Horizontal Flat Plate. A.I.Ch.E. J. 19, 998.

Robertson, G. E. 1975 Ph.D. dissertation, California Institute of Technology.

Table 1: Self-Similar Diffusive Wake Solutions

$$u_1 = -\frac{Re}{2\pi Pe^{1/6}|x|^{2/3}} \int_0^\infty s \cos \eta s \exp(-s^3) ds$$

$$u_{2_d} = \mp \frac{Pe^{1/2} Re}{2\pi |x|} \int_0^\infty s^2 \cos \eta s \exp(-s^3) ds$$

$$u_{2_s} = \pm \frac{Pe^{1/3} Re}{2\pi |x|^{2/3}} \int_0^\infty s \sin \eta s \exp(-s^3) ds$$

$$u_3 = \mp \frac{Re}{2\pi Pe^{1/3}|x|^{4/3}} \int_0^\infty s^3 \sin \eta s \exp(-s^3) ds$$

$$v_1 = \mp \frac{Re}{2\pi Pe^{1/3}|x|^{4/3}} \int_0^\infty s^3 \sin \eta s \exp(-s^3) ds$$

$$v_{2_d} = -\frac{Pe^{1/3} Re}{2\pi |x|^{5/3}} \int_0^\infty s^4 \sin \eta s \exp(-s^3) ds$$

$$v_{2_s} = -\frac{Pe^{1/6} Re}{2\pi |x|^{4/3}} \int_0^\infty s^3 \cos \eta s \exp(-s^3) ds$$

$$v_3 = +\frac{Re}{2\pi Pe^{1/2}|x|^2} \int_0^\infty s^5 \cos \eta s \exp(-s^3) ds$$

$$p_1 = \mp \frac{Pe^{1/6}}{2\pi |x|^{1/3}} \int_0^\infty \cos \eta s \exp(-s^3) ds$$

$$p_{2_d} = -\frac{Pe^{5/6}}{2\pi |x|^{2/3}} \int_0^\infty s \cos \eta s \exp(-s^3) ds$$

$$p_{2_s} = +\frac{Pe^{2/3}}{2\pi |x|^{1/3}} \int_0^\infty \sin \eta s \exp(-s^3) ds$$

$$p_3 = -\frac{1}{2\pi |x|} \int_0^\infty s^2 \sin \eta s \exp(-s^3) ds$$

$$\theta_1 = \begin{matrix} + \\ - \end{matrix} \frac{Pe^{1/3}Re}{2\pi|x|^{2/3}} \int_0^\infty s \sin \eta s \exp(-s^3) ds$$

$$\theta_{2_d} = + \frac{Pe}{2\pi|x|} \int_0^\infty s^2 \sin \eta s \exp(-s^3) ds$$

$$\theta_{2_s} = + \frac{Pe^{5/6}}{2\pi|x|^{2/3}} \int_0^\infty s \cos \eta s \exp(-s^3) ds$$

$$\theta_3 = - \frac{Pe^{1/6}Re}{2\pi|x|^{4/3}} \int_0^\infty s^3 \cos \eta s \exp(-s^3) ds$$

Figure Captions

Figure 1: $\bar{u}_1(\bar{x},\bar{y}) = 3.418\, u_1(x = 3.418\bar{x},\ y = 3.418\bar{y})$ for Re = 11.68, Pr = 0.7

—— Oseen solutions; ---- Self-similar solutions

(a) $\bar{x} = x/3.418 = 2.5,\ 25,\ 250$

(b) $\bar{x} = x/3.418 = -2.5,\ -25$

Figure 2: $\bar{u}_3(\bar{x},\bar{y}) = 3.418\, u_3(x = 3.418\bar{x},\ y = 3.418\bar{y})$ for Re = 11.68, Pr = 0.7

—— Oseen solutions; ---- Self-similar solutions

(a) $\bar{x} = x/3.418 = 2.5,\ 25$

(b) $\bar{x} = x/3.418 = -2.5,\ -25$

Figure 3: $\bar{u}_{2_d}(\bar{x},\bar{y}) = 3.418\, u_{2_d}(x = 3.418\bar{x},\ y = 3.418\bar{y})$ for Re = 11.68, Pr = 0.7

—— Oseen solutions; ---- Self-similar solutions

(a) $\bar{x} = x/3.418 = 2.5,\ 25,\ 250$

(b) $\bar{x} = x/3.418 = -2.5,\ -25$

Figure 4: $\bar{u}_{2_s}(\bar{x},\bar{y}) = u_{2_s}(x = 3.418\bar{x},\ y = 3.418\bar{y})$ for Re = 11.68, Pr = 0.7

—— Oseen solutions; ---- Self-similar solutions

(a) $\bar{x} = x/3.418 = 2.5,\ 25,\ 250$

(b) $\bar{x} = x/3.418 = -2.5,\ -25$

Figure 5: $\bar{u}_1(\bar{x},\bar{y}) = \frac{40}{Re}\, u_1(x = 40\bar{x}/Re,\ y = 40\bar{y}/Re)$ for Pr = 0.7; Re = 6.325, 11.68, 25.2

—— Oseen solutions; ---- Self-similar solution for Re = 6.325

(a) $\bar{x} = xRe/40 = 2.5$ (b) $\bar{x} = xRe/40 = -2.5$

Figure 6: $\bar{u}_3(\bar{x},\bar{y}) = \frac{40}{Re}\, u_3(x = 40\bar{x}/Re,\ y = 40\bar{y}/Re)$ for Pr = 0.7;
Re = 6.325, 11.68, 25.2

—— Oseen solutions; ---- Self-similar solution for Re = 6.325

(a) $\bar{x}$ = xRe/40 = 2.5 (b) $\bar{x}$ = xRe/40 = -2.5

Figure 7: $\bar{u}_{2_d}(\bar{x},\bar{y}) = \frac{40}{Re}\, u_{2_d}(x = 40\bar{x}/Re,\ y = 40\bar{y}/Re)$ for Pr = 0.7;
Re = 6.325, 11.68

—— Oseen solutions; ---- Self-similar solution for Re = 6.325

(a) $\bar{x}$ = xRe/40 = 2.5 (b) $\bar{x}$ = xRe/40 = -2.5

Figure 8: $\bar{u}_{2_s}(\bar{x},\bar{y}) = u_{2_s}(x = 40\bar{x}/Re,\ y = 40\bar{y}/Re)$ for Pr = 0.7; Re = 6.325, 11.68
—— Oseen solutions; ---- Self-similar solution for Re = 6.325

(a) $\bar{x}$ = xRe/40 = 2.5 (b) $\bar{x}$ = xRe/40 = -2.5

Figure 9: $\bar{\psi}_1(\bar{x},\bar{y})$ for Pr = 0.7

(a) $\gamma' = 0$; $\bar{\psi}_1(\bar{x},\bar{y}) = \psi_1(x_\phi = 40\bar{x},\ y_\phi = 40\bar{y})$ = -0.10, -0.15, -0.30, -0.35, -0.40, -0.425, -0.45 with -0.10 corresponding to the lowermost streamline

(b) Re = 25.2; $\bar{\psi}_1(\bar{x},\bar{y}) = \psi_1(x = 1.586\bar{x}, y = 1.586\bar{y})$ = -0.001, -0.1 , -0.2, -0.3, -0.4, -0.5, -0.6, -0.7, -0.8, -0.9, -1.0 with -0.001 corresponding to the lowermost streamline

(c) Re = 11.68; $\bar{\psi}_1(\bar{x},\bar{y}) = \psi_1(x = 3.418\bar{x}, y = 3.418\bar{y})$ = -0.001, -0.05, -0.1, -0.2, -0.3, -0.4, -0.5, 0.05, 0.10, 0.15 with -0.001 corresponding to the lowermost streamline

(d) Re = 6.325; $\bar{\psi}_1(\bar{x},\bar{y}) = \psi_1(x = 6.325\bar{x}, y = 6.325\bar{y})$ = -0.001, -0.05, -0.10, -0.15, -0.20, -0.30, 0.02, 0.04 with -0.001 corresponding to the lowermost streamline

Figure 10: $\bar{\psi}_3(\bar{x},\bar{y})$ for Pr = 0.7

(a) $\gamma' = 0$; $\bar{\psi}_3(\bar{x},\bar{y}) = \psi_3(x_\phi = 40\bar{x},\ y_\phi = 40\bar{y}) = -0.466, -0.366, -0.316, -0.266, -0.216, -0.166, -0.116, -0.066, -0.016, +0.014, 0.054$ with -0.466 corresponding to the streamline closest to the origin

(b) $Re = 25.2$; $\bar{\psi}_3(\bar{x},\bar{y}) = \psi_3(x = 1.586\bar{x},\ y = 1.586\bar{y}) = -0.40, -0.30, -0.20, -0.10, -0.05, -0.001, 0.05, 0.10, 0.20, 0.30, 0.40$ with -0.40 corresponding to the streamline closest to the origin

(c) $Re = 11.68$; $\bar{\psi}_3(\bar{x},\bar{y}) = \psi_3(x = 3.418\bar{x},\ y = 3.418\bar{y}) = -0.20, -0.15, -0.10, -0.05, -0.001, 0.05, 0.10, 0.20, 0.30$ with -0.20 corresponding to the streamline closest to the origin

(d) $Re = 6.325$; $\bar{\psi}_3(\bar{x},\bar{y}) = \psi_3(x = 6.325\bar{x},\ y = 6.325\bar{y}) = -0.10, -0.05, -0.001, 0.05, 0.125, 0.20$ with -0.10 corresponding to the innermost streamline just upstream of the origin

Figure 11: $\bar{\psi}_{2_d}(\bar{x},\bar{y})$ for $Pr = 0.7$

(a) $\gamma' = 0$; $\bar{\psi}_{2_d}(\bar{x},\bar{y}) = \psi_{2_d}(x_\phi = 40\bar{x},\ y_\phi = 40\bar{y}) = 0.10, 0.15, 0.20, 0.25, 0.30, 0.35, 0.40$ with 0.10 corresponding to the lowermost streamline

(b) $Re = 25.2$; $\bar{\psi}_{2_d}(\bar{x},\bar{y}) = \psi_{2_d}(x = 1.586\bar{x},\ y = 1.586\bar{y}) = 0.001, 0.1, 0.2, 0.3, 0.4, 0.5, 0.6, 0.7, 0.8, 0.9$ with 0.001 corresponding to the lowermost streamline

(c) $Re = 11.68$; $\bar{\psi}_{2_d}(\bar{x},\bar{y}) = \psi_{2_d}(x = 3.418\bar{x},\ y = 3.418\bar{y}) = 0.001, 0.1, 0.2, 0.3, 0.4, -0.05, -0.10, -0.15, -0.20$ with 0.001 corresponding to the lowermost streamline

(d) $Re = 6.325$; $\bar{\psi}_{2_d}(\bar{x},\bar{y}) = \psi_{2_d}(x = 6.325\bar{x},\ y = 6.325\bar{y}) = 0.001, 0.05, 0.10, 0.20, -0.025, -0.05, -0.10$ with 0.001 corresponding to the lowermost streamline just upstream

of the origin

Figure 12: $\bar{\psi}_{2_s}(\bar{x},\bar{y})$ for Pr = 0.7

(a) Re = 11.68; $\bar{\psi}_{2_s}(\bar{x},\bar{y}) = \psi_{2_s}(x = 3.418\bar{x},\ y = 3.418\bar{y})/3.418 =$ 0.6, 0.5, 0.4, 0.3, 0.2, 0.1, 0.001, -0.1, -0.2, -0.3, -0.4 with 0.6 corresponding to the streamline closest to the origin

(b) Re = 6.325; $\bar{\psi}_{2_s}(\bar{x},\bar{y}) = \psi_{2_s}(x = 6.325\bar{x},\ y = 6.325\bar{y})/6.325 =$ 0.10, 0.08, 0.06, 0.04, 0.02, -0.05, -0.075, -0.10 with 0.10 corresponding to the streamline closest to the origin

Figure A1: Minimum Distance Requirements for Valid Solutions; Pr = 0.7

(a) $|x| = Re^{2}Pr^{-1}$; for self-similar solutions for each singularity type considered

(b) $|x| = 0.61\ Re^{5/4}Pr^{-1/4}$; estimate for Oseen solution for horizontal momentum source with $K_1 = 1$

(c) $|x| = 0.53\ Re^{1/2}Pr^{-1/4}$; estimate for Oseen solution for vertical momentum source with $K_3 = 1$

(d) $|x| = 0.50\ Re^{1/2}Pr^{1/2}$; estimate for Oseen solution for heat source or vertically oriented heat dipole singularity with $K_2 = 1$

0: for Oseen solution for horizontal momentum source with $K_1 = 1$

Figure 1

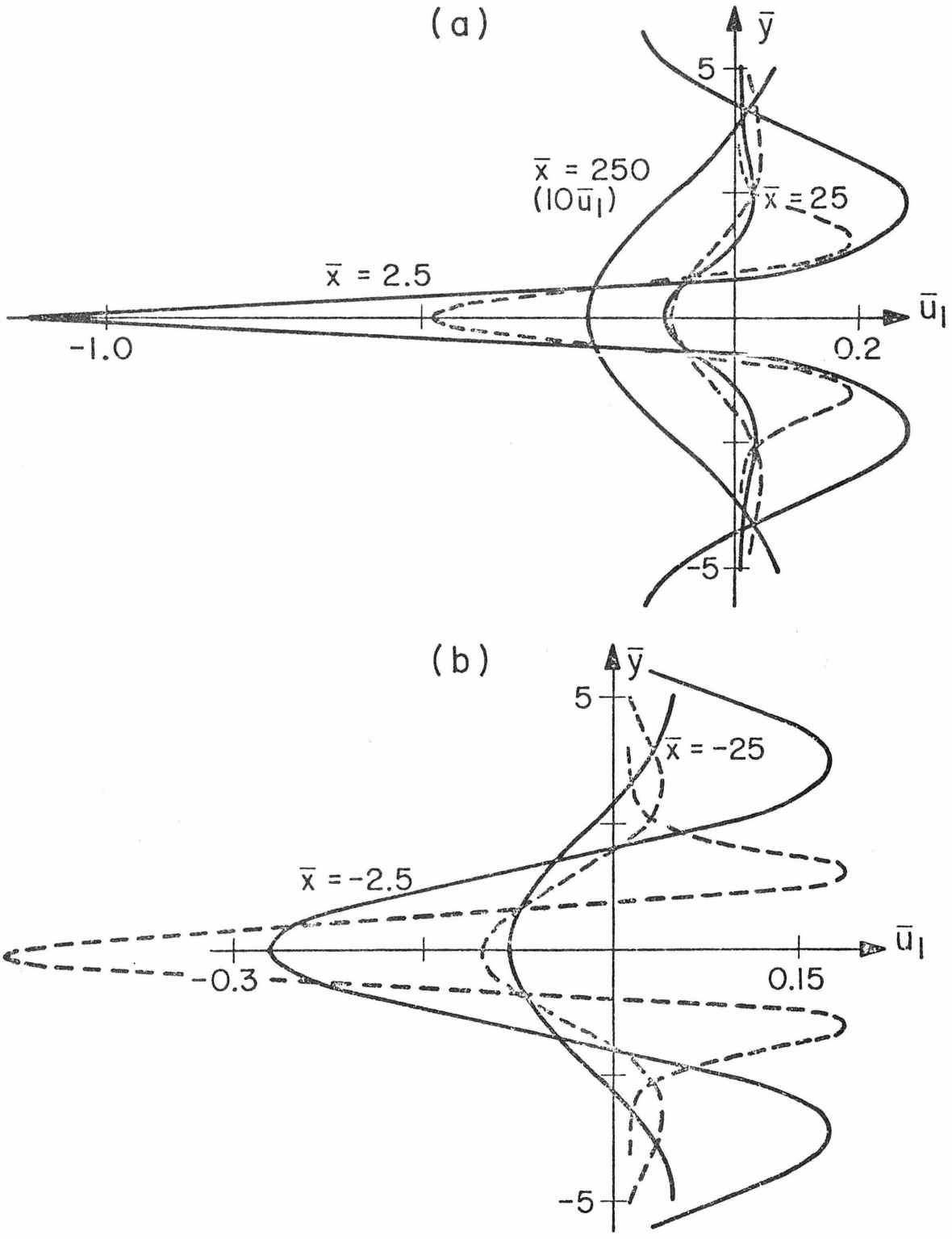
(a)
$\bar{y}$
5
$\bar{x}$ = 250
($10\bar{u}_1$)
$\bar{x}$ = 25
$\bar{x}$ = 2.5
$\bar{u}_1$
-1.0
0.2
-5
(b)
$\bar{y}$
5
$\bar{x}$ = -25
$\bar{x}$ = -2.5
$\bar{u}_1$
-0.3
0.15
-5

Figure 2

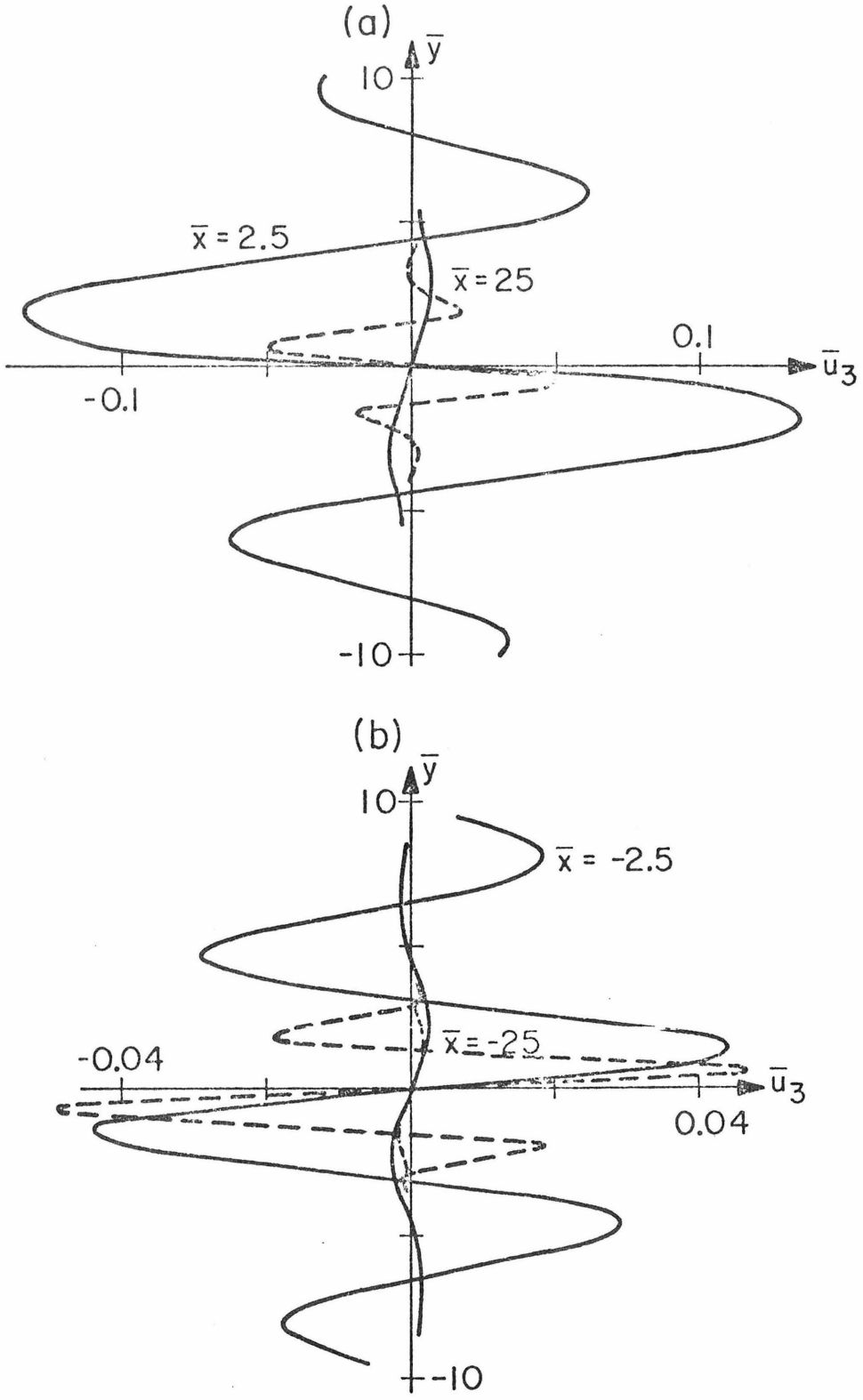
(a)
$\bar{y}$
10
$\bar{x} = 2.5$
$\bar{x} = 25$
0.1
$\bar{u}_3$
-0.1
-10
(b)
$\bar{y}$
10
$\bar{x} = -2.5$
$\bar{x} = -25$
-0.04
$\bar{u}_3$
0.04
-10

Figure 3

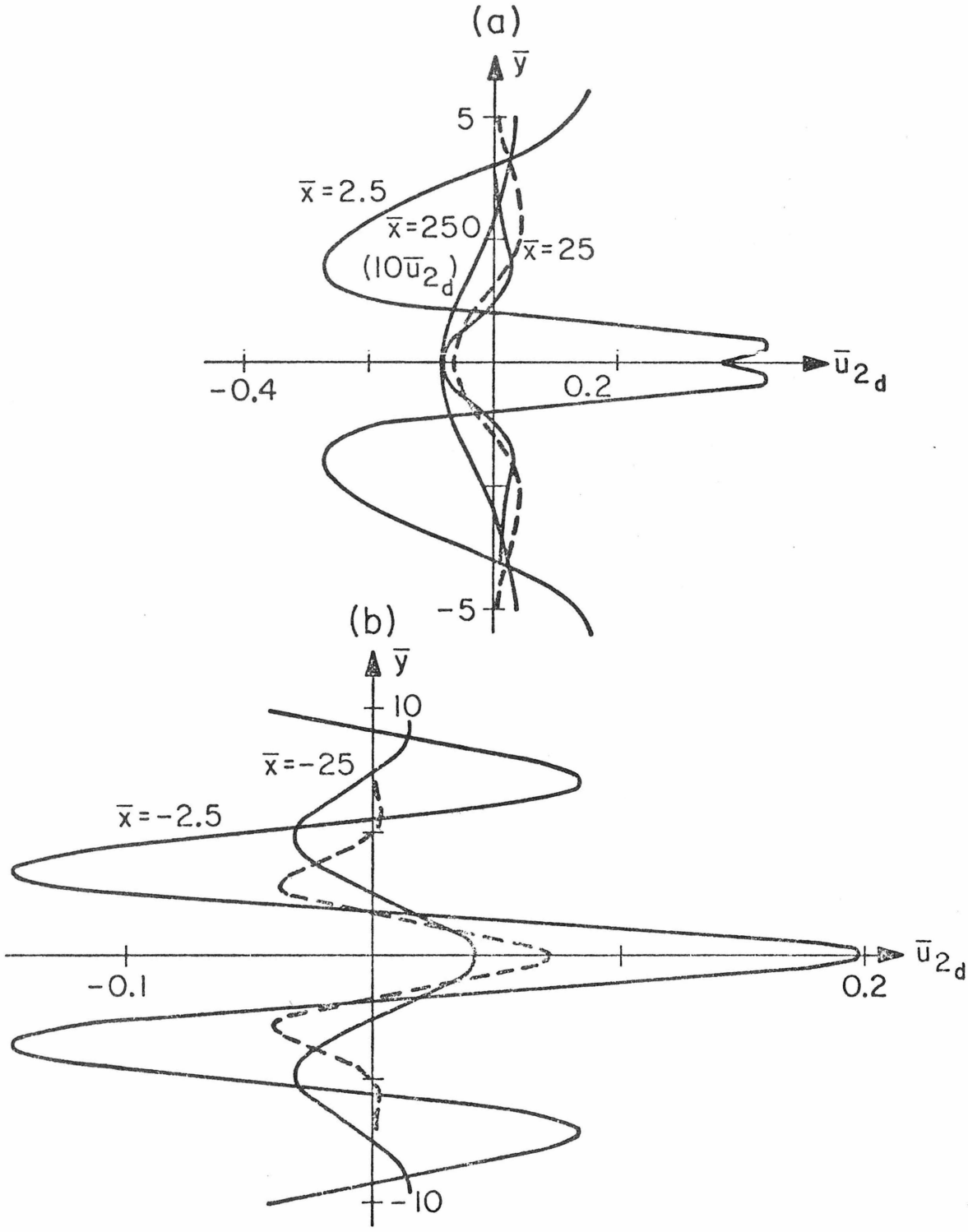
(a)
$\bar{y}$
5
$\bar{x}=2.5$
$\bar{x}=250$
$(10\bar{u}_{2_d})$
$\bar{x}=25$
$\bar{u}_{2_d}$
-0.4
0.2
-5
(b)
$\bar{y}$
10
$\bar{x}=-25$
$\bar{x}=-2.5$
$\bar{u}_{2_d}$
-0.1
0.2
-10

Figure 4

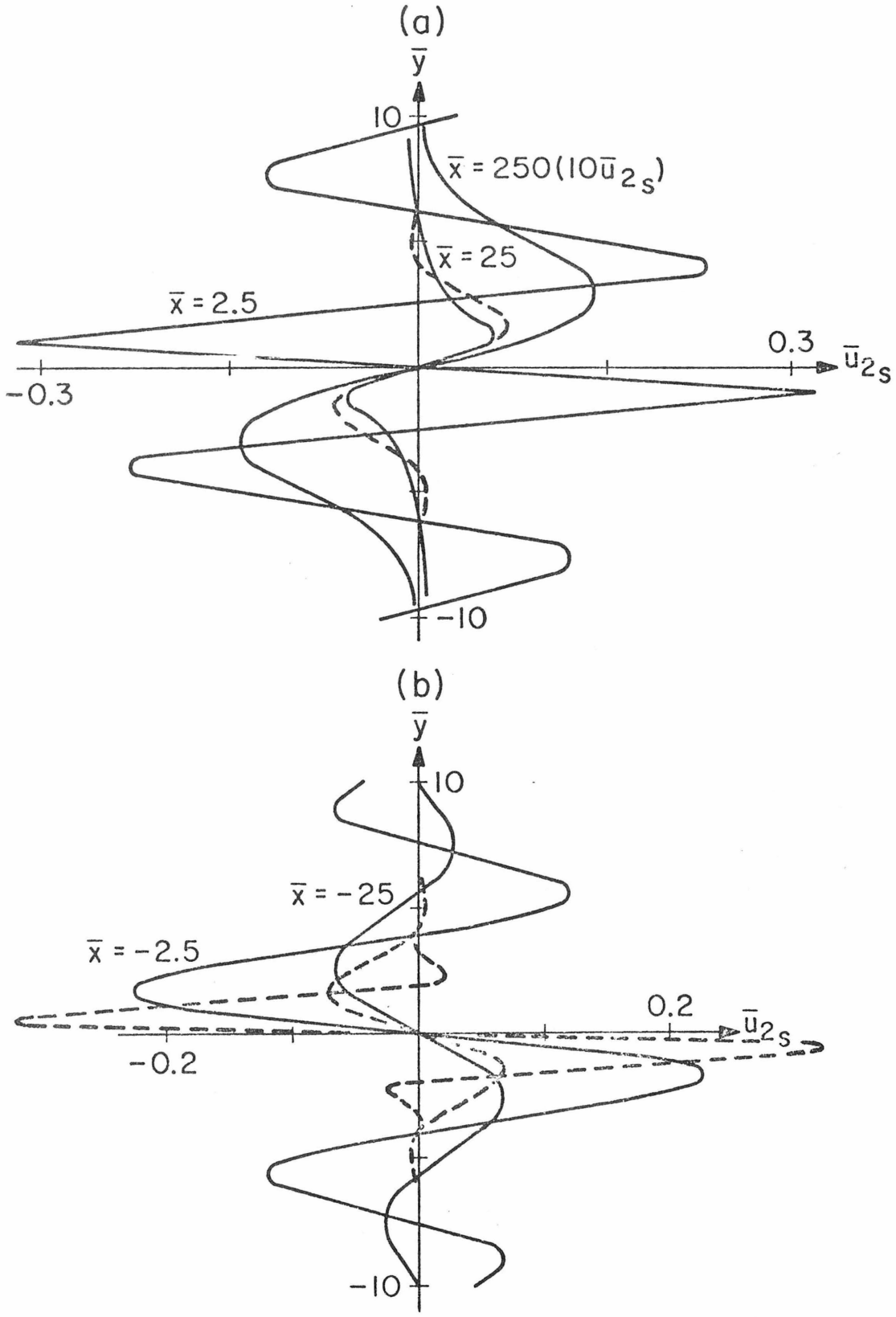
(a)
$\bar{y}$
10
$\bar{x} = 250(10\bar{u}_{2s})$
$\bar{x} = 25$
$\bar{x} = 2.5$
0.3
$\bar{u}_{2s}$
-0.3
-10
(b)
$\bar{y}$
10
$\bar{x} = -25$
$\bar{x} = -2.5$
0.2
$\bar{u}_{2s}$
-0.2
-10

Figure 5

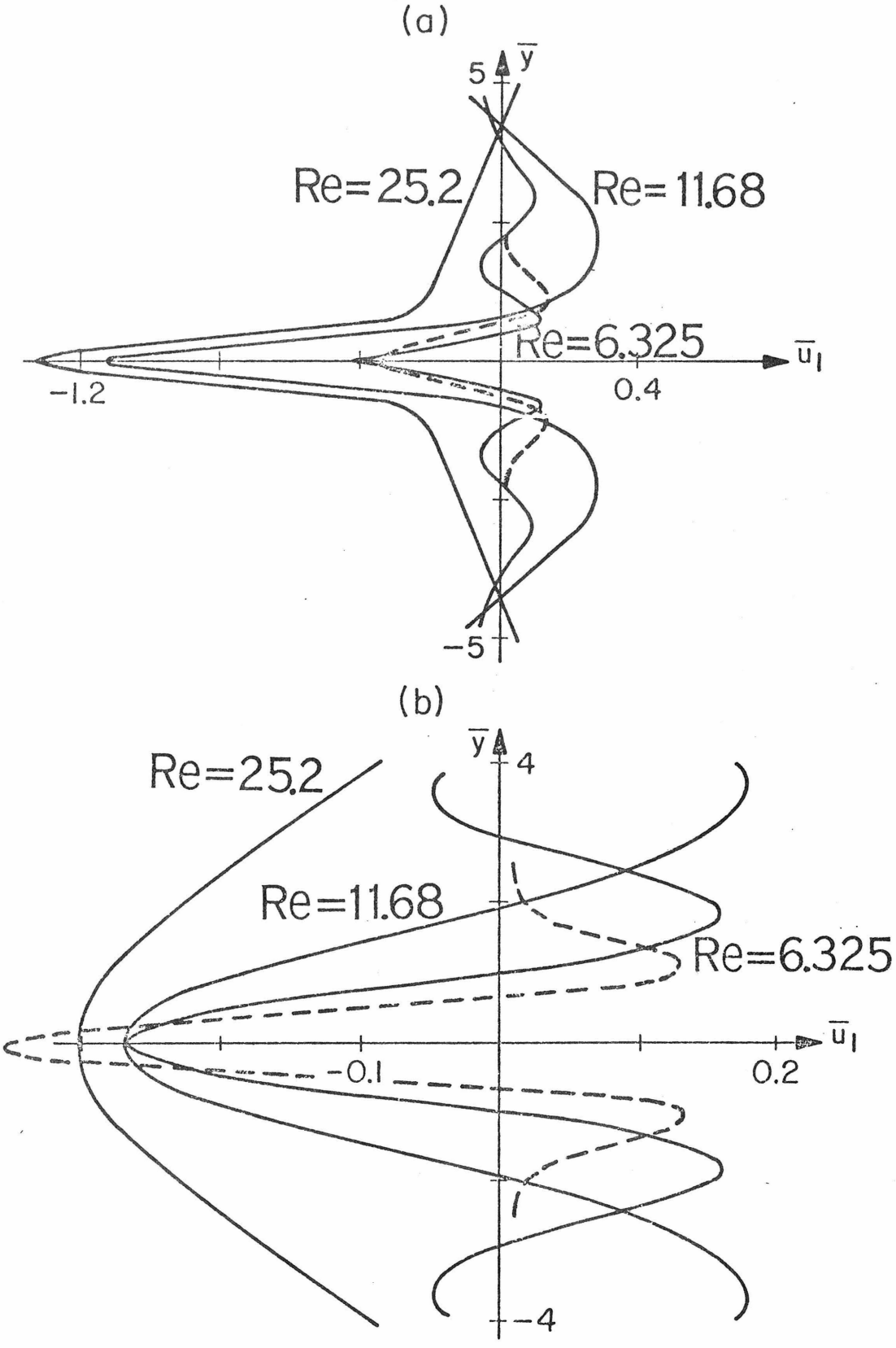
(a)
$\bar{y}$
5
Re=25.2
Re=11.68
Re=6.325
$\bar{u}_1$
-1.2
0.4
-5
(b)
$\bar{y}$
4
Re=25.2
Re=11.68
Re=6.325
$\bar{u}_1$
-0.1
0.2
-4

Figure 6

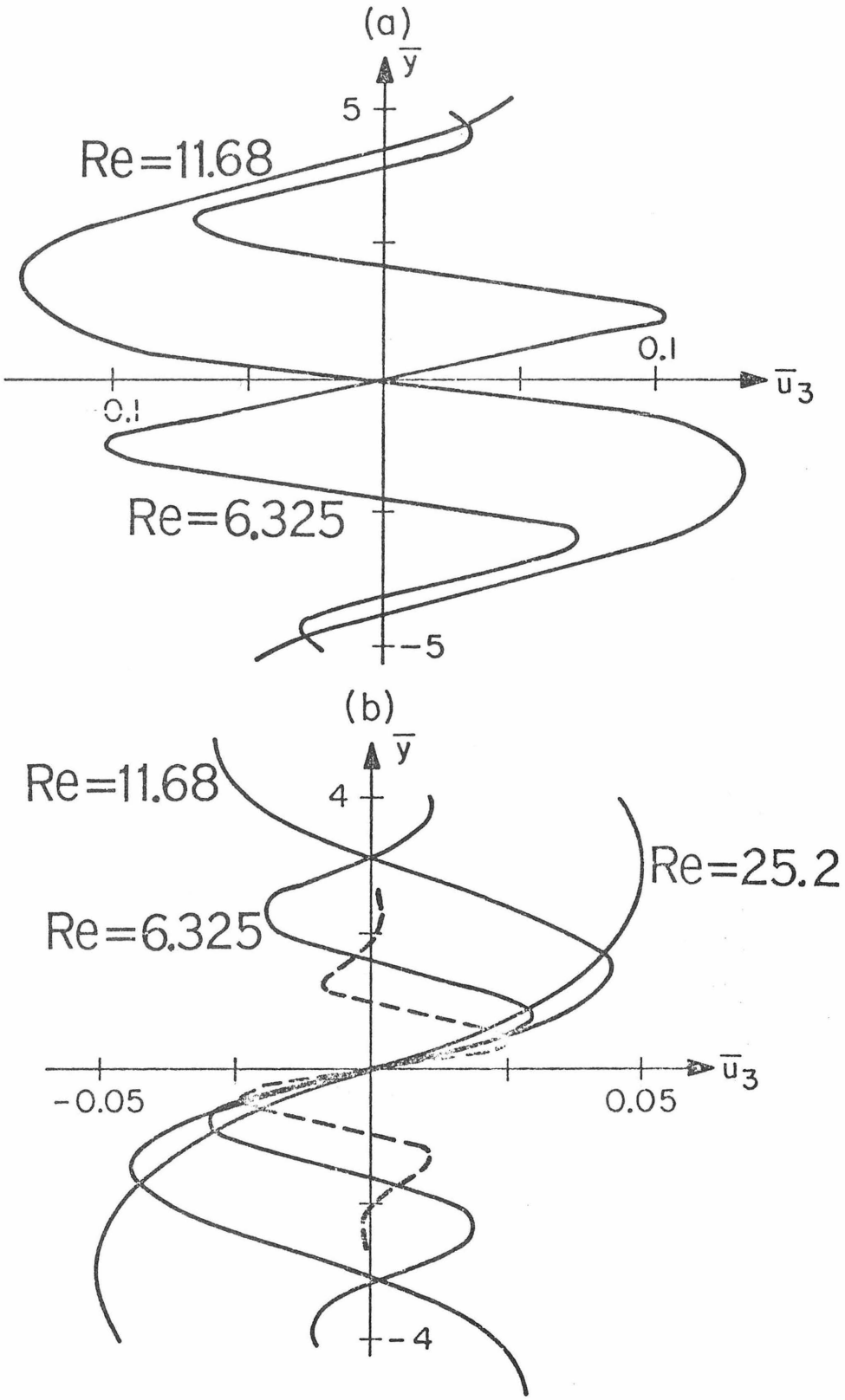
(a)
$\bar{y}$
5
Re=11.68
0.1
$\bar{u}_3$
-0.1
Re=6.325
-5
(b)
$\bar{y}$
Re=11.68
4
Re=25.2
Re=6.325
$\bar{u}_3$
-0.05
0.05
-4

Figure 7

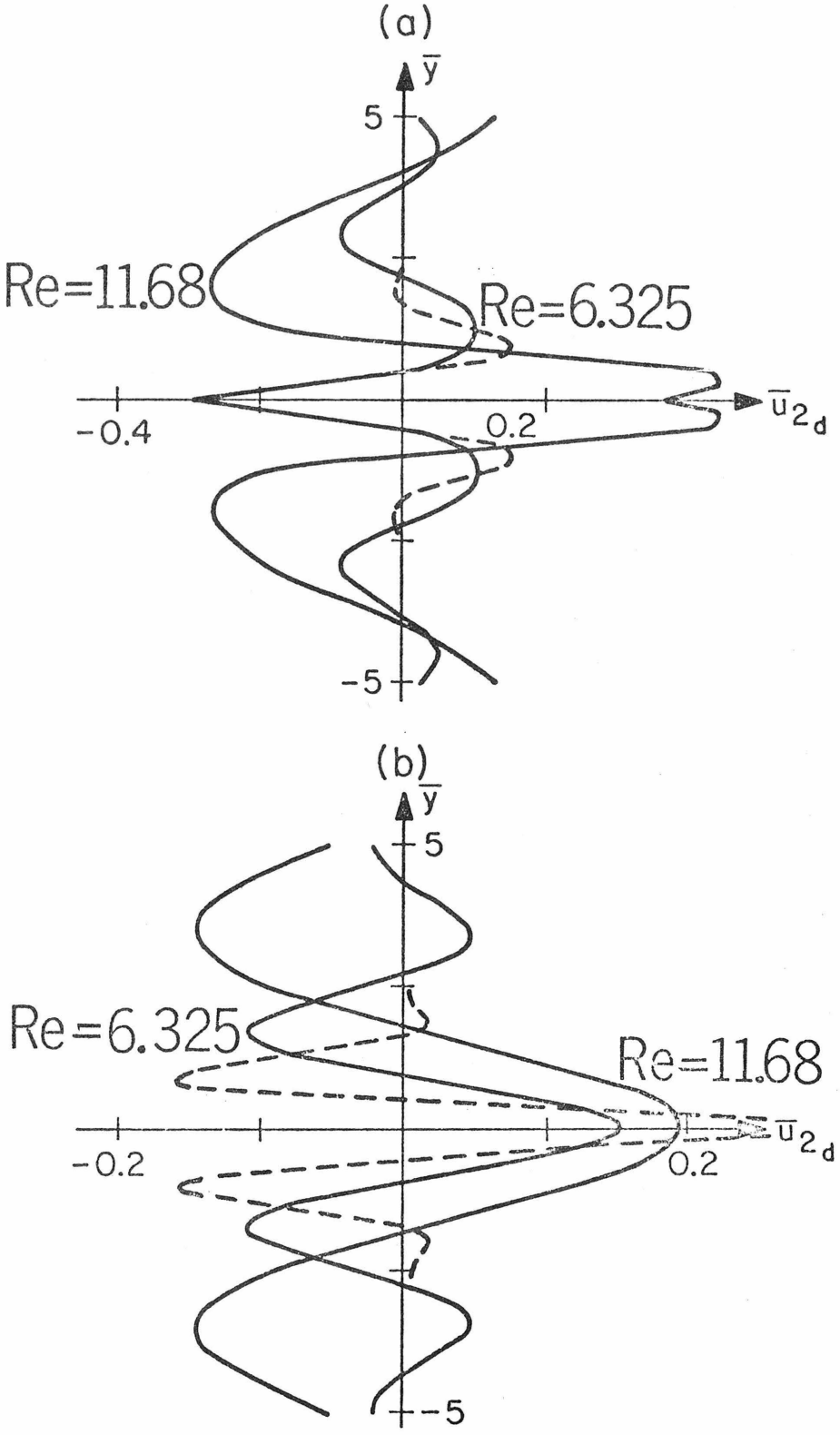
(a)
$\bar{y}$
5
Re=11.68
Re=6.325
$\bar{u}_{2_d}$
-0.4
0.2
-5
(b)
$\bar{y}$
5
Re=6.325
Re=11.68
$\bar{u}_{2_d}$
-0.2
0.2
-5

Figure 8

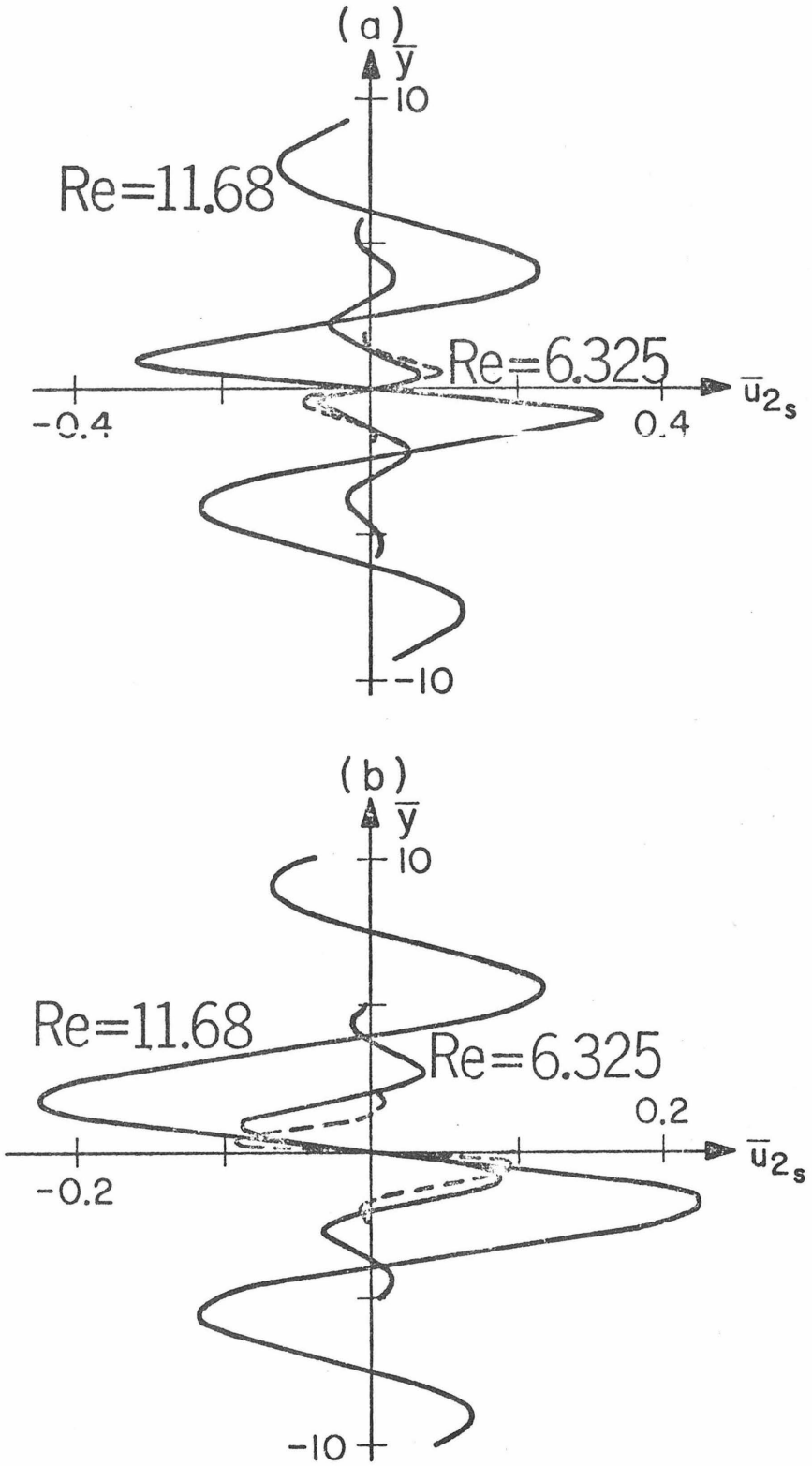
(a)
$\bar{y}$
10
Re=11.68
Re=6.325
$\bar{u}_{2_s}$
-0.4
0.4
-10
(b)
$\bar{y}$
10
Re=11.68
Re=6.325
0.2
$\bar{u}_{2_s}$
-0.2
-10

Figure 9

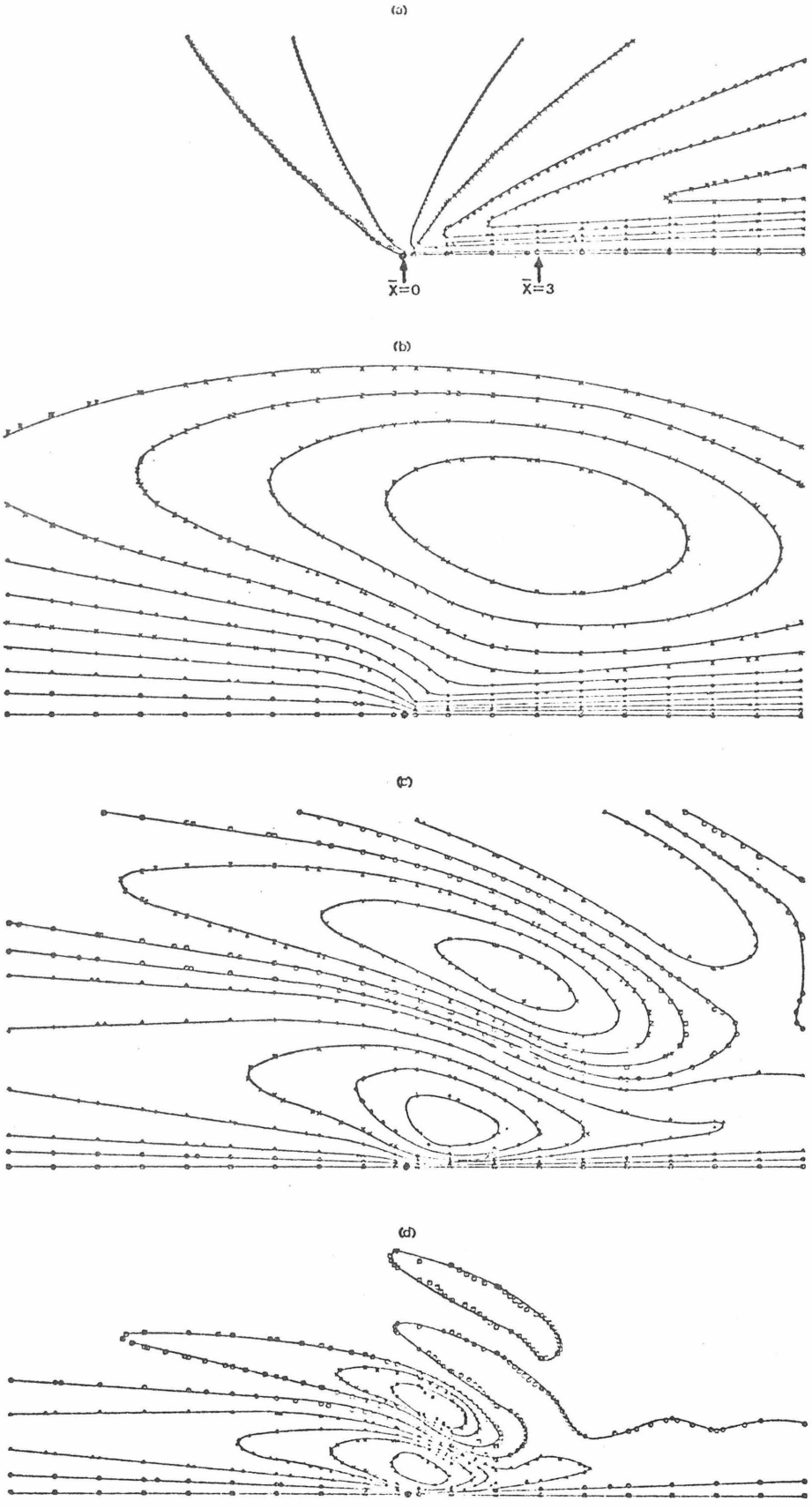

Figure 10

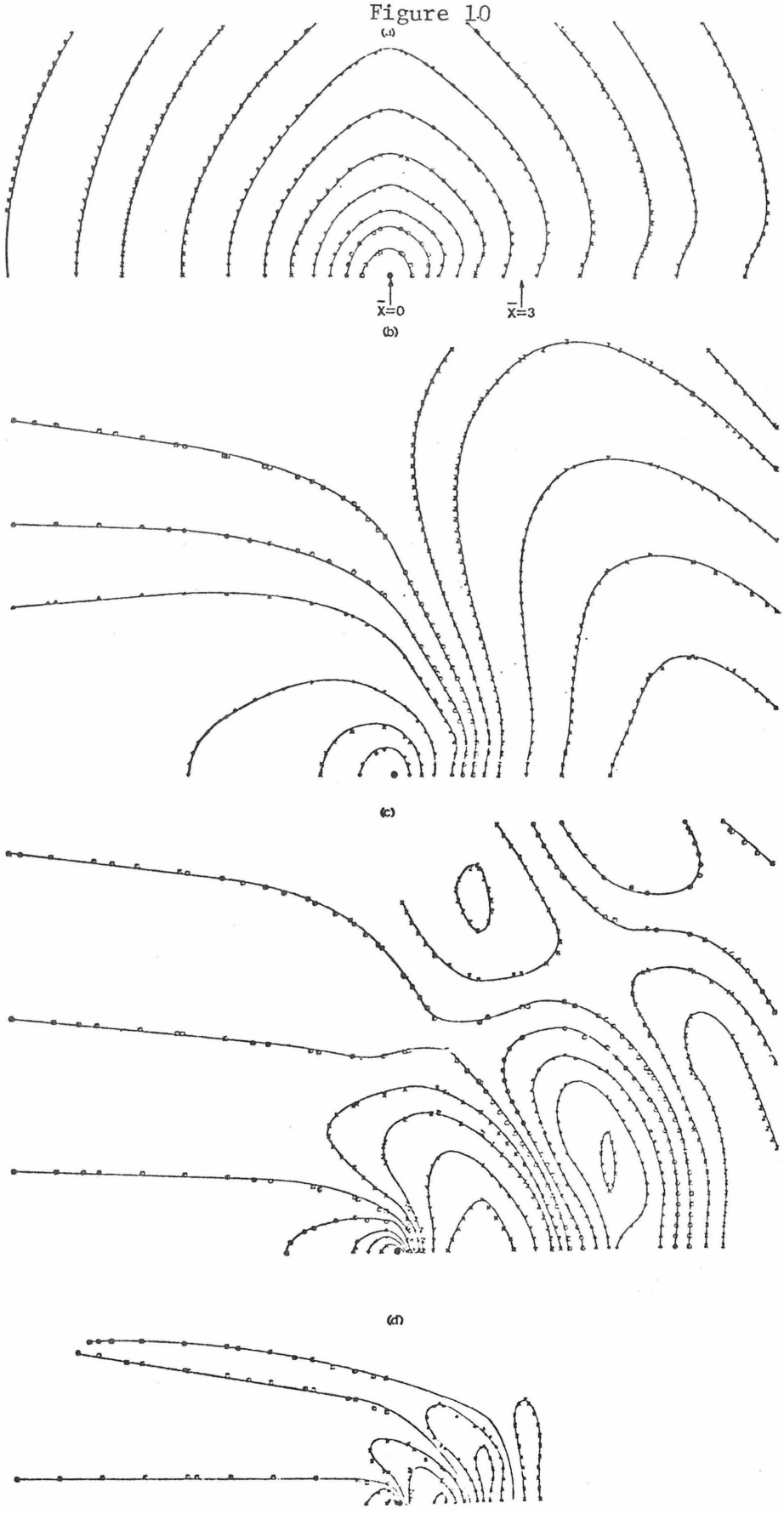

Figure 11

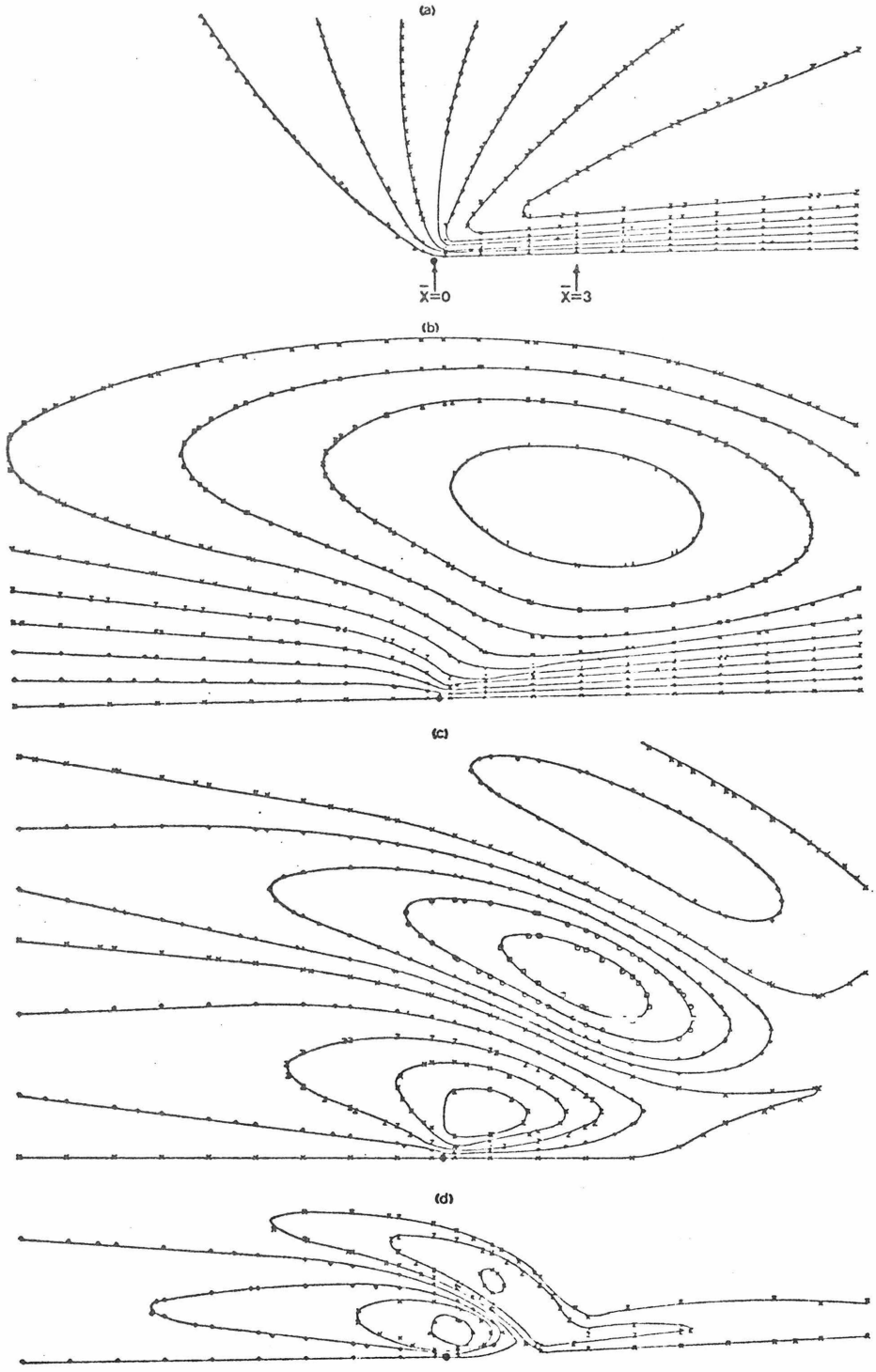

Figure 12

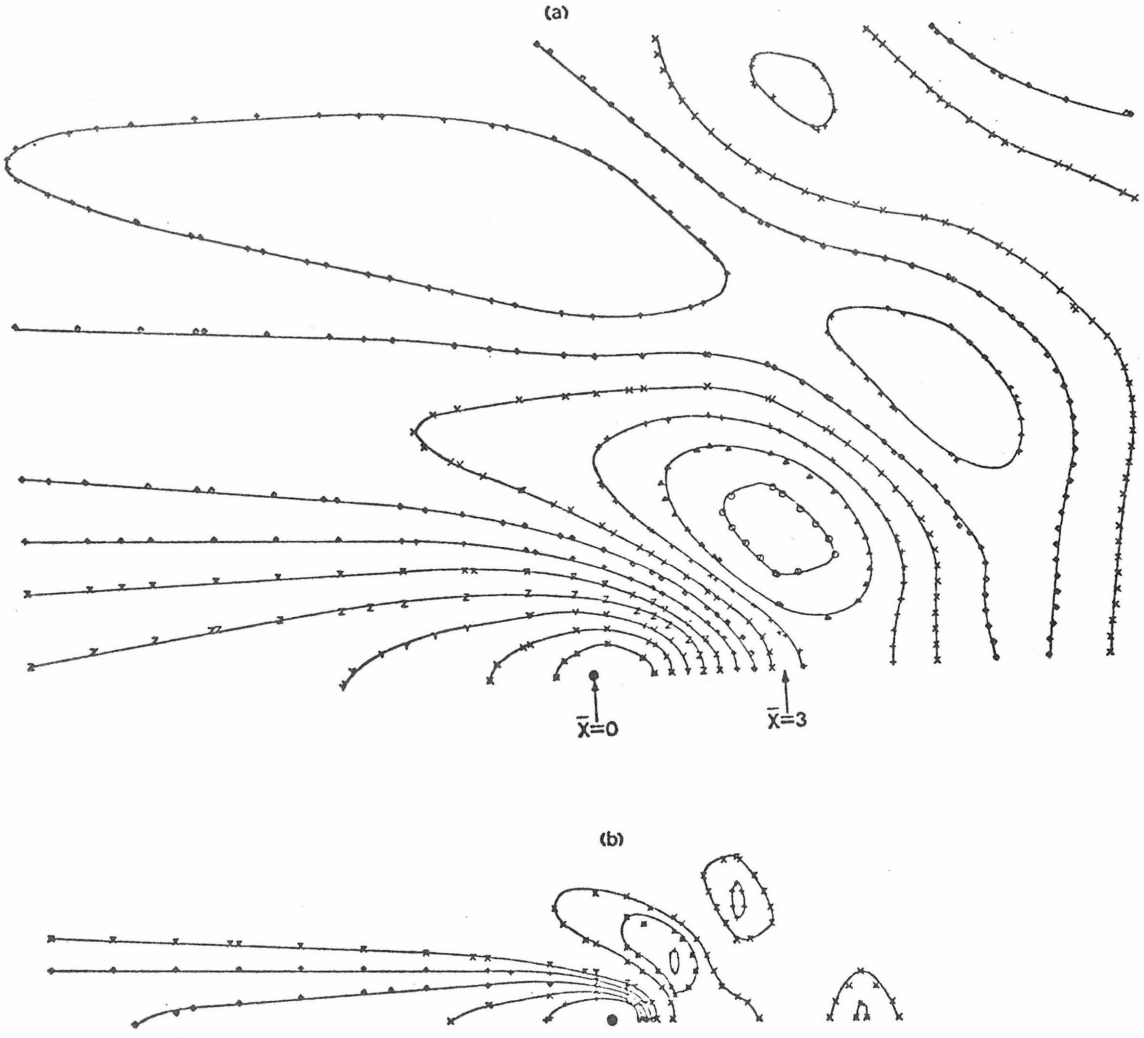

Figure A1

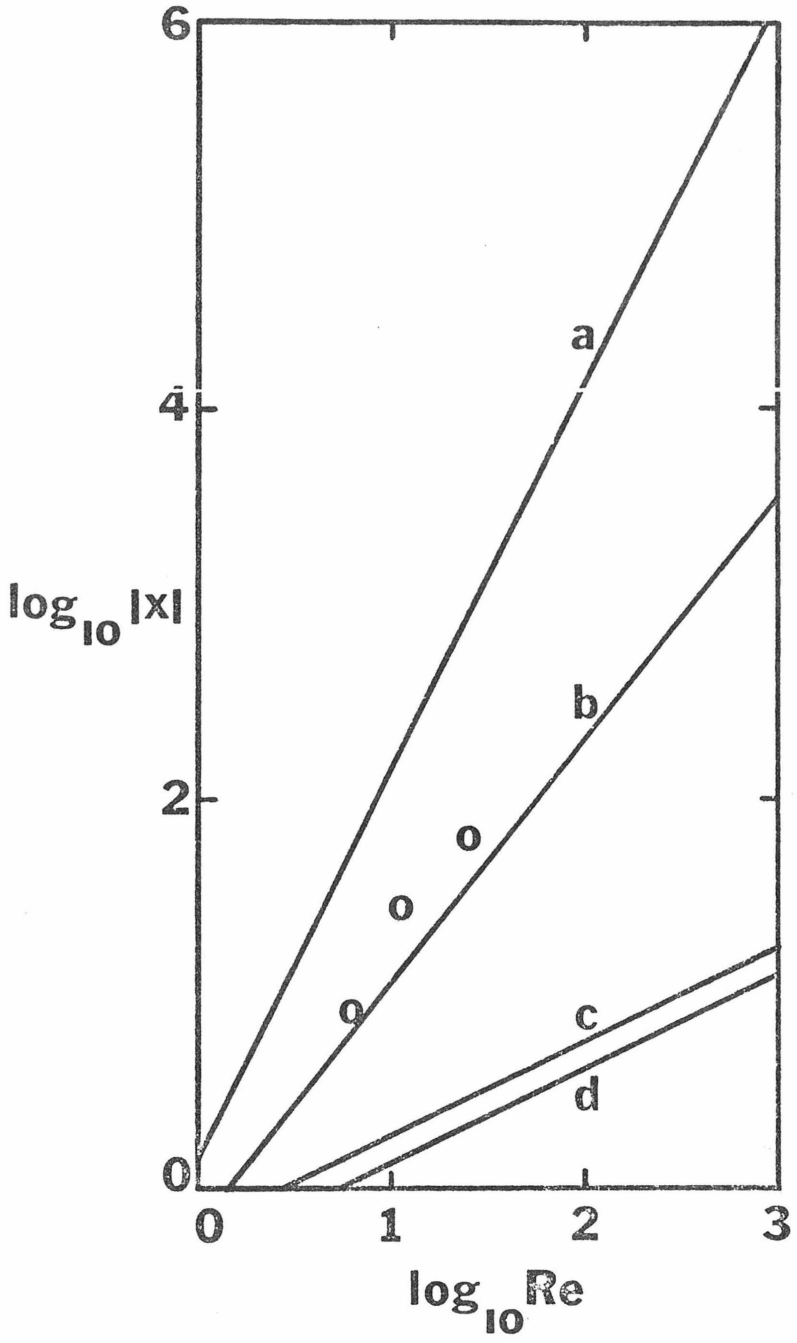

Appendix 2-A: Additional Tables and Figures

This appendix presents the Tables and Figures referred to in but, for brevity, omitted from the main body of Chapter 2.

TABLE CAPTIONS

Table 1: Functions $J_\zeta(k_2; y)$ and $K_\zeta(k_1, k_2; Re, Pe)$ for the various physical variables ζ.

Table 2: Functions A_ζ, B_{0_ζ}, B_{1_ζ}, B_{2_ζ}, B_{3_ζ}, C_ζ, D_ζ, E_ζ, F_ζ, G_ζ, L_ζ, M_ζ, N_ζ, and P_ζ for the physical variables $\zeta = u_1$, u_{2_s}, u_{2_d}, and u_3.

TABLE 1

ζ	$J_\zeta(k_2; y)$	$K_\zeta(k_1,k_2; Re, Pe)$
u_1	$k_2^2 \cos k_2 y$	$ik_1 + \frac{k_1^2 + k_2^2}{Pe}$
u_{2_s}	$k_2 \sin k_2 y$	ik_1
u_{2_d}	$- k_2^2 \cos k_2 y$	ik_1
u_3	$- k_2 \sin k_2 y$	$ik_1\left(ik_1 + \frac{k_1^2 + k_2^2}{Pe}\right)$
v_1	$- k_2 \sin k_2 y$	$ik_1\left(ik_1 + \frac{k_1^2 + k_2^2}{Pe}\right)$
v_{2_s}	$- \cos k_2 y$	k_1^2
v_{2_d}	$- k_2 \sin k_2 y$	k_1^2
v_3	$\cos k_2 y$	$k_1^2\left(ik_1 + \frac{k_1^2 + k_2^2}{Pe}\right)$
p_1	$\cos k_2 y$	$- ik_1 \left[\left(ik_1 + \frac{k_1^2 + k_2^2}{Re}\right)\left(ik_1 + \frac{k_1^2 + k_2^2}{Pe}\right) + \frac{1}{Re}\right]$
p_{2_s}	$- k_2 \sin k_2 y$	$ik_1 + \frac{k_1^2 + k_2^2}{Re}$
p_{2_d}	$k_2^2 \cos k_2 y$	$ik_1 + \frac{k_1^2 + k_2^2}{Re}$
p_3	$k_2 \sin k_2 y$	$\left(ik_1 + \frac{k_1^2 + k_2^2}{Re}\right)\left(ik_1 + \frac{k_1^2 + k_2^2}{Pe}\right)$

TABLE 1 (continued)

ζ	$J_\zeta(k_2; y)$	$K_\zeta(k_1, k_2; Re, Pe)$
θ_1	$k_2 \sin k_2 y$	ik_1
θ_{2_s}	$-\cos k_2 y$	$\left(ik_1 + \frac{k_1^2 + k_2^2}{Re}\right)\left(k_1^2 + k_2^2\right)$
θ_{2_d}	$-k_2 \sin k_2 y$	$\left(ik_1 + \frac{k_1^2 + k_2^2}{Re}\right)\left(k_1^2 + k_2^2\right)$
θ_3	$-\cos k_2 y$	k_1^2

TABLE 2

Function	$\zeta = u_1$	$\zeta = u_{2_s}$, $\zeta = u_{2_d}$	$\zeta = u_3$
A_ζ	$-\left(k_2^2 - Pe\ s_1 - s_1^2\right)$	$Pe\ s_1$	$-s_1 A_{u_1}$
B_{0_ζ}	k_2^2	0	0
B_{1_ζ}	$-Pe\lvert s_2\rvert$	$-Pe\lvert s_2\rvert$	$-\lvert s_2\rvert k_2^2$
B_{2_ζ}	$-\lvert s_2\rvert^2$	0	$Pe\lvert s_2\rvert^2$
B_{3_ζ}	0	0	$\lvert s_2\rvert^3$
C_ζ	$-\left(k_2^2 - Pe\ s_1 - s_1^2\right)$	$Pe\ s_1$	$-s_1 C_{u_1}$
D_ζ	$-\left(k_2^2 - Pe\ s_2 - s_2^2\right)$	$Pe\ s_2$	$-s_2 D_{u_1}$
E_ζ	$-\left(k_2^2 - Pe\ s_3 - s_3^2\right)$	$Pe\ s_3$	$-s_3 E_{u_1}$
F_ζ	$\left(k_2^2 - Pe\ s_4 - s_4^2\right)$	$-Pe\ s_4$	$-s_4 F_{u_1}$
G_ζ	$\left(k_2^2 - Pe\ s_5 - s_5^2\right)$	$-Pe\ s_5$	$-s_5 G_{u_1}$
L_ζ	$\left(k_2^2 - Pe\ s_6 - s_6^2\right)$	$-Pe\ s_6$	$-s_6 L_{u_1}$
M_ζ	F_{u_1}	$F_{u_{2_s}}\left(= F_{u_{2_d}}\right)$	F_{u_3}
N_ζ	G_{u_1}	$G_{u_{2_s}}\left(= G_{u_{2_d}}\right)$	G_{u_3}
P_ζ	L_{u_1}	$L_{u_{2_s}}\left(= L_{u_{2_d}}\right)$	L_{u_3}

FIGURE CAPTIONS

Figure 1: Integrals as a Function of the Similarity Variable η

a: $\int_0^\infty \cos \eta s \exp(-s^3) ds$

b: $\int_0^\infty s \cos \eta s \exp(-s^3) ds$

c: $\int_0^\infty s^2 \cos \eta s \exp(-s^3) ds$

d: $\int_0^\infty s^3 \cos \eta s \exp(-s^3) ds$

e: $\int_0^\infty s^5 \cos \eta s \exp(-s^3) ds$

Figure 2: Integrals as a Function of the Similarity Variable η

a: $\int_0^\infty \sin \eta s \exp(-s^3) ds$

b: $\int_0^\infty s \sin \eta s \exp(-s^3) ds$

c: $\int_0^\infty s^2 \sin \eta s \exp(-s^3) ds$

d: $\int_0^\infty s^3 \sin \eta s \exp(-s^3) ds$

e: $\int_0^\infty s^4 \sin \eta s \exp(-s^3) ds$

Figure 3: $\bar{y} + 0.6\bar{\psi}_1(\bar{x}, \bar{y}) = 0.001, 0.2, 0.4, 0.6, 0.8, 1.0, 1.5, 2.0, 3.0, 4.0$, with 0.001 corresponding to the lowermost streamline, for Pr = 0.7.

(a) $\gamma' = 0$; $\bar{y} + 0.6\bar{\psi}_1(\bar{x}, \bar{y}) = y_\phi/40 + 0.6\psi_1(x_\phi = 40\ \bar{x}, y_\phi = 40\ \bar{y})$

(b) Re = 25.2; $\bar{y} + 0.6\bar{\psi}_1(\bar{x}, \bar{y}) = y/1.586 + 0.6\psi_1(x = 1.586\ \bar{x}, y = 1.586\ \bar{y})$

(c) —— Re = 11.68; $\bar{y} + 0.6\bar{\psi}_1(\bar{x}, \bar{y}) = y/3.418 + 0.6\psi_1(x = 3.418\ \bar{x}, y = 3.418\ \bar{y})$

– – – $\gamma' = 0$

(d) $Re = 6.325$; $\bar{y} + 0.6\bar{\psi}_1(\bar{x}, \bar{y}) = y/6.325 + 0.6\psi_1(x = 6.325\,\bar{x}, y = 6.325\,\bar{y})$

Figure 4: $\bar{y} + 0.6\bar{\psi}_3(\bar{x}, \bar{y}) = -2.0, -1.0, -0.75, -0.60, -0.40, -0.25, 0.001, 0.25, 0.50, 0.75, 1.0, 2.0$, with -2.0 corresponding to the lowermost streamline, for $Pr = 0.7$.

(a) $\gamma' = 0$; $\bar{y} + 0.6\bar{\psi}_3(\bar{x}, \bar{y}) = y_\phi/40 + 0.6\psi_3(x_\phi = 40\,\bar{x}, y_\phi = 40\,\bar{y})$

(b) $Re = 25.2$; $\bar{y} + 0.6\bar{\psi}_3(\bar{x}, \bar{y}) = y/1.586 + 0.6\psi_3(x = 1.586\,\bar{x}, y = 1.586\,\bar{y})$

(c) $Re = 11.68$; $\bar{y} + 0.6\bar{\psi}_3(\bar{x}, \bar{y}) = y/3.418 + 0.6\psi_3(x = 3.418\,\bar{x}, y = 3.418\,\bar{y})$

(d) $Re = 6.325$; $\bar{y} + 0.6\bar{\psi}_3(\bar{x}, \bar{y}) = y/6.325 + 0.6\psi_3(x = 6.325\,\bar{x}, y = 6.325\,\bar{y})$

Figure 5: $\bar{y} + 0.6\bar{\psi}_{2_d}(\bar{x},\bar{y}) = 0.001, 0.2, 0.4, 0.6, 0.8, 1.0, 1.5, 2.0, 3.0, 4.0$, with 0.001 corresponding to the lowermost streamline, for $Pr = 0.7$.

(a) $\gamma' = 0$; $\bar{y} + 0.6\bar{\psi}_{2_d}(\bar{x}, \bar{y}) = y_\phi/40 + 0.6\psi_{2_d}(x_\phi = 40\,\bar{x}, y_\phi = 40\,\bar{y})$

(b) $Re = 25.2$; $\bar{y} + 0.6\bar{\psi}_{2_d}(\bar{x}, \bar{y}) = y/1.586 + 0.6\psi_{2_d}(x = 1.586\,\bar{x}, y = 1.586\,\bar{y})$

(c) —— $Re = 11.68$; $\bar{y} + 0.6\bar{\psi}_{2_d}(\bar{x},\bar{y}) = y/3.418 + 0.6\psi_{2_d}(x = 3.418\bar{x}, y = 3.418\bar{y})$; ---- $\gamma' = 0$

(d) $Re = 6.325$; $\bar{y} + 0.6\bar{\psi}_{2_d}(\bar{x},\bar{y}) = y/6.325 + 0.6\psi_{2_d}(x = 6.325\bar{x}, y = 6.325\bar{y})$

Figure 6: $\bar{y} + 0.6\bar{\psi}_{2_s}(\bar{x},\bar{y}) = -2.0,-1.0,-0.75,-0.60,-0.40,-0.25,0.001,$ $0.25,0.50,0.75,1.0,2.0$, with -2.0 corresponding to the lowermost streamline, for $Pr = 0.7$

(a) $Re = 11.68$; $\bar{y}+0.6\bar{\psi}_{2_s}(\bar{x},\bar{y})= y/3.418+0.6\psi_{2_s}(x=3.418\bar{x},$ $y=3.418\bar{y})/3.418$

(b) $Re = 6.325$; $\bar{y}+0.6\bar{\psi}_{2_s}(\bar{x},\bar{y})= y/6.325+0.6\psi_{2_s}(x=6.325\bar{x},$ $y=6.325\bar{y})/6.325$

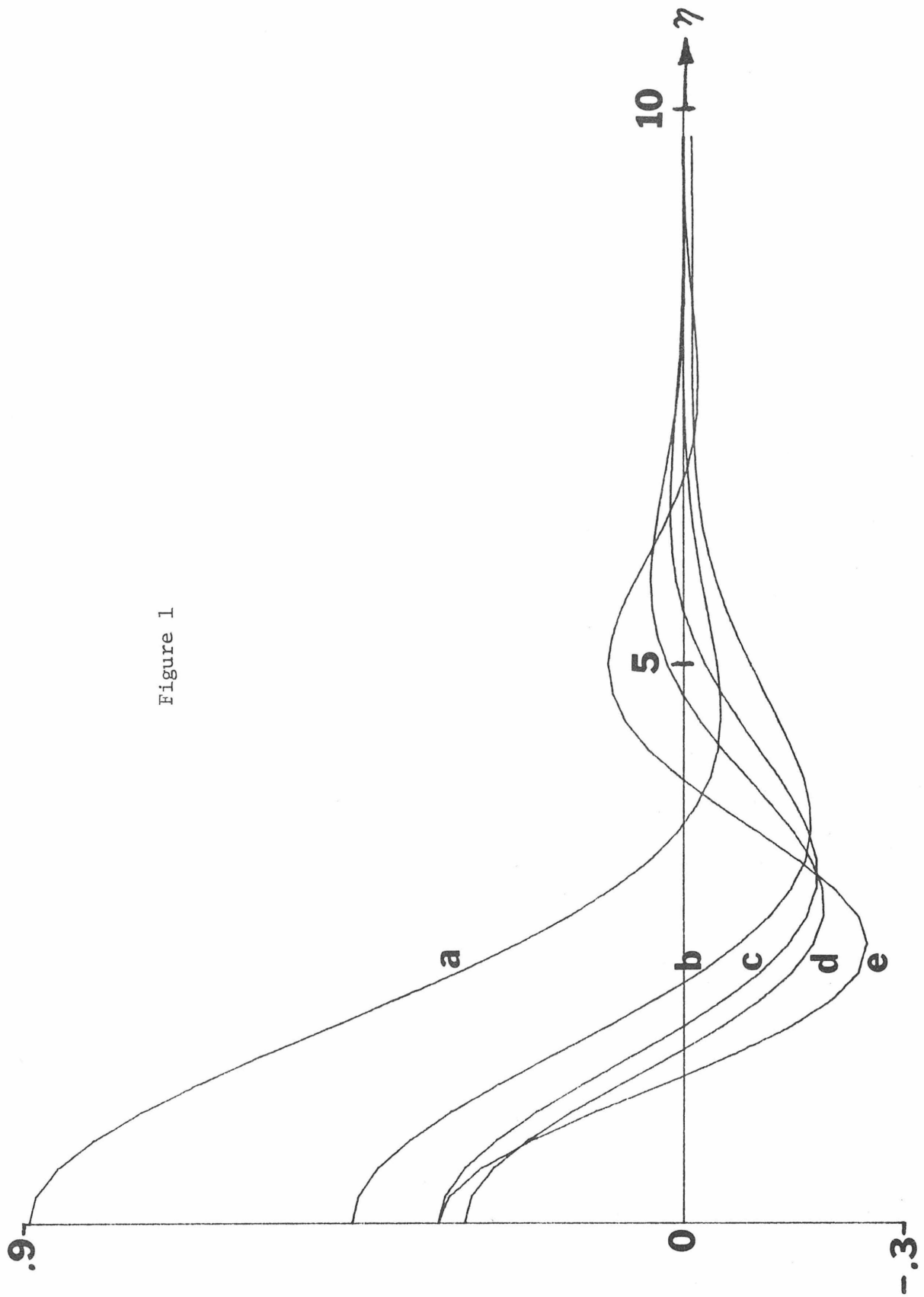

Figure 1

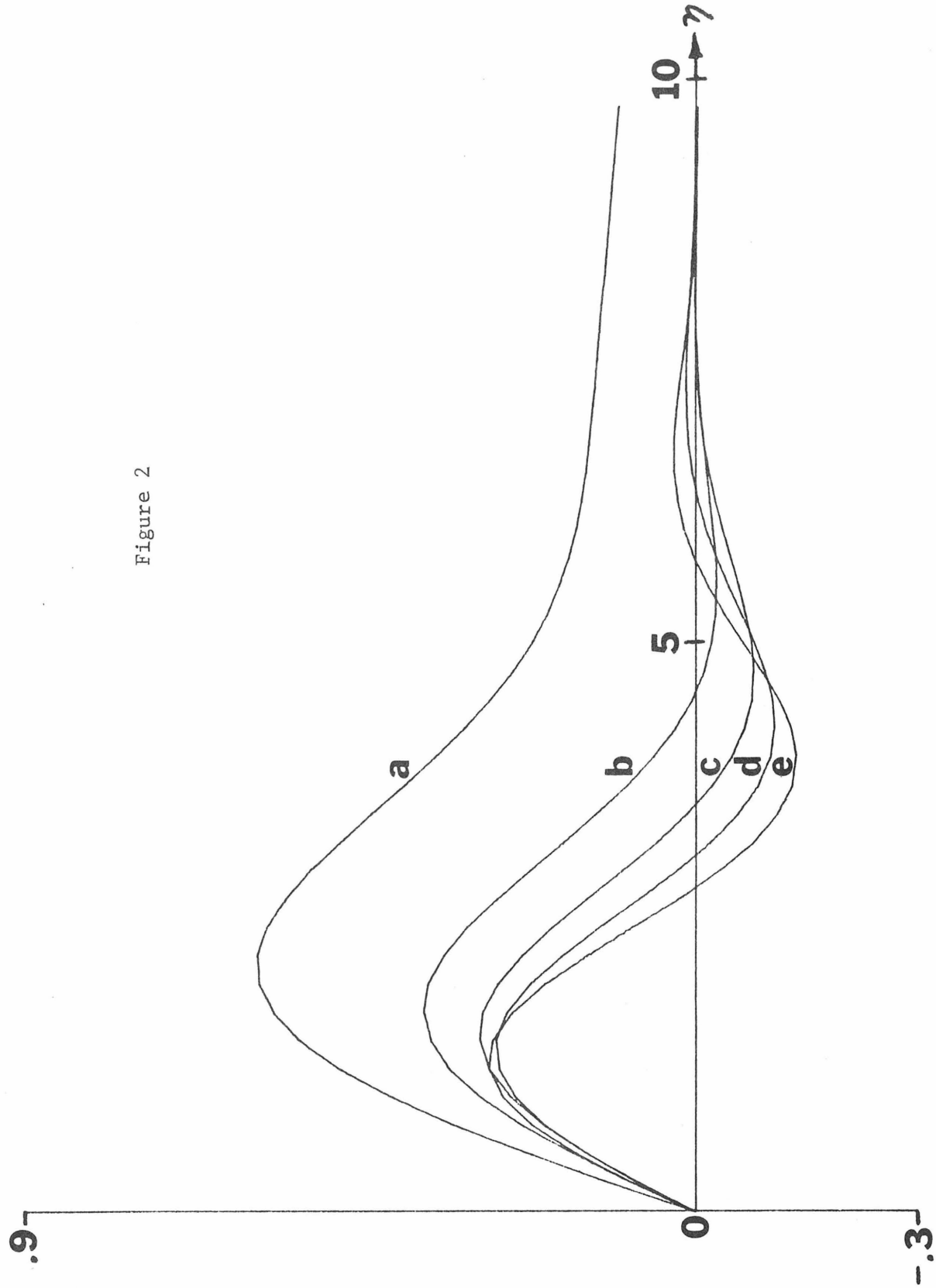

Figure 2

Figure 3

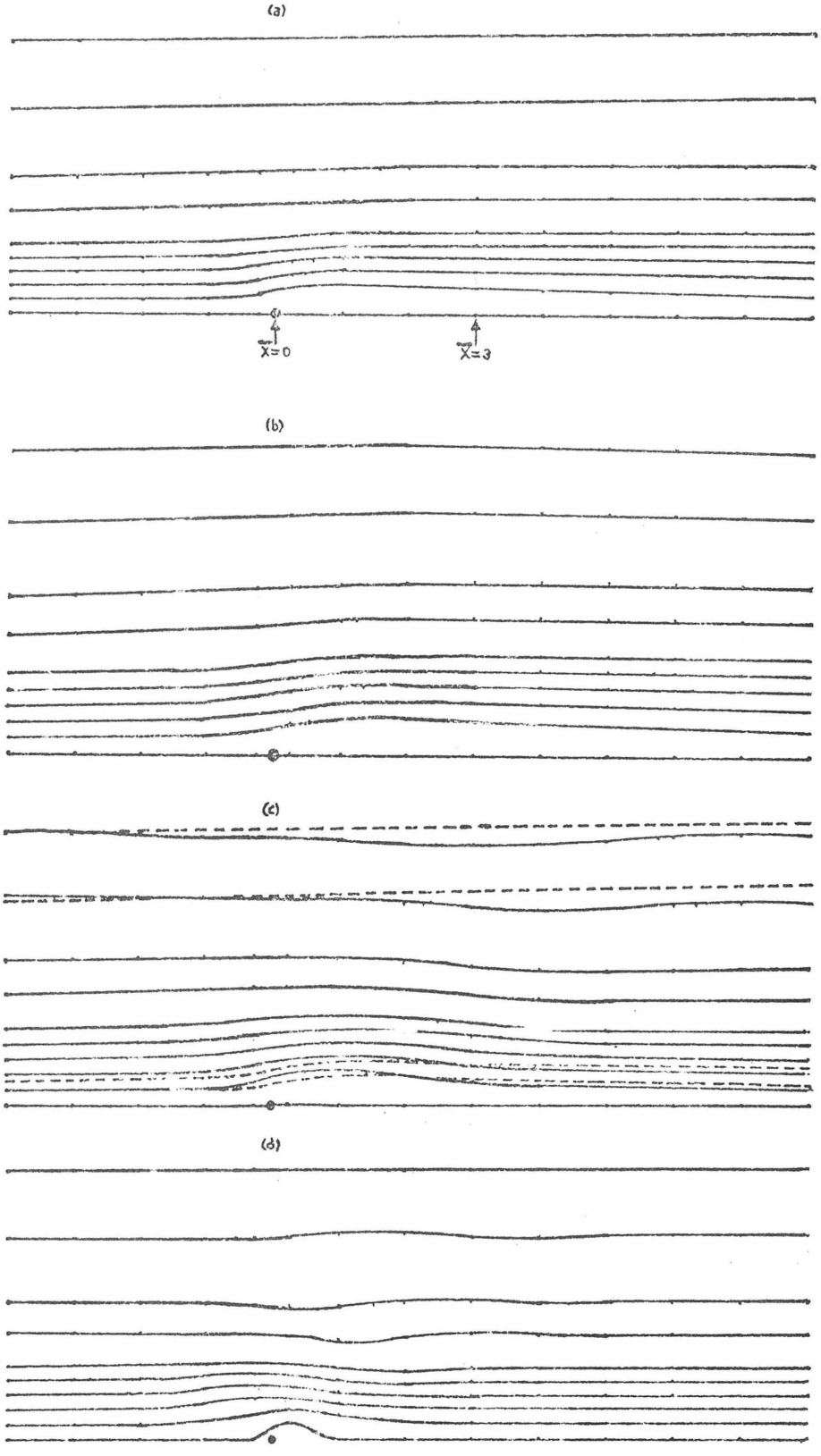

Figure 4

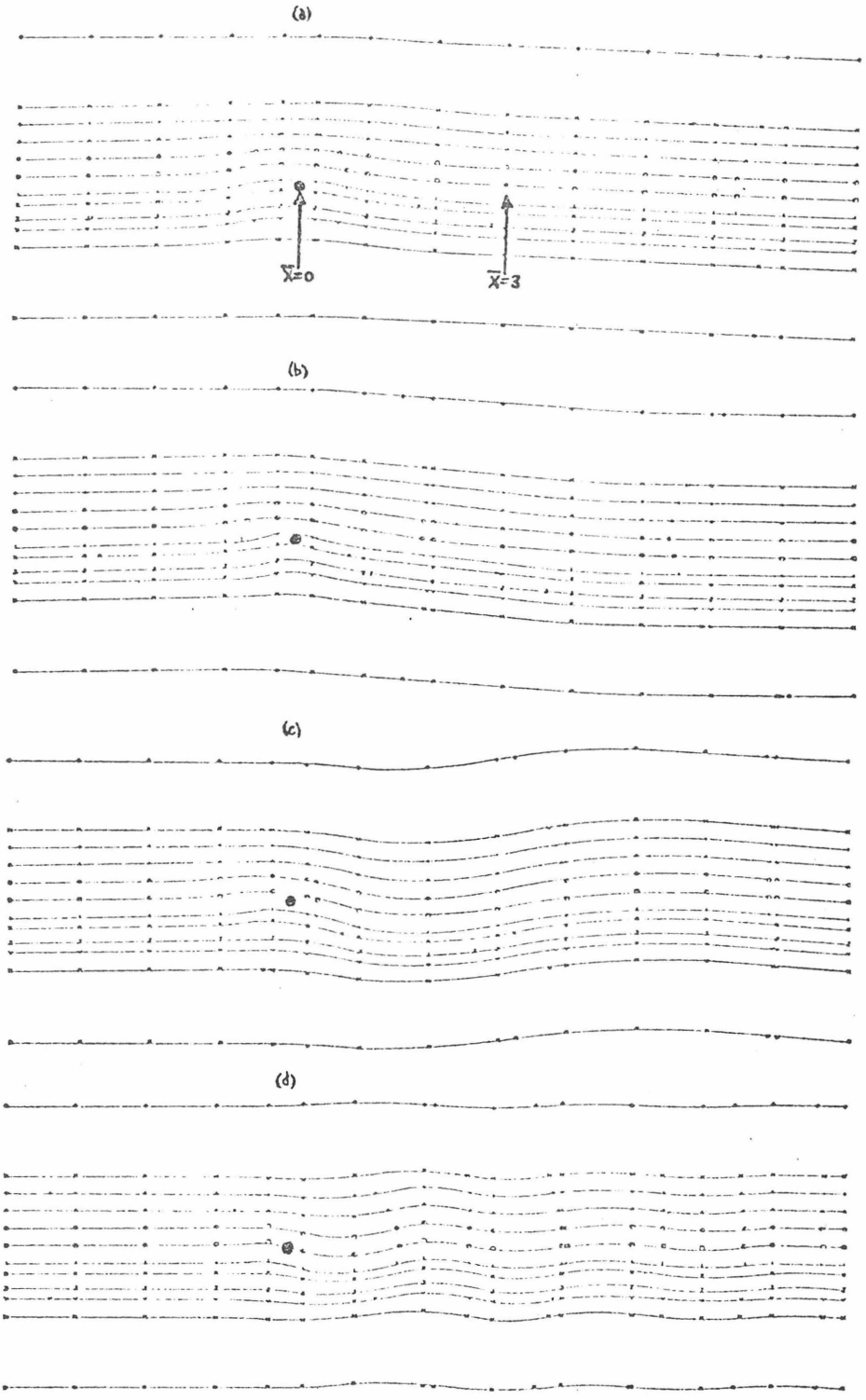

Figure 5

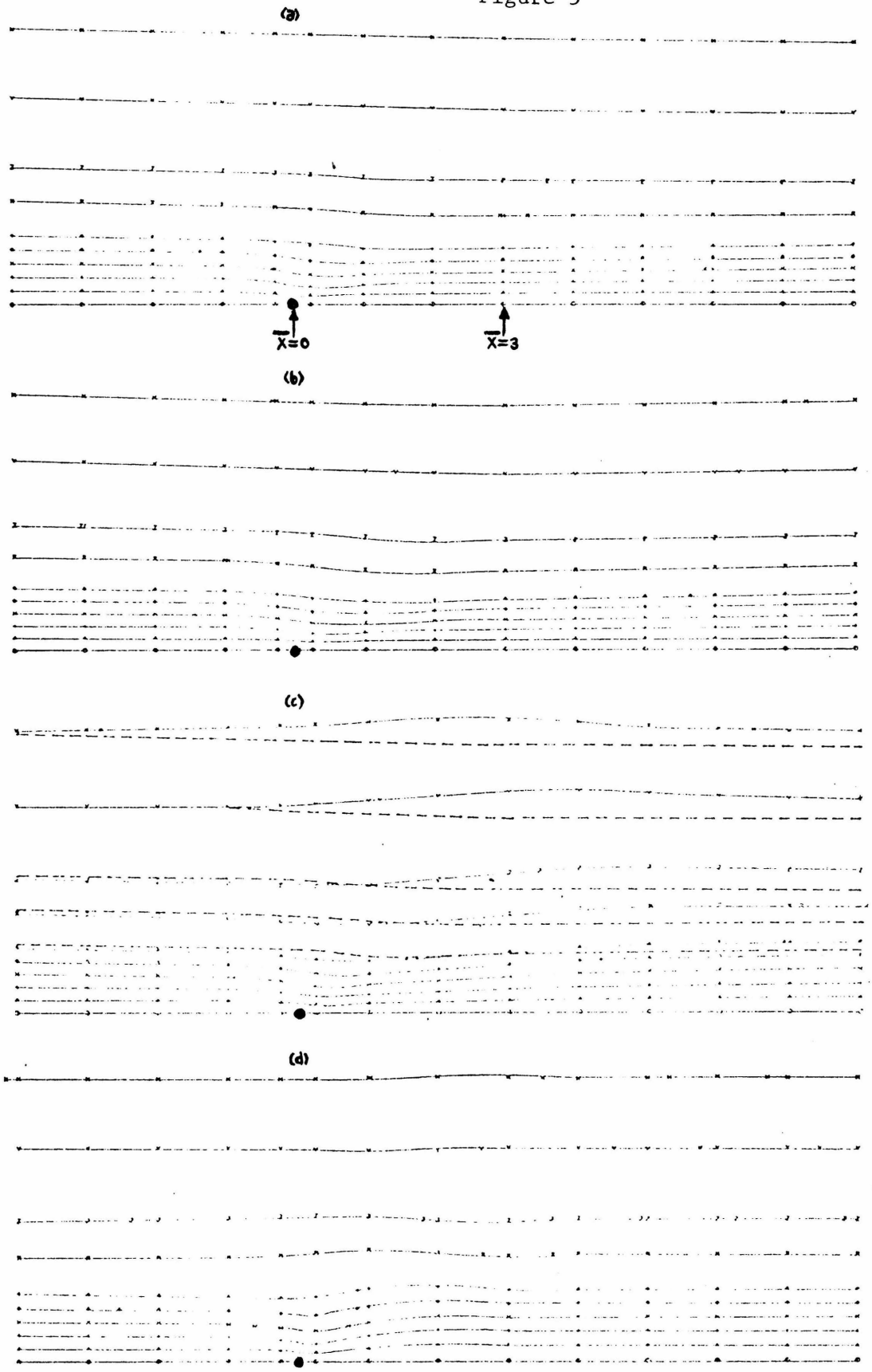

Figure 6

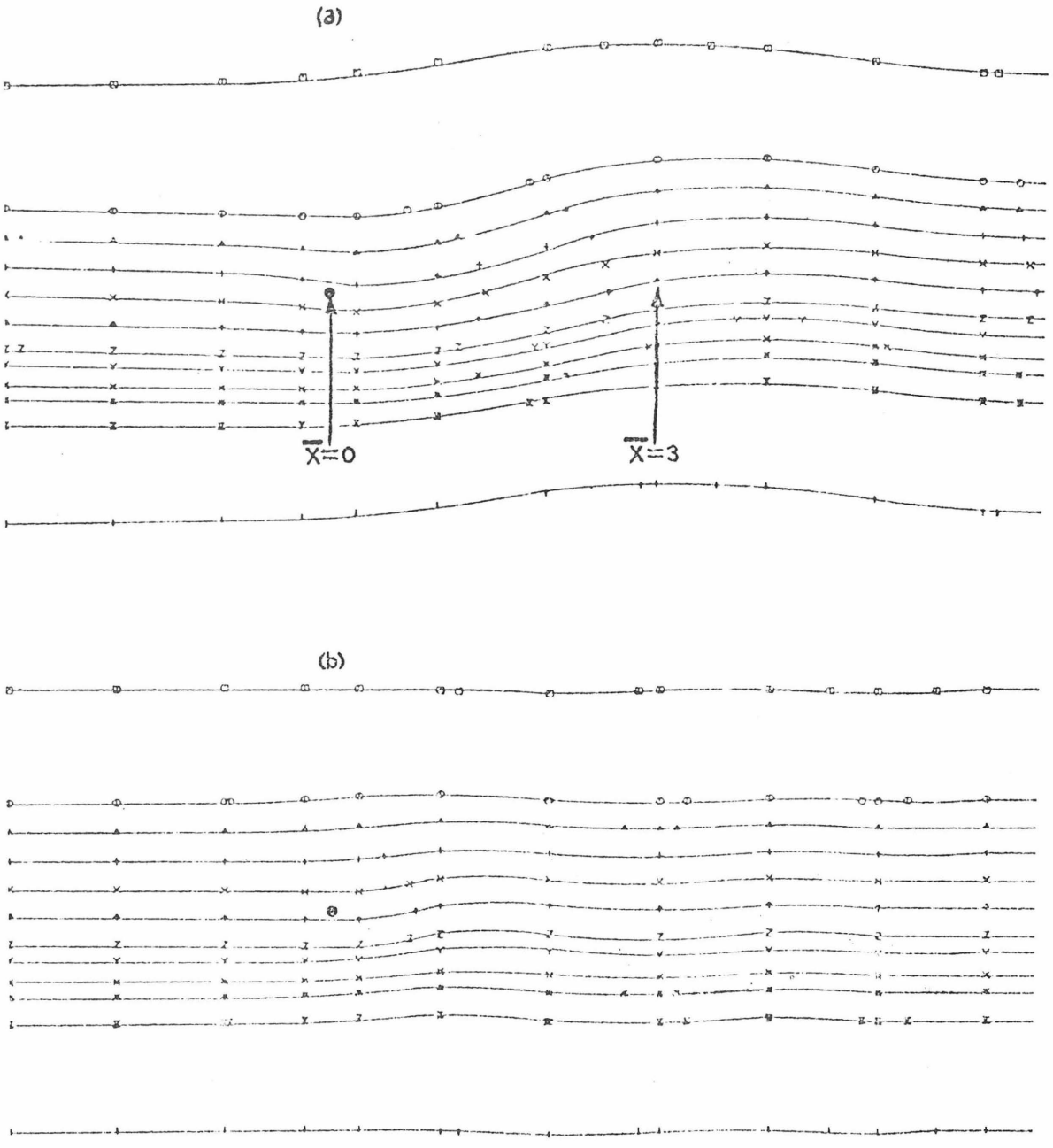

Chapter 3. The Near-Field Solution

This chapter investigates the effects of ambient stratification and locally produced buoyancy contributions on the velocity and temperature fields near a hot or cold horizontal flat plate of finite length. The flat plate is considered to act as a heat dipole; i.e., if the upper surface of the plate is at the uniform temperature $T_\infty + \Delta T$, then the lower surface is at a temperature $T_\infty - \Delta T$, corresponding to a situation in which there is no net heat transfer to the ambient fluid. The chief advantage of this configuration is that it produces a velocity field symmetric about the horizontal plane of the plate (allowing considerable savings of computation time), and exhibits many of the computational difficulties which are inherent in the more complicated heat source geometry. Also, from boundary-layer theory, it can be anticipated that the detailed structure of the velocity and temperature fields in the immediate vicinity of either the upper or lower surface of the plate will be essentially the same for the heat source and heat dipole problems, in spite of the fact that the structure of the downstream wake regions will be markedly different as seen in Chapter 2.

The numerical solution in the near-field of the full nonlinear partial differential equations representing the momentum, mass, and the thermal energy balances is discussed for neutrally-stratified fluids in Appendix 3-A and stably-stratified fluids in Appendix 3-B. Appendix 3-C details the finite-difference equations used in the near-field numerical solutions. Appendix 3-D derives the analytical far-field solutions used as the outer boundary conditions in the numerical solutions of Appendix 3-A for neutrally-stratified fluids. Appendix

3-E gives some near-field solutions for neutrally-stratified flows when the boundary conditions on the horizontal plane of the plate are different than for the heat doublet problem. Appendix 3-F indicates that Redekopp's (1971) stably-stratified fluid, boundary-layer analysis for the diffusive, inertia-viscous balance region reduces exactly to Sparrow and Minkowycz' (1962) neutrally-stratified fluid analysis.

References

Redekopp, L. G. 1971 "The boundary layer on a flat plate moving transversely in a rotating, stratified fluid". J. Fluid Mech. 46, 769.

Sparrow, E. M. and Minkowycz, W. J. 1962 "Buoyancy effects on horizontal boundary-layer flow and heat transfer". Int. J. Heat Mass Transfer 5, 505.

Appendix 3-A: Combined Forced and Free Convection Flow Past a Horizontal Flat Plate for a Neutrally-Stratified Fluid

This appendix consists of an article reprinted from the A.I.Ch.E. J. 19, 998 (1973).

Combined Forced and Free Convection Flow Past a Horizontal Flat Plate

The problem of simultaneous forced and free convection flow of a Newtonian fluid past a hot or cold horizontal flat plate is investigated by means of numerical solutions of the full equations of motion and thermal energy subject only to the Boussinesq approximation. These solutions span the parameter ranges $10 \leq Re \leq 100$, $0.1 \leq Pr \leq 10$, and $-2.215 \leq Gr/Re^{5/2} \leq 2.215$ where Re, Pr, and Gr are based on the ambient free stream fluid properties and the overall plate length l. When $Gr > 0$, the boundary flow near the plate surface is accelerated relative to the corresponding forced convection flow, with a resulting increase in both the local skin friction and heat transfer coefficients. When $Gr < 0$, the boundary flow is decelerated, the local skin friction and heat transfer are decreased, and the flow actually separates for $Gr/Re^{5/2} < -0.8$ when $Pr = 0.7$. In the latter circumstance, an increasing degree of upstream influence is observed as $Gr/Re^{5/2}$ is further decreased.

G. E. ROBERTSON
J. H. SEINFELD
and L. G. LEAL

Department of Chemical Engineering
California Institute of Technology
Pasadena, California 91109

SCOPE

The buoyancy effects induced by a hot or cold body can cause considerable deviations from the basic forced convection flow which would exist when the body and free stream fluid are at the same temperature. In some circumstances, such deviations may be of significance primarily because of the accompanying changes in the overall heat transfer rate; however, in general, one would be interested in a detailed understanding of the changes in flow structure, and a considerable body of literature has grown up in an attempt to achieve this goal. To date, the majority of this work has been concerned with the case in which a significant component of the buoyancy-induced body force is either parallel or antiparallel with the direction of the undisturbed fluid motion [compare the work of Acrivos (1966), Merkin (1969), and others on the combined forced and free convection flow past a vertical flat plate].

In this work, we utilize numerical solutions of the full equations of motion and thermal energy, subject to the Boussinesq approximation, to consider the laminar, two-dimensional flow of a Newtonian fluid past the upper surface of a hot or cold horizontal flat plate. The most significant previous investigations of this problem are the boundary-layer analyses of Sparrow and Minkowycz (1962) and Leal (1973a). In these papers, it is shown that the cross-stream buoyancy-induced body force acts effectively to produce a streamwise pressure gradient in the fluid adjacent to the plate surface: favorable, in the usual

Correspondence concerning this paper should be addressed to L. G. Leal.

boundary-layer sense, when the plate is hot, and adverse when the plate is cold. Hence, the local boundary flow is either accelerated or decelerated relative to the corresponding forced convection flow, and the local skin friction and heat transfer are predicted either to increase or decrease depending upon whether the plate is hot or cold. Although these results are of considerable interest, the corresponding analyses are strictly limited to situations in which the natural convection contribution remains as a small correction to the basic forced convection flow. In particular, although the basic boundary flow is decelerated near the plate surface and hence has the potential to separate, an explicit prediction of this effect is outside the scope of the existing boundary-layer analyses.

The present paper is thus addressed to two main points. First, what is the qualitative nature of the flow produced when the effect of buoyancy is not small; and, second, what is the particular nature of the fluid motion when the plate is sufficiently cold so that the boundary flow actually separates? Additionally, we consider the role of the fluid Prandtl number in determining the flow structure under these circumstances. In this paper, we concentrate particularly on the region in the immediate vicinity of the plate.

CONCLUSIONS AND SIGNIFICANCE

Numerical solutions of the full equations of motion and thermal energy have been obtained subject to the Boussinesq approximation for $10 \leq Re \leq 100$, $0.1 \leq Pr \leq 10$, and $-2.215 \leq Gr/Re^{5/2} \leq 2.215$, where Re is the Reynolds number, Pr the Prandtl number, and Gr the Grashof number based on the ambient, free stream fluid properties and the overall plate length l.

For the intermediate values of Re investigated, the flow structure exhibits the same qualitative features as predicted by existing boundary-layer theories which are valid for $Re \to \infty$ and $|Gr/Re^{5/2}| << 1$. Thus, the gravitationally induced streamwise pressure gradient produces either an acceleration or deceleration of the boundary flow compared with the corresponding forced convection case ($Gr = 0$) depending on whether the plate surface is hot or cold. When $Gr > 0$ and is increased, the local skin friction and heat transfer coefficients increase over the plate surface, and the flow structure remains qualitatively the same even as $|Gr/Re^{5/2}| = 0(1)$. On the other hand, when $Gr/Re^{5/2} < -0.8$ (for $Pr = 0.7$), the buoyancy-induced streamwise pressure gradient actually causes the flow to separate and a recirculating eddy develops adjacent to the plate surface. As Gr is further decreased, the recirculating eddy increases in size; but, more importantly, its leading edge moves forward along the plate surface until, finally, the reverse flow region is found to extend upstream beyond the leading edge of the plate. As Re or Pr is decreased, with $Gr/Re^{5/2}$ fixed, the size of the recirculating eddy is increased, as is the extent of its upstream influence on the flow. Finally, it should be noted that the onset of separation and growth of a large recirculating eddy is accompanied by a rather remarkable decrease in the overall frictional drag on the plate, as well as a smaller decrease in the overall heat transfer coefficient.

The presence of a recirculating flow upstream beyond the leading edge of the plate is, perhaps, the most interesting and significant result of the present work. Careful observation of the temperature, vorticity, and stream-function fields in a time-dependent numerical solution indicates that the mechanism for the progressive (in time) upstream movement of the recirculating eddy lies in the local stable density stratification which is produced as the fluid adjacent to the plate surface is cooled below the ambient, free stream temperature. It is, of course, well known that the presence of a finite two-dimensional body (in this case the recirculating eddy) can produce strong upstream disturbances when the ambient fluid is stably stratified; however, so far as we are aware, the presence of significant upstream influence due to a locally induced stratification has not hitherto been reported in the literature.

PHYSICAL PROBLEM AND BASIC EQUATIONS

We consider the laminar, two-dimensional motion of Newtonian fluid past a hot or cold flat plate of length l. As indicated in Figure 1, the free stream velocity and temperature are denoted by U_∞ and T_∞, the temperature at the upper surface of the plate by $T_\infty + \Delta T$, and the streamwise and normal coordinate directions by x and y. We are primarily concerned in this work with understanding the role of the temperature induced buoyancy forces in contributing to the flow structure in the immediate vicinity of the plate surface. Hence, in order to simplify the analysis, we consider the case in which the plate, as a whole, acts as a heat dipole; that is, we consider the temperature of the underside of the plate to be $T_\infty - \Delta T$, corresponding to a situation in which there is no net heat transfer to the ambient fluid. The advantage of this choice is that the velocity field produced is thereby symmetric about the plane $y = 0$. The alternate source problem, in which the underside temperature is $T_\infty + \Delta T$ is also of interest; however, it can be anticipated from boundary-layer theory that the detailed structure of the velocity and temperature fields in the immediate vicinity of either the upper or lower surface of the plate will be essentially the same for the source and dipole problems in spite of the

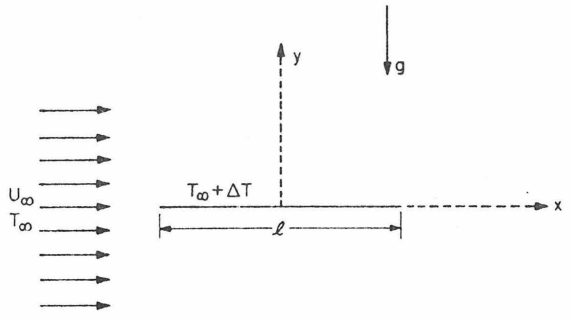

Fig. 1. The physical system.

fact that the structure of the downstream wake regions will be markedly different (a point which we shall consider in detail in a later communication).

Nondimensionalizing the basic conservation balances for momentum, mass, and thermal energy using the ambient (free stream) fluid properties, the free-stream velocity U_∞ and the plate length l, and invoking the usual Boussinesq approximation (Boussinesq, 1903; Spiegel and Veronis, 1960), we obtain the basic governing differential equations

$$\frac{\partial u}{\partial t} + u\frac{\partial u}{\partial x} + v\frac{\partial u}{\partial y} = -\frac{\partial p}{\partial x} + \frac{1}{Re}\left(\frac{\partial^2 u}{\partial x^2} + \frac{\partial^2 u}{\partial y^2}\right) \tag{1a}$$

$$\frac{\partial v}{\partial t} + u\frac{\partial v}{\partial x} + v\frac{\partial v}{\partial y} = -\frac{\partial p}{\partial y} + \frac{1}{Re}\left(\frac{\partial^2 v}{\partial x^2} + \frac{\partial^2 v}{\partial y^2}\right) + \frac{Gr}{Re^2}\theta \tag{1b}$$

$$\frac{\partial u}{\partial x} + \frac{\partial v}{\partial y} = 0 \tag{2}$$

$$\frac{\partial \theta}{\partial t} + u\frac{\partial \theta}{\partial x} + v\frac{\partial \theta}{\partial y} = \frac{1}{PrRe}\left(\frac{\partial^2 \theta}{\partial x^2} + \frac{\partial^2 \theta}{\partial y^2}\right) \tag{3}$$

in which

$$Re = \frac{\rho_\infty U_\infty l}{\mu_\infty}, \quad Pr = \frac{C_{p\infty}\mu_\infty}{k_\infty}, \quad \text{and} \quad Gr = \frac{l^3\beta g \Delta T \rho_\infty^2}{\mu_\infty^2}$$

where θ is defined as $(T - T_\infty)/\Delta T$, β is the coefficient of thermal expansion, and the subscript ∞ represents the free stream value.

With the present definition, it may be noted that $Gr > 0$ corresponds to the case in which the upper plate surface is hot relative to the ambient fluid, whereas $Gr < 0$ corresponds to the case in which it is cold. Clearly, the relevant buoyancy parameter is Gr/Re^2 according to (1). Leal (1973a) and Sparrow and Minkowycz (1962) both show that the equivalent parameter in the boundary-layer version of (1) to (3) is $Gr/Re^{5/2}$, a result which we shall utilize at a later point.

In view of the symmetry of the dipole problem, these equations need only be solved in the upper half plane. The appropriate boundary conditions are simply

$$\frac{\partial u}{\partial y} = v = \theta = 0 \quad ; \quad |x| > \frac{1}{2}, \; y = 0 \tag{4a}$$

$$u = v = 0, \; \theta = 1 \quad ; \quad |x| \leq \frac{1}{2}, \; y = 0 \tag{4b}$$

$$u \to 1, \; v \to 0, \; \theta \to 0; \quad r = (x^2 + y^2)^{1/2} \to \infty \tag{4c}$$

For purposes of obtaining a numerical solution to this problem, it is convenient to rewrite Equations (1) to (4) in terms of the streamfunction ψ and vorticity ω, defined by

$$u = \frac{\partial \psi}{\partial y}, \quad v = -\frac{\partial \psi}{\partial x}, \quad \omega = \frac{\partial v}{\partial x} - \frac{\partial u}{\partial y}$$

and to transform the resulting equations to an elliptical cylindrical coordinate system (ξ, η) in which

$$x = \frac{1}{2}\cosh\xi\cos\eta, \quad y = \frac{1}{2}\sinh\xi\sin\eta \tag{5}$$

hence yielding the governing equations

$$\frac{1}{4}M^2(\xi,\eta)\frac{\partial \omega}{\partial t} + J(\omega,\psi) = \frac{1}{Re}\left(\frac{\partial^2 \omega}{\partial \xi^2} + \frac{\partial^2 \omega}{\partial \eta^2}\right) + \frac{Gr}{2Re^2}\left(\sinh\xi\cos\eta\frac{\partial \theta}{\partial \xi} - \cosh\xi\sin\eta\frac{\partial \theta}{\partial \eta}\right) \tag{6}$$

$$\frac{\partial^2 \psi}{\partial \xi^2} + \frac{\partial^2 \psi}{\partial \eta^2} + \frac{1}{4}M^2(\xi,\eta)\,\omega = 0 \tag{7}$$

$$\frac{1}{4}M^2(\xi,\eta)\frac{\partial \theta}{\partial t} + J(\theta,\psi) = \frac{1}{PrRe}\left(\frac{\partial^2 \theta}{\partial \xi^2} + \frac{\partial^2 \theta}{\partial \eta^2}\right) \tag{8}$$

where $M^2(\xi,\eta) = \frac{1}{2}(\cosh 2\xi - \cos 2\eta)$ and the nonlinear, two-dimensional Jacobian is given by

$$J(\alpha,\gamma) = \frac{\partial \alpha}{\partial \xi}\frac{\partial \gamma}{\partial \eta} - \frac{\partial \alpha}{\partial \eta}\frac{\partial \gamma}{\partial \xi}$$

The advantage of elliptical cylindrical coordinates is that the region near the plate is effectively magnified, particularly the singular regions near the ends of the plate which are effectively resolved by a corresponding coordinate singularity (Leal and Acrivos, 1969). In this coordinate system the plate is located at $\xi = 0$, and the remaining portions of the x-axis ($|x| > \frac{1}{2}$, $y = 0$) are given by $\eta = 0$ ($x > \frac{1}{2}$) and $\eta = \pi$ ($x < -\frac{1}{2}$), respectively. Hence, the boundary conditions (4) can be expressed as

$$\psi = \omega = \theta = 0; \quad \eta = 0 \text{ and } \pi, \quad \text{all } \xi > 0 \tag{9a}$$

$$\frac{\partial \psi}{\partial \xi} = \psi = 0; \quad \theta = 1; \quad \xi = 0, \quad 0 \leq \eta \leq \pi \tag{9b}$$

and

$$\psi \to \frac{1}{2}\sinh\xi\sin\eta, \quad \omega \to 0, \quad \theta \to 0; \quad \xi \to \infty, \quad 0 \leq \eta \leq \pi \tag{9c}$$

We shall be concerned, in this paper, with the numerical solution of the problem represented by Equations (6) to (9).

NUMERICAL SOLUTION SCHEME

The basic numerical solution scheme utilized in this work was based on the explicit, Gauss-Seidel pointwise iteration applied to the appropriate finite-difference form of the Equations (6) to (9), with $\partial\theta/\partial t$ and $\partial\omega/\partial t$ set equal to zero. This steady state iterative algorithm (which is similar to that of Leal and Acrivos, 1969) converges more rapidly to the final steady state than most standard time-dependent schemes and hence was used to obtain all of the steady state solutions which comprise the major portion of the present investigation. The finite-difference approximations of (6) to (8) were obtained using the simple two-point central difference formula for spatial first derivatives and the familiar five-point approximation for the Laplacian operator. Hence they are accurate to $0(h^2)$, where h is the computational mesh size in the (ξ, η) plane. The more stable Arakawa (1966) eight-point approximation for the nonlinear Jacobians was also utilized in several cases with no discernable change in results. The influence of computational mesh size on the solution was carefully documented in every instance, and the final values used are listed in Table 1. Finally, it should be noted that two minor modifications of the straightforward iterative scheme were made to enhance numerical stability. First, relaxation parameters a_ψ, a_ω, and a_θ, chosen by numerical experimentation, were introduced such that the values of ψ, ω, and θ retained at each mesh point for use in subsequent calculations were a weighted average of the value from the previous iteration and the newly computed

TABLE 1. NUMERICAL PARAMETERS

Re	Gr/Re^2	Pr	h	x_∞	a_ψ	a_ω	a_θ
10	+7	0.7	$\pi/30$	5.8(11.6)	1.1	0.4	0.4
10	+5	0.7	$\pi/30$	5.8	1.1	0.4	0.4
10	0	0.7	$\pi/30$	5.8(11.6)	1.1	0.4	0.4
10	−5	0.7	$\pi/30$	11.6(17.4)	1.0	0.2	0.2
10	−7	0.7	$\pi/30$	11.6(17.4)	1.0	0.2	0.2
40	+8	10.0	$\pi/50$	3.08	0.7	0.05	0.05
40	+8	0.7	$\pi/50$	3.08	1.1	0.4	0.4
40	+5	0.7	$\pi/50$	3.08	1.1	0.4	0.4
40	0	10.0	$\pi/50$	3.08(1.54)	1.1	0.4	0.05
40	0	0.7	$\pi/50$	3.08(6.16)	1.1	0.4	0.4
40	−5	0.7	$\pi/50$	6.16(3.08)	1.0	0.2	0.2
40	−7	0.7	$\pi/50$	9.24(6.16)	0.9	0.1	0.1
40	−8	0.7	$\pi/50$	9.24(12.32)	0.9	0.1	0.1
40	−11	10.0	$\pi/50$	3.08	0.7	0.05	0.05
40	−11	0.7	$\pi/50$	9.24(12.32)	0.9	0.1	0.1
40	−14	0.7	$\pi/50$	9.24(12.32)	0.9	0.1	0.1
100	+14	0.7	$\pi/60$	2.5	1.1	0.4	0.4
100	0	10.0	$\pi/60$	2.5	1.1	0.4	0.025
100	0	0.7	$\pi/60$	2.5	1.1	0.4	0.4
100	0	0.1	$\pi/60$	7.5	1.1	0.4	1.5
100	−11	0.7	$\pi/60$	5.0(7.5)	1.0	0.2	0.2
100	−14	0.7	$\pi/60$	5.0(7.5)	1.0	0.2	0.2
100	−22.15	0.7	$\pi/60$	5.0(7.5)	0.7	0.025	0.025

value; for example,

$$\omega_{\text{retained}} = \omega_{\text{old}} + a_\omega(\omega_{\text{new}} - \omega_{\text{old}}) .$$

The values of a_ψ, a_θ, and a_ω utilized in each case are listed in Table 1. Secondly, the calculations were actually performed in terms of $\hat{\psi}$ rather than ψ, where $\hat{\psi} = \psi - \frac{1}{2}\sinh\xi\sin\eta$.

In applying the boundary conditions (9b), the no-slip condition at the plate surface, $\partial\psi/\partial\xi|_{\xi=0} = 0$ was replaced by an equivalent condition relating the surface vorticity ω_0 to the values of the streamfunction on adjacent rows (Leal and Acrivos, 1969). Utilizing a Taylor series expansion, the value of the streamfunction ψ_1 at $\xi = h$ can be expressed in terms of ψ and its derivatives at the plate surface as

$$\psi_1 = \psi|_{\xi=0} + h\left.\frac{\partial\psi}{\partial\xi}\right|_{\xi=0} + \frac{h^2}{2!}\left.\frac{\partial^2\psi}{\partial\xi^2}\right|_{\xi=0} + 0(h^3) \tag{10}$$

Utilizing Equation (7) and the boundary conditions (9b), and truncating series (10) after the term of $0(h^2)$, we obtain

$$\omega_0 = -\frac{8\psi_1}{h^2M^2(0,\eta)} + 0(h) \tag{11}$$

Similarly, by including the term of $0(h^3)$, a more accurate condition can be derived in terms of ψ_1 and ψ_2 $(\psi|_{\xi=2h})$,

$$\omega_0 = \frac{2(\psi_2 - 8\psi_1)}{h^2M^2(0,\eta)} + 0(h^2) \tag{12}$$

However, for the fluid motion problem alone [that is, Equations (6) and (7) with $Gr = 0$ and appropriate boundary conditions], the expression (12) is less stable than (11) in the numerical scheme (compare Thom and Apelt, 1956; Janssen, 1957; Leal and Acrivos, 1969). Therefore, relation (11) was employed for the majority of each calculation with the more accurate formula (12) being used only as a check on the solution once convergence was achieved.

The most troublesome feature of the present calculations, at least compared with the corresponding forced convection problem, is the approximation of the boundary conditions (9c), since the region covered by the finite difference mesh system must obviously be restricted to finite values of r. The simplest and most common approach, which has been widely utilized in studies of fluid mechanics alone (for example, Rimon, 1969; Son and Hanratty, 1969; Dennis and Chang, 1970; Masliyah and Epstein, 1970; Leal, 1973b), is simply to use the uniform stream conditions (9c) applied at a large but finite value of r (or equivalently, of ξ). Numerical experimentation showed this method to be computationally feasible in the present case also, provided $Gr \geq 0$. Unfortunately, however, for $Gr < 0$ this simple approach was found to be entirely unsatisfactory. In this case, as the fluid passes above the plate, it is cooled and thus becomes stably stratified. As a result the fluid in the wake region downstream is also stably stratified and hence exhibits the phenomenon common to such flows of very strong upstream propagation of disturbances (see Long, 1953, 1955, 1972; Janowitz, 1968). For this reason, the solution close to the plate becomes much more sensitive to errors in the downstream boundary conditions than for the corresponding flow with $Gr > 0$. Thus, the uniform stream conditions are not adequate for numerical solution at least in the sense that the values of ξ_∞ required to ensure an accurate solution near the plate are too large to be economically feasible. After considerable trial and error, two alternative approaches were found to produce satisfactory results. The first involves the use of a far-field correction to the simple free stream condition, which is the first term of an infinite series expansion that converges asymptotically for $\xi >> 1$. Imai (1951) and Chang (1961) have discussed this far-field correction in some detail for the fluid mechanics problem alone ($Gr = 0$), and we have utilized the formalism of Chang to obtain a similar correction in the present case in which the buoyancy contribution plays an important role. The details of this calculation will be reported in a future communication. For the present purposes it is enough simply to quote the results

$$\left.\begin{aligned} &\theta \sim A\dot{y}x^{-3/2}\exp(-PrRey^2/4x) + o(r^{-1/2}); \quad x > 0 \\ &\theta = 0; \quad x < 0 \end{aligned}\right\} \tag{14}$$

$$\left.\begin{aligned} &\psi \sim y + \frac{m}{2\pi}\tan^{-1}\left(\frac{y}{x}\right) \\ &\quad + \sqrt{\frac{\pi}{PrRe}}\left\{\left[g(0) - \frac{K_1}{1-Pr}\right]\sqrt{Pr}\ \mathrm{erf}\left(\frac{\sqrt{Re}}{2}\frac{y}{\sqrt{x}}\right) + \frac{K_1}{1-Pr}\mathrm{erf}\left(\frac{\sqrt{PrRe}}{2}\frac{y}{\sqrt{x}}\right)\right\} + o(1); \quad x > 0 \\ &\psi \sim y + \frac{m}{2}\left[-1 + \frac{1}{\pi}\tan^{-1}\frac{y}{x}\right]; \quad x < 0 \end{aligned}\right\} \tag{15}$$

$$\left.\begin{aligned} &\omega \sim \frac{Re}{2}\frac{y}{x^{3/2}}\left\{\left[g(0) - \frac{K_1}{1-Pr}\right]\exp\left(-\frac{Re}{4}\frac{y^2}{x}\right) + \frac{PrK_1}{1-Pr}\exp\left(-\frac{PrRe}{4}\frac{y^2}{x}\right)\right\} + o(r^{-1/2}); \quad x > 0 \\ &\omega = 0; \quad x < 0 \end{aligned}\right\} \tag{16}$$

in which

$$A \equiv \frac{x_0^{1/2}}{2}\left(Nu - \int_{-x_0}^{-1/2} \left.\frac{\partial\theta}{\partial y}\right|_{y=0} dx - \int_{1/2}^{x_0} \left.\frac{\partial\theta}{\partial y}\right|_{y=0} dx \right)$$

$$K_1 \equiv A\,\frac{Gr}{Re^2}\cdot\frac{2}{PrRe}$$

$$g(0) \equiv -\frac{C_d}{2}\sqrt{\frac{Re}{\pi}} + K_1\left(\frac{1-\sqrt{Pr}}{1-Pr}\right)$$

$$m \equiv -\frac{2\sqrt{\pi}}{\sqrt{PrRe}}\left[\sqrt{Pr}\,g(0) + K_1\left(\frac{1-\sqrt{Pr}}{1-Pr}\right)\right]$$

In the latter expressions, Nu is the overall Nusselt number based on the total heat transfer at the upper surface of the plate,

$$Nu \equiv -\int_0^{\pi} \left.\frac{\partial\theta}{\partial\xi}\right|_{\xi=0} d\eta \qquad (17)$$

and C_d is the corresponding drag coefficient

$$C_d \equiv -\frac{1}{Re}\int_0^{\pi} \omega_0 \sin\eta\, d\eta \qquad (18)$$

Finally, in evaluating the expressions (14) to (16) at a particular point (x, y), the value x_0 is utilized to denote the x-intercept of the circular arc $r = (x^2 + y^2)^{1/2} =$ constant. It should be noted that the parameter A vanishes as $x_0 \to \infty$. In view of the definitions (17) and (18) it may be seen that the parameters A and $g(0)$ provide a direct coupling between the far-field solutions (14) to (16) and the numerical solution near the plate. The key idea in utilizing the far-field corrections at a large but finite value of r instead of the simple free stream conditions at the same position is to minimize the difference between the imposed values of ψ, ω, and θ, and the values which would exist at the same position if one had an exact solution. Using (14) to (18), the choice of ξ_∞ required for an accurate solution near the plate was reduced to an economically feasible value in all cases. The values used are listed in Table 1 ($x_\infty = \frac{1}{2}\cosh\xi_\infty$). We estimate these as the minimum value necessary to produce accurate solutions in the vicinity of the plate. In most cases, these values were actually confirmed by comparison with a similar solution obtained using the somewhat larger (or smaller) values listed in parentheses under x_∞ in Table 1. For $Gr = 0$, the values of x_∞ chosen correspond to those independently determined by Leal and Acrivos (1969) for a similar fluid mechanics problem. In addition, we note that the values listed in Table 1 are essentially equivalent to those utilized by Takami and Keller (1969) for flow past a circular cylinder with a similar wake correction when account is taken of the overall length of the cylinder plus the attached closed-streamline wake. It is noteworthy that the required distance decreases as Re increases, all else being fixed, while generally increasing as Gr is decreased to negative values or as Pr is decreased.

As an alternative to the far-field correction, the recently developed Milne's extrapolation procedure was also utilized to produce boundary values at ξ_∞ from the internal solution itself. Denoting the value of θ at $\xi = \xi_\infty - mh$ as θ_{N-m}, Milne's procedure for extrapolation outward in ξ along a line of constant η is defined by

$$\theta_N = \theta_{N-5} - 5\theta_{N-4} + 10\theta_{N-3} - 10\theta_{N-2} + 5\theta_{N-1} + 0(h^5) \qquad (19)$$

Similar expressions can be written for the streamfunction and vorticity. This formula, which was first derived by Lin and Apelt (1970), is based on the familiar Milne's predictor formula used to integrate ordinary differential equations (Lapidus and Seinfeld, 1971). The chief advantage of (19) compared with extrapolation schemes which have been previously proposed for estimating ψ, ω, and θ at the outermost boundary (compare Thoman and Szewczyk, 1969; Estoque, 1962; Yamada and Meroney, 1971), is that no explicit (and unjustified) assumption need be made of the functional dependence of these variables on ξ other than simple differentiability. The chief disadvantage of the extrapolation formulation compared with the scheme involving (14) to (18) is that the numerical algorithm is less stable, and distortions in the fields are produced if the initial fields are too inaccurate (Lin and Apelt 1970; Yamada and Meroney, 1971). On the other hand, the advantage of the extrapolation scheme is that the solution near the outer boundary is not directly coupled with that near the plate. In view of the unusually strong interaction already inherent in the stably stratified wake flow when the plate is cold, one may logically ask whether, in using (14) to (18), an incorrect value for C_d or Nu leading to an inaccurate boundary-value for $\xi = \xi_\infty$ at some intermediate point in the calculation might not lead to further inaccuracies in C_d or Nu and hence to some convergent but inaccurate solution in the vicinity of the plate. In order to ensure that this possibility did not actually occur, the calculations for the cold plate were first carried to near-convergence utilizing the stable far-field approximations, and then run to completion using both the far-field solutions and the extrapolation scheme independently. In general, the solutions so obtained were virtually identical. However, as Gr was made increasingly negative some small (2 to 3%) differences were noted in the vorticity distribution near the plate and, hence, by (18), in the drag coefficients as well. In these instances, the results reported here are based on the solution obtained using the extrapolation procedure since these appeared to introduce somewhat smaller disturbances in the flow near ξ_∞.

Finally, it should be mentioned that convergence was achieved via an oscillatory mode similar to that described previously by Leal and Acrivos (1969) and Leal (1973b). Thus, for example, C_d was observed to oscillate with a monotonically decreasing amplitude about a fixed mean and a characteristic period of 0(100) iterations. Such oscillatory convergence is very appealing as upper and lower bounds on the various dependent variables are available throughout the calculation. The solution was generally assumed to have converged when these bounds were within 0.05% of the average value for C_d and Nu. However, the detailed fields for ψ, θ, and ω were also examined carefully to ensure that the solutions were uniformly convergent throughout the (x, y) plane.

COMPARISON WITH PREVIOUS SOLUTIONS

A variety of detailed tests were performed to ensure the accuracy of the solutions reported here. Considering first of all the case of forced convection $Gr = 0$ in which the fluid mechanics is uncoupled from the heat transfer problem, we may compare our results for $Re = 10$, 40, and 100 directly with those obtained by Dennis and Dunwoody (1966) who studied the fluid mechanics problem alone.

The values of C_d shown in Figure 2 for these cases are virtually identical with those of Dennis and Dunwoody. Furthermore, the variation of the local skin friction coefficient $-\omega_0$, as a function of position along the plate agrees closely with that reported by these authors.

There are no prior results of which we are aware for forced convection heat transfer with $\theta = 0$ on $y = 0$, $|x| > \frac{1}{2}$. However, Dennis and Smith (1966) have considered the case in which $\partial\theta/\partial y = 0$ on $y = 0$, $|x| > \frac{1}{2}$. Hence, we also solved this problem in order to provide a test for the accuracy of our numerical algorithm. Again, the values of Nu, which are reported in Table 2, and the variation of the local heat transfer coefficient, $-2\ \partial\theta/\partial\xi|_{\xi=0}/\sin\eta$, with position along the plate surface, agree very well with the results of Dennis and Smith. The numerical results for the case in which $\theta = 0$ on $y = 0$ and $Gr = 0$ are also qualitatively similar to those of Dennis and Smith. However, as expected on physical grounds, the actual numerical values for the local heat transfer coefficient are somewhat larger, particularly near the ends of the plate.

A further test on the accuracy of our numerical scheme is provided by examining the Reynolds number dependence of δ_θ, the dimensionless vertical distance between the plate surface at $x = 0$ and the isotherm $\theta = 0.1$. δ_θ is a measure of the thickness of the thermal layer and is given in Table 3 for $Pr = 0.7$ and $Gr = 0$. It may be seen that δ_θ is roughly proportional to $Re^{-\frac{1}{2}}$, which is the theoretically predicted boundary-layer behavior (though, of course, quantitative agreement with boundary-layer theory is not obtained or expected for $Re \leq 100$).

Finally, as indicated previously, we have obtained a limited number of solutions for $Pr = 10$ and 0.1 in order to evaluate the effect of this parameter on the overall flow structure. In Figure 3, we have plotted the numerical results for $Gr = 0$ and $Re = 100$ together with the classical boundary-layer estimates for $Pr << 1$, $Pr = 1$, and $Pr >> 1$. These provide further evidence for the validity of the numerical scheme in the sense that the solutions for $Pr = 0.7$ and $Pr = 10$ appear to be consistent with the expected asymptotic trends. The result for $Pr = 0.1$ is also qualitatively correct but appears to somewhat overestimate the actual value. The most likely explanation for this behavior is that the outer boundary (ξ_∞) is not sufficiently far away from the plate. This is suggested by the fact that the solution still changed somewhat as x_∞ was increased from twice to three times its value at $Pr = 0.7$. Unfortunately, the excessive computation times involved for such large values of ξ_∞ (at this Reynolds number and Prandtl number) preclude any attempt to consider larger values of ξ_∞ directly. We shall return to discuss these results in more detail in the next section of this paper.

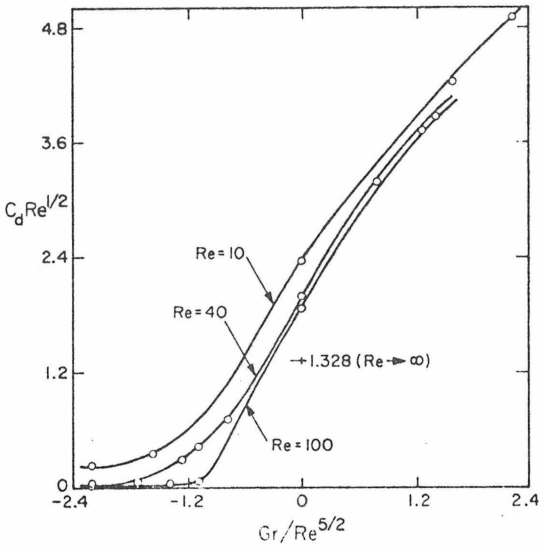

Fig. 2. $C_dRe^{1/2}$ as a function of the boundary-layer parameter, $Gr/Re^{5/2}$, for $Pr = 0.7$.

Table 2. Nu for $Gr = 0$, $Pr = 0.7$, and $\partial\theta/\partial y = 0$ on $y = 0$, $|x| > 1/2$

Investigators	$Re = 10$	$Re = 40$	$Re = 100$
Dennis and Smith	2.43	4.37	6.75
Present	2.43	4.32	6.74

Table 3. δ_θ for $Gr = 0$, $Pr = 0.7$

Re	10	40	100
δ_θ	0.86	0.41	0.26

Table 4. $C_dRe^{1/2}$ and $NuRe^{-1/2}$ for $Pr = 10.0$ and $Re = 40$

$Gr/Re^{5/2}$	−1.74	0	1.265
$C_dRe^{1/2}$	1.56	2.00	2.22
$NuRe^{-1/2}$	1.85	1.94	1.98

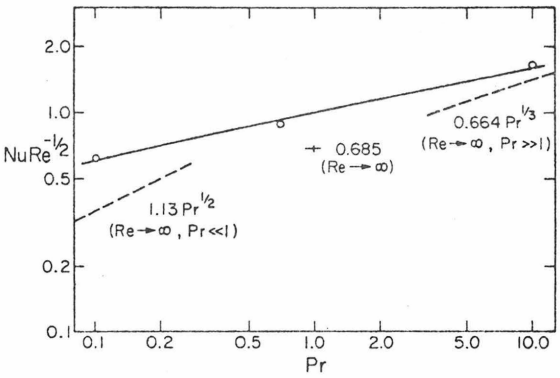

Fig. 3. $NuRe^{-1/2}$ as a function of Pr for $Gr = 0$: comparison of the numerical results for $Re = 100$ and the boundary-layer estimates for $Pr << 1$, $Pr = 1$, and $Pr >> 1$.

RESULTS AND DISCUSSION

We previously mentioned the expected boundary-layer flow structure for large Re, and $|Gr/Re^{5/2}|$* suitably small. In particular, we have noted that the cross-stream buoyancy force acts effectively to produce a streamwise pressure gradient at the upper plate surface which is favorable in the usual boundary-layer sense when the plate is hot and adverse when it is cold. Hence, the local boundary-layer flow is either accelerated or decelerated relative to the corresponding forced convection flow, with a concurrent increase or decrease in the local skin friction and heat transfer rates, depending upon whether the plate is hot or cold.

* Note that whereas the original Equation (1) depends on the parameters Re, Pr, and Gr/Re^2, the corresponding laminar boundary-layer equations for $Pr = O(1)$ contain only Pr and $Gr/Re^{5/2}$ as explicit parameters.

The main thrust of the present work has been to determine the effect of buoyancy on the flow structure and temperature distribution under circumstances in which $Gr/Re^{5/2}$ (and hence the natural convection contribution to the flow) is not necessarily small. In the first part of this section, we consider the effect of variable Re and Gr/Re^2 at a fixed value of $Pr = 0.7$. In the second, we briefly examine the change in flow structure as Pr is increased to 10 and decreased to 0.1 with $Re = 40$ and 100, and values of Gr/Re^2 equal to 8, 0, and -11. Finally, in the last part of this section we consider, in some detail, the structure of the recirculating eddy which results from flow separation at sufficiently negative values of Gr/Re^2.

Effects of Gr and Re on Flow Structure; Fixed $Pr = 0.7$

In order to achieve a relatively complete description of the dependence of the flow structure and temperature distribution on Re and Gr/Re^2 we have obtained steady state numerical solutions for $Re = 10$, 40, and 100 and a variety of positive and negative values of Gr/Re^2 as listed in Table 1. Typical streamline, vorticity and temperature plots are shown in Figures 4, 5, and 6, respectively, for $Re = 40$, $Pr = 0.7$ and $Gr/Re^2 = 8$, 0, -5 and -14. The flow is from left to right. Three features are worthy of special note. First, as expected from the boundary layer analyses (Sparrow and Minkowyz, 1962; Leal, 1973a), the gravitationally induced streamwise pressure gradient produces either an acceleration or deceleration of the flow near the plate with an accompanying narrowing or thickening of the boundary-layer region depending upon whether Gr is positive or negative (that is, the plate surface is hot or cold). When the surface temperature is sufficiently low (Gr sufficiently negative), the boundary flow actually separates and a recirculating eddy develops adjacent to the plate surface. Second, and perhaps the most interesting result from the numerical solutions, is the fact that this recirculating region can actually extend considerably upstream beyond the leading edge of the plate. Such a degree of upstream influence of the flat plate upon the basic flow structure seems to be an unex-

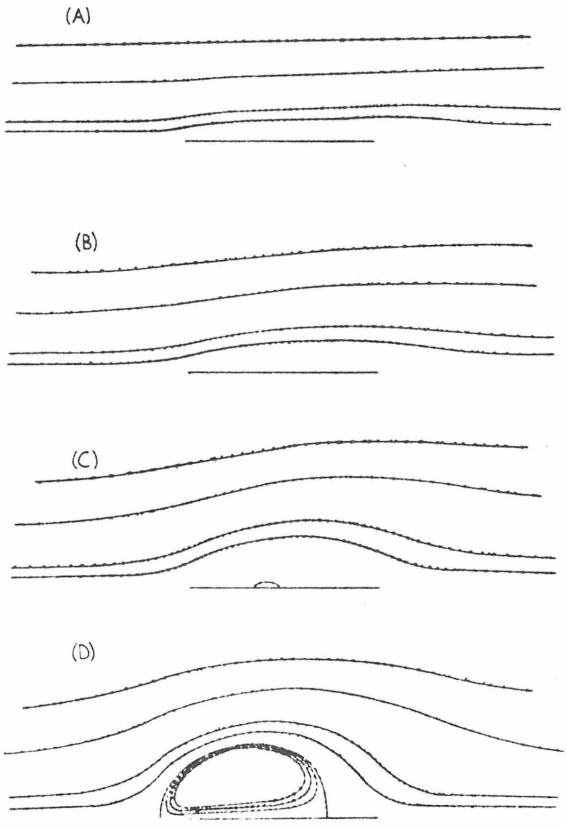

Fig. 4. Streamlines for $Re = 40$ and $Pr = 0.7$; $\psi = 0.5$, 0.3, 0.1, 0.05, 0, -0.005, -0.01, and -0.015 with 0.5 corresponding to the outermost streamline: (A) $Gr/Re^2 = 8$; (B) $Gr/Re^2 = 0$; (C) $Gr/Re^2 = -5$; (D) $Gr/Re^2 = -14$.

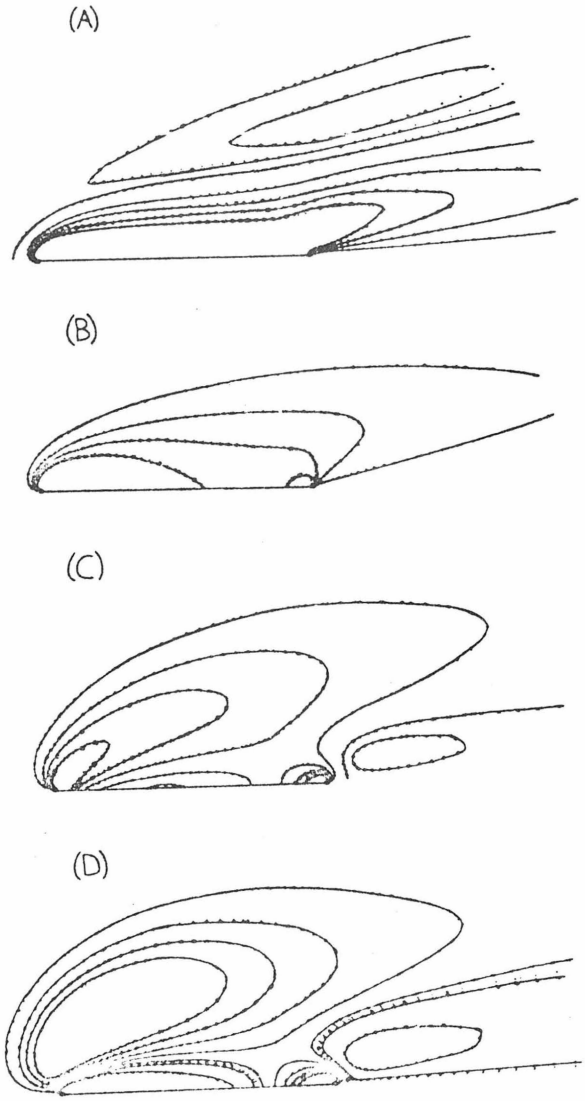

Fig. 5. Equivorticity lines for $Re = 40$ and $Pr = 0.7$: (A) $Gr/Re^2 = 8$; $\omega = -4$, -3, -2, -1, 0, 0.3, and 0.5 with -4 corresponding to the innermost curve; (B) $Gr/Re^2 = 0$; $\omega = -4$, -3, -2, and -1 with -1 corresponding to the outermost curve; (C) $Gr/Re^2 = -5$; $\omega = -4$, -3, -2, and -1 over the front and rear of the plate; $\omega = 0$ and 0.3 in the reverse flow region and downstream from the plate; (D) $Gr/Re^2 = -14$; $\omega = -4$, -3, -2, and -1 over the front and rear of the plate; $\omega = 0$, 0.5, and 2.0 in the reverse flow region and downstream from the plate.

pected and highly significant feature of the present problem, which we shall discuss in more detail at the end of this section. Thirdly, we note the existence, for $Gr \neq 0$, of closed equivorticity curves in the plots of Figure 5, indicating the presence of internal (nonboundary) sources for vorticity in these cases. The origin of these sources is the temperature induced density variations in the fluid, as can be easily seen from the vorticity transport equation for two-dimensional flow, namely,

$$\frac{\partial \omega}{\partial t} + u\frac{\partial \omega}{\partial x} + v\frac{\partial \omega}{\partial y} = \frac{1}{Re}\nabla^2\omega + \frac{Gr}{Re^2}\frac{\partial \theta}{\partial x}$$

The rate of vorticity production by variations in fluid density is given by $(Gr/Re^2)\dfrac{\partial \theta}{\partial x}$. In the upstream and downstream portions of the field, $\partial\theta/\partial x > 0$ and $\partial\theta/\partial x < 0$, respectively (see Figure 6). Hence, we expect that positive (negative) vorticity will be created on the upstream side for $Gr > 0$ ($Gr < 0$), and similarly negative (positive) vorticity on the downstream side for $Gr > 0$ ($Gr <$ 0); our results exhibit these features. The vorticity distribution at steady state and $Gr \neq 0$ thus represents a balance between convection and diffusion of vorticity produced by the internal source at each point, as well as that produced at the plate boundary. A discussion of vorticity production in density stratified flow under more general circumstances is available in Yih (1965, 1969).

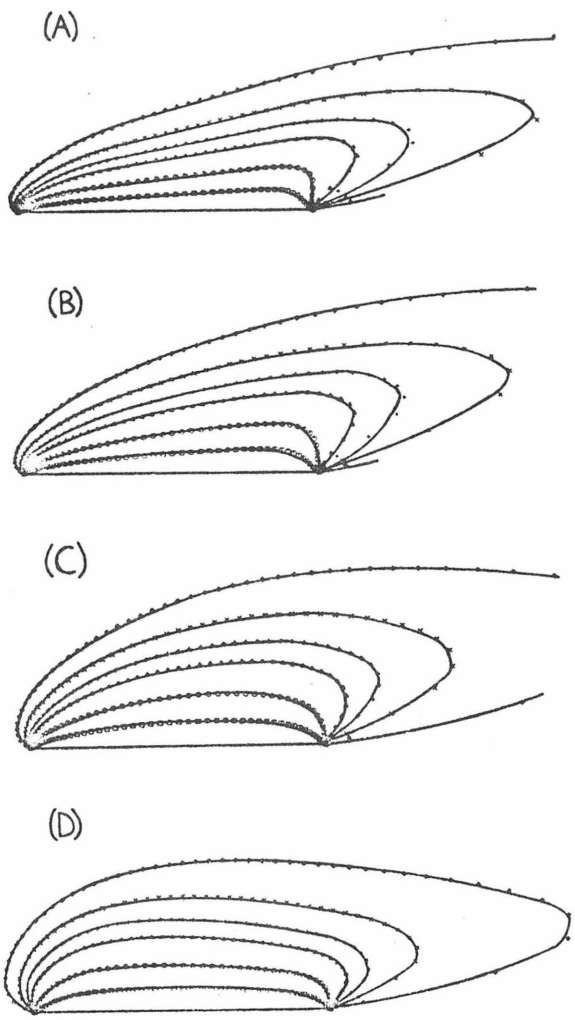

Fig. 6. Isotherms for $Re = 40$ and $Pr = 0.7$; $\theta = 0.8, 0.6, 0.4, 0.3, 0.2$, and 0.1 with 0.8 corresponding to the innermost isotherm: (A) $Gr/Re^2 = 8$; (B) $Gr/Re^2 = 0$; (C) $Gr/Re^2 = -5$; (D) $Gr/Re^2 = -14$.

The qualitative dependence of flow structure on Gr for $Re = 10$, 100, and $Pr = 0.7$ is similar to that described above for $Re = 40$. However, it is of interest to document more fully the dependence of flow structure on Re in order to provide an indication of the degree to which the small Gr boundary-layer behavior ($Pr = 0(1)$) of Sparrow and Minkowycz (1962) is preserved when Re is moderate and the natural convection effects are not intrinsically assumed to be small. Two overall parameters which have been frequently used to characterize the gross flow structure in problems of this sort are the drag coefficient C_d and Nusselt number Nu which we have defined in Equations (17) and (18). Figure 2 shows the dependence of $C_dRe^{1/2}$ on the boundary-layer parameter $Gr/Re^{5/2}$ for the various Reynolds numbers studied. For $|Gr/Re^{5/2}| << 1$ and fixed, and large Re, it is expected from boundary-layer theory that $C_dRe^{1/2}$ will be independent of Re. Surprisingly, even for Re as small as 40-100, $C_dRe^{1/2}$ appears to be qualitatively consistent with this behavior not only in the regime of small (positive) $Gr/Re^{5/2}$ but throughout the range studied up to +2.215. It should be noted, however, that $Re = 100$ is not sufficiently large to provide a quantitative comparison with boundary-layer behavior as evidenced by the fact that the value of $C_dRe^{1/2}$ calculated for $Gr = 0$, $Re = 100$ is still considerably above the theoretical boundary layer value of 1.328 (Dennis and Dunwoody, 1966). The divergence of the curves for negative Gr is viewed by us as a direct consequence of the existence of flow separation which corresponds to a total breakdown of the boundary-layer type flow structure which appears to be present for $Gr > 0$, even when $Gr/Re^{5/2}$ is not small. More interesting than the Reynolds number dependence is the very strong dependence of $C_dRe^{1/2}$ on Gr and particularly the very small although positive values of C_d which result for Gr negative and numerically large in absolute value. Although admittedly unusual from the point of view of classical fluid dynamics, the latter might be expected on physical grounds since the existence of a large recirculating eddy of the type pictured in Figure 4d implies that a large portion of the plate surface is subjected to reverse flow and, hence, negative skin friction. Figure 7 shows the calculated dependence of $NuRe^{-1/2}$ on $Gr/Re^{5/2}$ for $Re = 10$, 40, and 100. Clearly, the basic behavior is similar to that of the drag coefficient although the dependence on Gr is weaker and the dependence on Re somewhat stronger. The weak dependence on Gr is consistent with the boundary-layer predictions of Sparrow and Minkowycz (1962).

Effect of Pr on Flow Structure; Fixed Re and $Gr/Re^{5/2}$

Recently, Leal (1973a) considered the asymptotic boundary-layer structure for the present problem in the limits as $Pr \to \infty$ and $Pr \to 0$, respectively for $|Gr/Re^{5/2}|$ suitably restricted. The key qualitative result from this work was the suppression or enhancement of the buoyancy effect depending upon whether $Pr >> 1$ or $Pr << 1$, respectively, which arises from the fact that the thermal boundary layer is either very thin or very thick relative to the momentum boundary layer in these limits. When $Pr >> 1$ and the thermal layer is thin, the buoyancy driving force is confined essentially to the viscous layer near

the wall, and its effect on the dynamics is thereby diminished compared with the case $Pr = 1$. On the other hand, when $Pr << 1$, the thermal driving force is primarily effective in the nonviscous portion of the flow outside the momentum boundary-layer and its effect is thereby enhanced.

It is of interest to compare the qualitative dependence of the overall parameters $NuRe^{-1/2}$ and $C_dRe^{1/2}$ on Pr with the theoretical predictions from the boundary layer analysis of Leal (1973a). In Figure 3, we have plotted the numerical results for $Re = 100$ and $Gr = 0$ as discussed in the previous section. The finite value of Re is apparently reflected in the uniform upward displacement of the numerical results compared with the theoretical ones which are evident in the plot. In order to ascertain the practical effects of Pr on the flow dynamics for $|Gr/Re^{5/2}| = 0(1)$, numerical solutions were obtained at fixed $Re = 40$ and $Gr/Re^{5/2} = 1.265$, 0, and -1.74; Table 4 gives the results for $C_dRe^{1/2}$ and $NuRe^{-1/2}$ with $Pr = 10.0$. A dramatic example of the enhancement of the influence of buoyancy on the flow structure for decreasing Pr is that, for $Gr/Re^{5/2} = -1.74$, *no* separation occurs for $Pr = 10.0$ whereas a reverse flow region develops for $Pr = 0.7$ as will be evident from the next part of this section. For large and increasing Pr, Leal predicts that the corrections due to the buoyancy effect to the forced convection values of $C_dRe^{1/2}$ and $NuRe^{-1/2}$ should behave like $Pr^{-2/3}$ and $Pr^{-1/3}$, respectively. It is somewhat surprising in view of the restrictions on Gr which are implicit in the boundary-layer analysis that our results for $Gr/Re^{5/2} = 1.265$ exhibit qualitatively the same behavior (although the theory only requires that $Pr >> 1$ and $Gr/Re^{5/2} << Pr^{2/3}$). No attempt was made to obtain results at $Pr = 0.1$, in addition to the case $Re = 100$ and $Gr = 0$, in view of the large values of x_s required; however, it is expected that the results would be qualitatively similar for $Gr \geq 0$ to those predicted by the boundary-layer analysis of Leal.

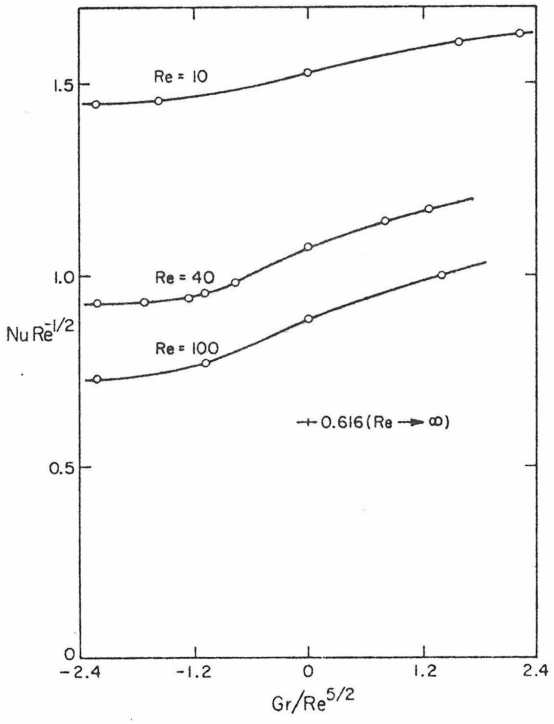

Fig. 7. $NuRe^{-1/2}$ as a function of the boundary-layer parameter, $Gr/Re^{5/2}$, for $Pr = 0.7$.

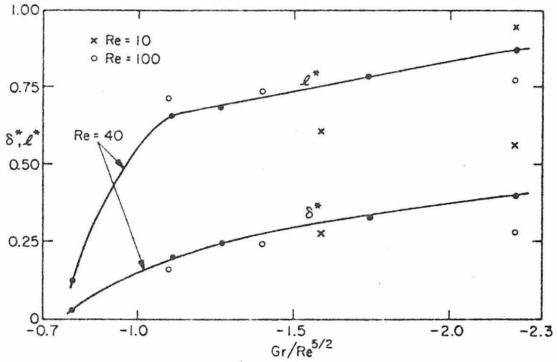

Fig. 8. δ^* and l^*, as a function of the boundary-layer parameter, $Gr/Re^{5/2}$, for $Pr = 0.7$.

Structure of the Recirculating Eddy; Fixed $Pr = 0.7$

We have previously noted that when the plate is cold and Gr is sufficiently large, the adverse pressure gradient which is induced causes the boundary flow to separate with the resultant formation of a recirculating eddy whose nominal dimensions may sometimes approach that of the plate. In the remainder of this section, we return to a more detailed consideration of the structure of this region for $Gr < 0$ and $Pr = 0.7$. In particular, we consider three geometric features of the recirculating eddy: the dimensionless overall length between its leading and trailing edges measured at $y = 0$ (l°), the dimensionless maximum vertical height δ°, and the dimensionless position of its leading edge x°, again measured at $y = 0$. Since the inception of the separation process for large Re is governed by the boundary-layer equations, it should be expected that all of these physical features would have a common origin, independent of Reynolds number, when plotted against the sole boundary layer parameter $Gr/Re^{5/2}$, provided only that Re is sufficiently large.

In Figure 8, we have plotted δ° as a function of $Gr/Re^{5/2}$ for $Re = 10$, 40, and 100. As expected, the numerical data do appear to collapse onto a universal curve for small values of $|Gr/Re^{5/2}|$, with a common origin of approximately -0.8. The continued correlation at higher $|Gr/Re^{5/2}|$ is possibly fortuitous since the boundary-layer theory is not directly applicable in this domain. The main additional feature of interest in Figure 8 is the monotonic increase in the vertical extent δ° as the plate is increasingly cooled to lower temperatures. We have also observed very similar behavior for the overall length of the recirculating region l° as shown in Figure 8. Finally, we turn to the streamwise position of the upstream edge of the recirculating eddy x°, which is plotted as a function of $Gr/Re^{5/2}$ in Figure 9. Clearly, as we have noted previously, the recirculating region does extend upstream beyond the leading edge of the plate for a sufficiently cooled plate. However, the most significant feature of this plot is the fact that, at least through $Gr/Re^{5/2} = -2.3$, x° is increasing monotonically with increasing values of $|Gr/Re^{5/2}|$. Whether this trend will continue as $|Gr/Re^{5/2}|$ increases is, of course, a question of some importance which the present work cannot answer.

The phenomena of buoyancy induced upstream influence is, of course, widely known to occur in circumstances where the entire fluid is stably stratified. A reasonably comprehensive discussion is presented by Yih (1965, 1969), following the initial, extensive work of Long (1953,

1955). However, so far as we are aware, the present investigation is the first to report such an effect which is completely due to locally produced density gradients. In the absence of this effect, one would expect the boundary separation to occur somewhere on the plate surface, certainly downstream of its leading edge. A logical question, therefore, is whether a mechanism is available which could possibly account for the leading edge of the recirculating eddy flow moving upstream in such a dramatic fashion. In order to investigate this point in detail, we numerically studied the time-dependent development of a reverse flow region for $Re = 10$ and $Pr = 0.7$ by starting with the forced convection solution ($Gr/Re^2 \equiv 0$) and changing instantaneously at $t = 0$ from this condition to $Gr/Re^2 = -7$. Several streamline and temperature plots for subsequent points in time are shown in Figures 10 and 11. These appear to suggest the following explanation for the locally-induced upstream influence effect. The fluid directly above the plate is stably stratified as a result of being cooled in passing over its surface. Initially the streamwise variations in the density profile produce only an adverse pressure distribution and the flow separates in the usual manner. For $Re = 10$, $Pr = 0.7$, and $Gr/Re^2 = -7$, the initial separation point is approximately $x_s = -0.25$. This separation leads to a recirculating eddy of finite cross section which the boundary flow must pass over. However, the flow upstream of x_s is stably stratified and the recirculating eddy thus tends to block the flow. This blockage (which is strictly a locally induced phenomenon) causes the pressure distribution to be modified upstream in such a way that the separation process is enhanced and

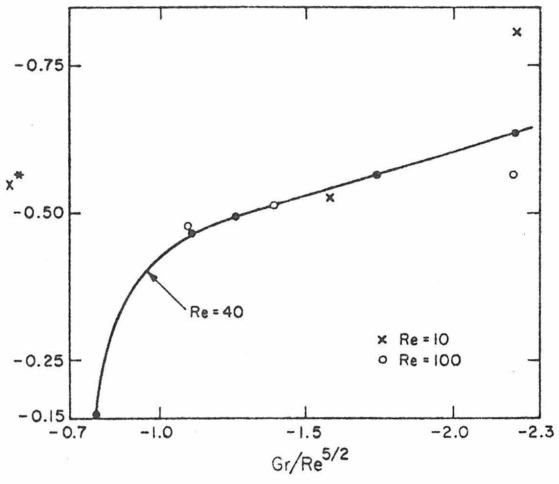

Fig. 9. x^* as a function of the boundary-layer parameter, $Gr/Re^{5/2}$, for $Pr = 0.7$.

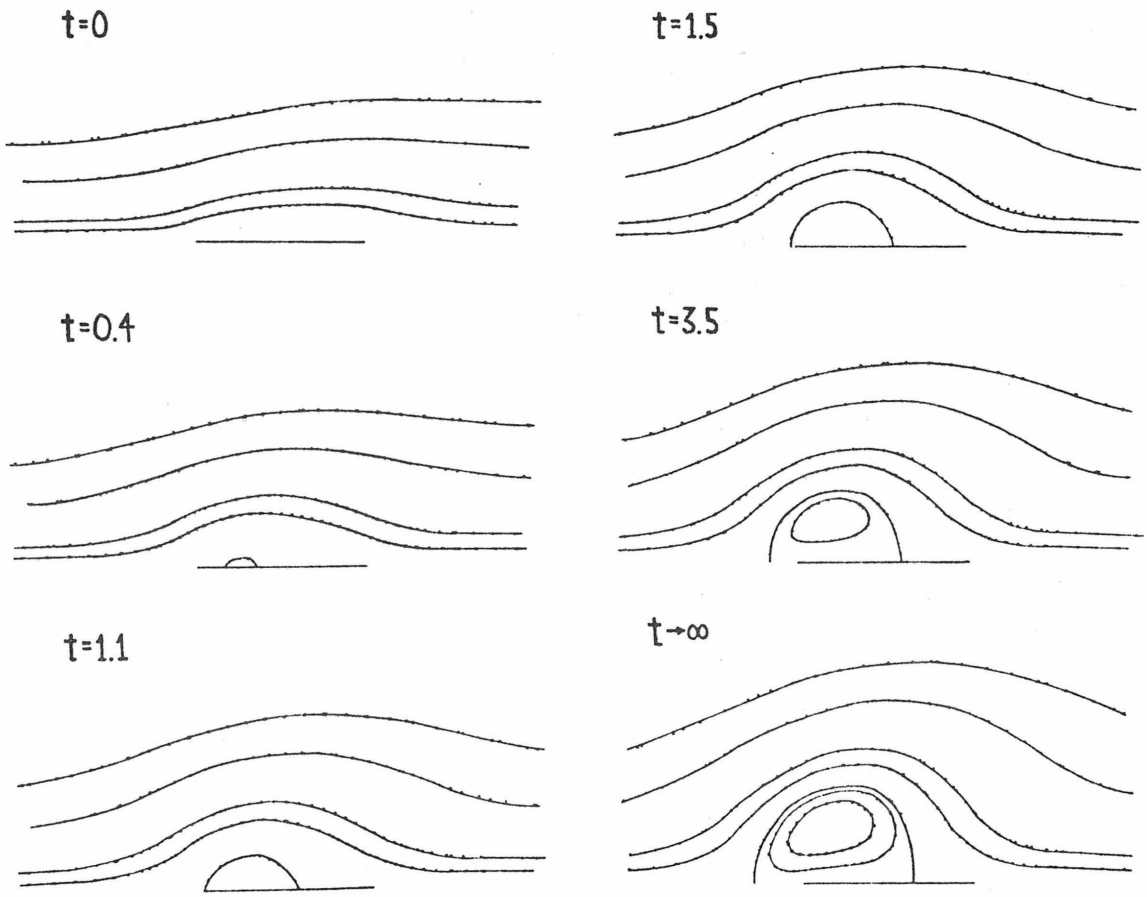

Fig. 10. Streamlines for $Re = 10$, $Pr = 0.7$, and $Gr/Re^2 = -7$; $\psi = 0.5, 0.3, 0.1, 0.05, 0, -0.01, -0.025$ with 0.5 corresponding to the outermost streamline.

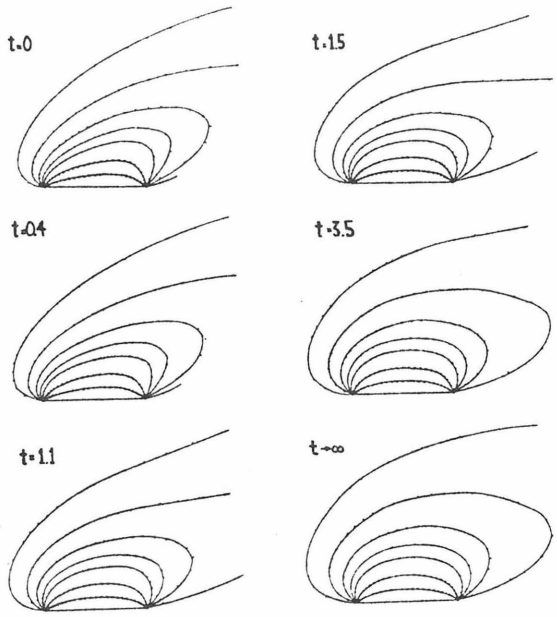

Fig. 11. Isotherms for $Re = 10$, $Pr = 0.7$, and $Gr/Re^2 = -7$; $\theta = 0.8, 0.6, 0.4, 0.3, 0.2, 0.1$, and 0.03 with 0.8 corresponding to the innermost isotherm

occurs more quickly. Ultimately, the leading edge of the eddy moves beyond the leading edge of the plate. At this point, the stratified fluid upstream can only be a result of local cooling of the fluid outside the eddy by the fluid inside. For a given fixed value of Gr, the upstream edge thus attains a finite equilibrium position. It is indeed significant from this point of view that the temperature field precedes the recirculating eddy in moving upstream; it is the region of stably stratified fluid that is produced which apparently allows the reverse flow region to propagate beyond the leading edge of the plate.

In conclusion, it will be of considerable interest to extend the present results to a locally induced flow stratification of the type reported here, coupled with an ambient free stream stratification. In this regard, it is of interest to note that Estoque (1962), in a large-scale numerical analysis of turbulent, stratified, boundary layer flow, predicted the presence of a recirculating region extending over land for an imposed prevailing breeze from warm land to a cool body of water.

ACKNOWLEDGMENT

This work was supported in part by National Science Foundation Grant GK-35476.

LITERATURE CITED

Acrivos, A., "On the Combined Effect of Forced and Free Convection Heat Transfer in Laminar Boundary Layer Flows," *Chem. Eng. Sci.*, 21, 343 (1966).

Arakawa, A., "Computational Design for Long-Term Numerical Integration of the Equations of Fluid Motion: Two-Dimensional Incompressible Flow, Part I," *J. Comp. Phys.*, 1, 119 (1966).

Boussinesq, J., *Theorie Analytique de la Chaleur*, Vol. 2, Gathier-Villars, Paris (1903).

Chang, I.-D., "Navier-Stokes Solutions at Large Distances from a Finite Body," *J. Math. Mech.*, 10, 811 (1961).

Dennis, S. C. R., and G.-Z. Chang, "Numerical Solutions for Steady Flow past a Circular Cylinder at Reynolds Numbers up to 100," *J. Fluid Mech.*, 42, 471 (1970).

Dennis, S. C. R., and J. Dunwoody, "The Steady Flow of a Viscous Fluid past a Flat Plate," *ibid.*, 24, 577 (1966).

Dennis, S. C. R., and N. Smith, "Forced Convection from a Heated Flat Plate," *ibid.*, 509.

Estoque, M. A., "The Sea Breeze as a Function of the Prevailing Synoptic Situation," *J. Atm. Sci.*, 19, 244 (1962).

Imai, I., "On the Asymptotic Behavior of Viscous Fluid Flow at a Great Distance from a Cylindrical Body, with Special Reference to Filon's Paradox," *Proc. Roy. Soc. London*, A208, 487 (1951).

Janowitz, G. S., "On Wakes in Stratified Fluids," *J. Fluid Mech.*, 33, 417 (1968).

Janssen, E., "Flow past a Flat Plate at Low Reynolds Numbers," *ibid.*, 3, 329 (1957).

Lapidus, L., and J. H. Seinfeld, *Numerical Solution of Ordinary Differential Equations*, Academic Press, New York (1971).

Leal, L. G., "Combined Forced and Free Convection Heat Transfer from a Horizontal Flat Plate," Z.A.M.P., in press (1973a).

———., "Steady Separated Flow in a Linearly Decelerated Free Stream," *J. Fluid Mech.*, in press (1973b).

———., and A. Acrivos, "Structure of Steady Closed Streamline Flows within a Boundary Layer," *Phys. Fluids Supplement II*, 12, II-105 (1969).

Lin, J.-T., and C. J. Apelt, "Stratified Flow over an Obstacle; A Numerical Experiment," Project THEMIS, Tech. Rept. No. 7, CER69-70JTL-CJA25, Fluid Dynamics Diffusion Lab., Colorado St. Univ., Fort Collins (1970).

Long, R. R., "Some Aspects of the Flow of Stratified Fluids. I A Theoretical Investigation," *Tellus*, 5, 42 (1953).

———., "Some Aspects of the Flow of Stratified Fluids. III Continuous Density Gradients," *ibid.*, 7, 341 (1955).

———., "Finite Amplitude Disturbances in the Flow of Inviscid Rotating and Stratified Fluids over Obstacles," in *Ann. Review of Fluid Mechanics*, Vol. 4, p. 69, Annual Reviews, Palo Alto, Cal. (1972).

Masliyah, J. H., and N. Epstein, "Numerical Study of Steady Flow Past Spheroids," *J. Fluid Mech.*, 44, 493 (1970).

Merkin, J. H., "The Effect of Buoyancy Forces on the Boundary-Layer Flow over a Semi-Infinite Vertical Flat Plate in a Uniform Free Stream," *ibid.*, 35, 439 (1969).

Rimon, Y., "Numerical Solution of the Incompressible Time-Dependent Viscous Flow past a Thin Oblate Spheroid," *Phys. Fluids Supplement II*, 12, II-65 (1969).

Son, J. S., and T. J. Hanratty, "Numerical Solution for the Flow around a Cylinder at Reynolds Numbers of 40, 200, and 500," *J. Fluid Mech.*, 35, 369 (1969).

Sparrow, E. M., and W. J. Minkowycz, "Buoyancy Effects on Horizontal Boundary-Layer Flow and Heat Transfer," *Intern. J. Heat Mass Transfer*, 5, 505 (1962).

Spiegel, E. A., and G. Veronis, "On the Boussinesq Approximation for a Compressible Fluid," *Astrophys. J.*, 131, 442 (1960).

Takami, H., and H. B. Keller, "Steady Two-Dimensional Viscous Flow of an Incompressible Fluid Past a Circular Cylinder," *Phys. Fluids Supplement II*, 12, II-51 (1969).

Thom, A., and C. J. Apelt, "Note on the Convergence of Numerical Solutions of the Navier-Stokes Equations," Aeronautical Res. Council Rep. Mem. (GB), No. 3061 (1956).

Thoman, D. C., and A. A. Szewczyk, "Time-Dependent Viscous Flow Over a Circular Cylinder," *Phys. Fluids Supplement II*, 12, II-76 (1969).

Yamada, T., and R. N. Meroney, "Numerical and Wind Tunnel Simulation of Response of Stratified Shear Layers to Nonhomogeneous Surface Features," Project THEMIS, Tech. Rept. No. 9, CER-70-71TY-RNM62. Fluid Dynamics Diffusion Lab., Colorado St. Univ., Fort Collins (1971).

Yih, C.-S., *Dynamics of Nonhomogeneous Fluids*, MacMillan Co., New York (1965).

———., "Stratified Flows," in *Annual Review of Fluid Mechanics*, p. 79, Vol. 1, Annual Reviews, Palo Alto, Cal. (1969).

Manuscript received March 2, 1973; revision received May 3 and accepted May 4, 1973.

Appendix 3-B: Combined Forced and Free Convection Flow Past a Horizontal Flat Plate for a Stably-Stratified Fluid

This appendix consists of a manuscript prepared for publication (with co-authors Dr. L. G. Leal and Dr. J. H. Seinfeld). The Figures omitted in the manuscript for brevity are given in Appendix 3-BB.

The simultaneous forced and free convection flow of a stably-stratified fluid past the hot or cold upper surface of a horizontal flat plate is investigated by numerically solving the full equations of motion and thermal energy subject only to the Boussinesq approximation. The solutions for Ri = 0, 1 and 6.325, and $-11 \leq Gr/Re^2 \leq +8$ are discussed when Re = 40 and Pr = 0.7. For all stratifications, a hot plate accelerates the boundary flow near the plate surface relative to the corresponding forced convection flow, thereby increasing both the local skin friction and heat transfer coefficients. For all stratifications, a cold plate decelerates the boundary flow and decreases the local skin friction and heat transfer. The flow can actually separate for sufficiently cold plates with the separation being enhanced by further cooling or increasing the amount of ambient stratification, Ri. When the effect of the ambient stratification dominates that of local heating or cooling, the boundary-layer displacement decreases for increasing Ri, due to the increasing buoyancy restoring force, thus increasing the drag. The increase in the drag, for the same increase in Ri, decreases (increases) by slightly heating (cooling) the plate. When the effect of local heating or cooling dominates that of the ambient stratification, the drag is decreased by increasing Ri. A wave-structure exists only for stably-stratified fluids, with the amplitudes and wavelengths of the waves being decreased for increasing Ri.

A. Introduction

An old and important problem is the simultaneous forced and free convection heat transfer from a heated or cooled body to a fluid of constant ambient temperature (and density). An example is the laminar, two-dimensional flow past the hot or cold upper surface of a horizontal flat plate, which we studied earlier (Robertson et al., 1973, hereafter denoted as I). Earlier boundary-layer studies (Sparrow and Minkowycz, 1962; Redekopp, 1971; and Leal, 1973) had shown that the dominant buoyancy-induced effect in the fluid near the plate is a streamwise pressure gradient which can either accelerate or decelerate the flow depending upon whether the upper surface of the plate is hot or cold relative to the ambient fluid. When the plate is hot and the flow is accelerated, the boundary layer analyses showed that the shear stress at the plate surface is increased. Similarly, when the flow is decelerated, the shear stress is decreased. More significantly, the induced adverse pressure gradient in the latter case means that the boundary flow has the potential to separate. However, no explicit prediction of separation could be obtained from the boundary-layer analyses since they were all restricted to small buoyancy effects, i.e. to small Grashof numbers, Gr.

The purpose of our study in I was to extend the range of Gr in order to investigate the changes in flow structure which occur when the buoyancy effects are not small. Using numerical solutions of the full Boussinesq approximated equations of motion, it was shown that the various qualitative trends predicted by the boundary-layer theories actually carry over for $-2.215 \leqslant Gr/Re^{5/2} \leqslant 2.215$, $10 \leqslant Re \leqslant 100$, and

$0.1 \lesssim Pr \lesssim 10$, where Re and Pr denote the Reynolds and Prandtl numbers, respectively. In particular, flow separation was demonstrated for $Gr/Re^{5/2} < -0.8$ when $Pr = 0.7$, with the result being a large region of recirculating flow adjacent to the plate surface.

In the present paper we again use numerical solutions of the full Boussinesq equations of motion and thermal energy to investigate the additional effect of an ambient stable temperature (density) stratification on the flow structure. The simultaneous presence of ambient stratification and natural convection induced by local heat sources is a common characteristic of many natural and man-related geophysical fluid flows. Qualitatively, it is well-known that the presence of a stable stratification will tend to inhibit changes in vertical elevation of a fluid element. Since such changes are a dominant feature of the flow induced by a cooled plate in the absence of ambient stratification (see I), it may be anticipated that substantial changes will occur in the flow structure when the ambient density stratification is taken into account. This is especially true for the separated flows which produce a large recirculating eddy adjacent to the plate. Since the heat transfer from the plate induces a local density stratification in the fluid, it may at first seem that the dynamic effect of the local heating could be accounted for by simply considering a somewhat enhanced or weakened vertical stratification relative to the stratified flow which would exist with no local heat transfer. As we shall see, however, this qualitative idea is overly simplified and, in fact, quite misleading in many cases. The key to understanding the numerically observed behavior is to remember that the dominant dynamical influence of the <u>locally</u> induced

stratification by itself is the horizontal (streamwise) pressure gradient which arises from the streamwise gradients of density, rather than the vertical gradients which at first seems more likely.

B. Physical Problem and Basic Equations

The physical system is the same as that studied earlier in I, except that the free stream fluid is stably stratified, with the free stream temperature distribution given by

$$T_s = T_\infty (1 + \gamma y) , \qquad \gamma \geq 0$$

For convenience we have sketched the flow configuration in Figure 1. As in our previous study, we confine our attention to the case in which the temperatures at the upper and lower surfaces of the plate are $T_\infty + \Delta T$ and $T_\infty - \Delta T$, so that the plate acts as a heat dipole. This configuration has the advantage of producing a velocity field which is symmetric about $y = 0$, while still yielding a flow near the plate which is similar to that for the more familiar problem in which the plate acts as a heat source or sink of constant surface temperature.

The governing differential equations are the basic conservation balances for momentum, mass and thermal energy heat, simplified by application of the Boussinesq approximation. When these equations are non-dimensionalized using the ambient fluid properties at $y = 0$, the free stream velocity U_∞ and the plate length ℓ, they can be simply expressed in terms of the Cartesian coordinates of Figure 1 as

$$\frac{\partial u}{\partial t} + u \frac{\partial u}{\partial x} + v \frac{\partial u}{\partial y} = - \frac{\partial p}{\partial x} + \frac{1}{Re} \left(\frac{\partial^2 u}{\partial x^2} + \frac{\partial^2 u}{\partial y^2} \right) \qquad (1a)$$

$$\frac{\partial v}{\partial t} + u\frac{\partial v}{\partial x} + v\frac{\partial v}{\partial y} = -\frac{\partial p}{\partial y} + \frac{1}{Re}\left[\frac{\partial^2 v}{\partial x^2} + \frac{\partial^2 v}{\partial y^2}\right] + \frac{Gr}{Re^2}\theta \qquad (1b)$$

$$\frac{\partial u}{\partial x} + \frac{\partial v}{\partial y} = 0 \qquad (2)$$

$$\frac{\partial \theta}{\partial t} + u\frac{\partial \theta}{\partial x} + v\frac{\partial \theta}{\partial y} + \frac{Ri}{Gr/Re^2}v = \frac{1}{PrRe}\left[\frac{\partial^2 \theta}{\partial x^2} + \frac{\partial^2 \theta}{\partial y^2}\right] \qquad (3)$$

where θ is defined as $(T - T_s)/\Delta T$. The four dimensionless parameters in equations (1) and (3) are the Reynolds number, $Re \equiv U_\infty \ell/\nu_\infty$, the Prandtl number, $Pr \equiv c_{p_\infty}\mu_\infty/k_\infty$, the Grashof number, $Gr \equiv \ell^3 \beta g \Delta T/\nu_\infty^2$, and the Richardson number, $Ri \equiv \beta g T_\infty \ell\gamma/U_\infty^2$.† The parameter β which appears in Gr and Ri is the coefficient of thermal expansion. The Richardson number, $Ri \geqslant 0$, provides a measure of the relative magnitudes of buoyancy forces due to ambient stratification, and the inertia forces, whereas the Grashof number, Gr, is a measure of the magnitude of the buoyancy forces which are directly caused by the heat transfer from the hot ($Gr > 0$) or cold ($Gr < 0$) upper surface of the plate. Equations (1) to (3) are valid for all combinations of Ri and Gr, except for the limit $Gr \to 0$, $Ri > 0$. In that case the dimensionless temperature which we have used is inappropriate and must be replaced by $\hat{\theta} = \frac{Gr}{Re^2}\theta + Ri\ y$.

Due to the symmetry of the heat dipole problem, equations (1) to (3) need only be solved in the upper half plane. The appropriate boundary conditions are

$$\frac{\partial u}{\partial y} = v = \theta = 0 \quad ; \qquad |x| > \frac{1}{2}, \quad y = 0 \qquad (4a)$$

$$u = v = 0, \quad \theta = 1 \ ; \qquad |x| \leqslant \frac{1}{2}, \quad y = 0 \qquad (4b)$$

† We note, for future reference, that the group $RiRe^2/Gr$, which appears in equation (3) may also be expressed as γ/Δ, where $\Delta = \Delta T/T_\infty$.

$$u \to 1,\ v \to 0,\ \theta \to 0\ ; \qquad r = (x^2 + y^2)^{1/2} \to \infty \qquad (4c)$$

As in I, we shall restrict our investigation to the numerical solution of equations (1) to (4). In order to focus on the coupled roles of ambient and locally induced stratification, we shall consider only a single intermediate combination of Reynolds and Prandtl numbers, Re = 40 and Pr = 0.7, but allow Gr and Ri to vary over a moderately wide range of values.

C. Numerical Solution Scheme and Preliminary Computational Experiments

The basic numerical solution scheme used in this work is described in I. For present purposes we thus require only a brief recapitulation.

The numerical algorithm is based on the explicit, Gauss-Seidel pointwise iteration applied to the steady-state, finite-difference form of equations (1) to (4), transformed into elliptical cylindrical coordinates (ξ, η) and expressed in terms of the streamfunction, ψ, vorticity, ω, and temperature, θ. The specific cases studied are listed in Table 1, together with empirically determined (non-optimal) values for the relaxation parameters a_ψ, a_ω and a_θ. Also listed are the same data from I for the cases when Ri = 0. In all cases the computational mesh size in the (ξ, η) plane was chosen to be $h = \pi/50$.

The freestream boundary conditions (4c) cannot be satisfied exactly, since the computational domain is clearly limited to some large, but finite, value of r (or equivalently of ξ). In general, the influence of any errors associated with these conditions will depend upon the value of ξ chosen (ξ_∞), and the parameters Ri, Gr, Pr and Re. For the unstratified

problem ($Ri \equiv 0$), it has gradually become accepted that a solution valid in the vicinity of the body may always be obtained by simply imposing the free-stream conditions at some sufficiently large value of ξ_∞. Although the free-stream condition does produce an error when applied at a finite ξ_∞, the error is largely confined to the narrow wake-like region behind the body. Because the governing differential equations are almost parabolic in this region, the errors are not propagated very efficiently back upstream into the interior of the computational domain. Thus, although many studies, including I, have used higher-order (far-field) corrections to the free-stream conditions for $Ri = 0$, it is largely done as an economic measure rather than as a fundamental necessity. However, for stably stratified fluids ($Ri > 0$), the situation is completely changed. In particular, errors introduced at ξ_∞ can be propagated both downstream by convection (as in the unstratified problem), and upstream through the mechanism of internal traveling waves (for some examples of buoyancy-induced upstream influence, see Long, 1959, 1962; Yih, 1965). Furthermore, it is possible that errors which are introduced internally or at the upstream boundary may reflect at the downstream boundary and be trapped in a resonant form inside the computational domain. For some values of the dimensionless parameters, such effects are known to occur (Klemp, 1972). In order to investigate the potential difficulties in the present problem, a number of preliminary computational experiments were carried out.

The first of these preliminary studies was intended to investigate the possibility that an error introduced at some intermediate point in the calculation could propagate through the solution in time to produce

an apparent steady-state solution which is in error. In addition, it was hoped that the preliminary calculation would provide some insight into the efficiency of the reflection of information from the downstream boundary. The calculation was performed for Re = 40, Pr = 0.7 and h = $\pi/50$ with uniform flow conditions ($\psi = y$, $\omega = 0$, $\hat{\theta} = Riy$) imposed at the outer boundary, $x_\infty = \frac{1}{2}\cosh \xi_\infty = 3.08$, and on y = 0 for all x (i.e. the plate was not present). Initially, the uniform stream conditions were also imposed at all interior mesh points except for a large disturbance ($\psi = y + 0.5$, $\omega = -0.5$, and $\hat{\theta} = Riy + 0.5$) which was introduced in the interior of the field. The calculation was carried out to steady state for three values of the Richardson number: Ri = 0.1 ($a_\psi = 1.1$, $a_\omega = 0.4$, $a_{\hat{\theta}} = 0.4$); Ri = 1.0 ($a_\psi = 1.1$, $a_\omega = 0.4$, $a_{\hat{\theta}} = 0.4$); and Ri = 10 ($a_\psi = 0.8$, $a_\omega = 0.05$, $a_{\hat{\theta}} = 0.05$). In all cases, the disturbance was found to decay rapidly. A representative series of plots for the decays of the vorticity and streamfunction disturbances with Ri = 1.0 is shown in Figures 2 and 3. Initially the vorticity spreads by diffusion and convection, as expected, but after some time has passed the transport by these mechanisms begins to be dominated by the suppression of the disturbance by the ambient stratification. So far as we can tell, the disturbance is almost completely damped before it has any chance to reflect from the downstream boundary. Similar results were also obtained for Ri = 0.1 and Ri = 10.0. However, as the ambient stratification is increased (i.e. Ri from 0.1 to 1.0), the efficiency of damping of the disturbance is increased, so that the disturbance at any intermediate point in the calculation is decreased. In addition, the wave length of the remaining disturbance is also slightly decreased.

The decay of the disturbance can also be seen by observing $\|\omega\|^2$, $\|\psi - y\|^2$ and $\|\hat{\theta} - Riy\|^2$, with the norm calculated according to

$$\|\phi\|^2 = \sum_i \sum_j (\phi_{i,j})^2$$

where the subscripts represent the finite difference mesh coordinates. Figure 4 illustrates the decay of the various norms for Ri = 1.0. For Ri = 1.0, Figure 2 illustrates that positive vorticity develops due to the initially large negative vorticity disturbance, causing $\|\omega\|^2$ to increase initially in Figure 4, although $\int_{-\infty}^{\infty}\int_{-\infty}^{\infty} \omega \, dxdy$ is decreasing.

The second preliminary study was intended to determine the qualitative influence of a constant error at the outer boundary on the solution in the vicinity of the plate. The particular question which we wished to answer was whether, in the presence of the plate, the use of a simple free stream boundary condition at some large, but finite, value of ξ_∞, could yield acceptably small errors in the region near the plate. In order to answer this question, we assumed that an order of magnitude estimate of the error produced in the interior of the field by using the free stream conditions at ξ_∞ in the presence of the plate can be calculated by studying the case when the plate is absent and using the first-order far-field corrections to the free stream profiles (which were obtained by us in an earlier paper; Robertson et al., 1975) as if a plate were present. Thus, numerical solutions of the full finite difference equations were obtained with this Oseen linearized correction imposed at ξ_∞, with appropriate symmetry about y = 0 and in the absence of the plate, for Ri = 1.0 and 6.325. A typical case is illustrated in Figure 5, where we have x_∞ = 3.08, Re = 40, Pr = 0.7, and Ri = 1.0.

Although the maximum disturbance is confined to the region near ξ_∞, there is still a moderately strong wave-like structure induced in the interior of the field. Similar results were obtained for other combinations of Ri and ξ_∞ with the magnitude of the induced wave being decreased as ξ_∞ is increased for a fixed value of Ri. However, it was found that no value of ξ_∞ generally existed where the wave-like disturbance was reduced to an acceptable level and which was still sufficiently small for an economical solution of the full nonlinear problem. Thus, the free stream conditions applied at a large, but finite, value of ξ_∞ generally do not produce an acceptable numerical calculation for Ri > 0.

The present numerical solutions were obtained using the accurate Oseen far-field corrections to the uniform stream conditions which were obtained by us in Robertson et al. (1975). The purpose of using this correction is simply to minimize the error between the imposed values of ψ, ω, and θ at ξ_∞ and the values which would exist at the same position if one had an exact solution. In this way it is hoped that any errors introduced at the outer boundary are decreased in the interior of the field to an acceptable level. Even with this more accurate estimate of ψ, ω, and θ at ξ_∞, it was still necessary to investigate carefully the influence of the value of $\xi_\infty(x_\infty)$ on the solution near the plate for each Gr and Ri. This was accomplished by actually calculating convergent solutions at x_∞ = 3.08, 6.16, 9.24, ..., and comparing the results for each case using visual comparison of the ψ, ω, and θ fields, plus the additional requirement that the fractional change in C_d (the drag coefficient) and Nu (the Nusselt number or dimensionless heat flux from the plate) be less than .05. The values of x_∞ listed in Table 1 represent

the minimum values, determined in this manner, required to obtain acceptable solutions (2 to 3% accuracy) in the vicinity of the plate. It is satisfying that these empirically established values for x_∞ compare favorably with estimates given by Robertson et al. (1975) of the minimum distances required for validity of the Oseen far-field corrections, namely $|x| \geq 4.75$ for Ri = 1 and $|x| \geq 3$ for Ri = 6.325. The latter values reflect only the magnitudes of the horizontal velocity corrections which decrease as Ri increases (see Robertson et al., 1975), and do not provide, in any sense, for the effect of Ri on the efficiency of the propagation of errors from the boundaries.

Finally, it may be noted that convergence for fixed x_∞, Gr and Ri was established by visual comparison of ψ, θ and ω fields at intervals of 200 iterations. In addition, it was required that the fractional change in the drag coefficient (C_d) and Nusselt number (Nu) be less than 0.05 after 200 iterations. Typical cases were found to converge in the order of 1000 iterations, although wide variations were found depending primarily on the accuracy of the initial guess for ψ, ω and θ throughout the domain. Typical computation times on the IBM 370/155 were thus 15-20 minutes.

D. Results

As we have indicated earlier in this paper, the primary goal of the present study is to assess the role played by an ambient stable density stratification on the flow structure for simultaneous forced and free convection heat transfer from a horizontal flat plate. In keeping with that objective, numerical solutions were obtained for fixed Re = 40, Pr = 0.7 and various values of Gr and Ri. A number of streamline plots are shown in Figures 6 to 10. For convenience, we have also plotted the overall drag coefficient

$$C_d \equiv \frac{2}{Re} \int_{-1/2}^{1/2} \left(\frac{\partial u}{\partial y}\right)_{y=0} dx$$

as a function of Gr/Re^2 for various Ri in Figure 11. A similar plot for the Nusselt number

$$Nu \equiv \int_{-1/2}^{1/2} \left(\frac{\partial \theta}{\partial y}\right)_{y=0} dx$$

is shown in Figure 12.

1. The Effect of Gr on Flow Structure for Fixed Ri $\geq$ 0

We have noted in the introduction that previous studies for Ri = 0 (including I) have shown that the main dynamic effect of natural convection near the plate is to induce a streamwise gradient of pressure along the plate surface, which either accelerates or decelerates the flow compared with the case Gr = 0, depending upon whether the plate is heated or cooled with respect to the ambient fluid. When the flow is accelerated both the drag coefficient and Nusselt number increase, as shown in Figures 11 and 12. When the flow is decelerated, both C_d and Nu are decreased also. The present solutions for Ri = 1 and Ri = 6.325 show that the same qualitative

effect of natural convection (Gr) is preserved even when the ambient fluid is stably stratified. The streamline plots show an increasing degree of acceleration for Gr increasing and positive, and of deceleration (with separation in many instances) for Gr decreasing and negative. In addition, the behavior of the drag coefficient and Nusselt numbers is qualitatively similar for Ri = 0, 1, or 6.325.

2. The Effect of Stratification for Fixed Gr

The effects of stratification on the flow structure for fixed values of Gr is more complicated as may be seen by examination of either Figure 11 or 12. For purposes of discussion, it is convenient to consider separately the cases Gr = 0, |Gr| small, and |Gr| large.

When Gr = 0, the plate is neither heated nor cooled with respect to the ambient fluid at the same level, and the only influence of buoyancy on the flow is due to the ambient stratification. Examination of either Figure 6 or 11 shows that as Ri is increased, the flow near the plate is somewhat accelerated compared to the Ri = 0 case, thereby increasing the velocity gradients near the plate and therefore C_d. The physical explanation for these changes is simply that the increasing degree of ambient stratification causes the fluid elements (i.e. streamlines) to be displaced less upward by the boundary-layer than they are for Ri = 0, thus producing a local acceleration as observed in the numerical solutions.

For |Gr| nonzero, but small, the main effect of buoyancy on the flow structure is still the ambient stratification. Thus, increasing Ri again suppresses the vertical displacement of streamlines due to the boundary-layer, and the flow is accelerated compared with the case Ri = 0. In this case, however, the effective density stratification in the vicinity of the plate is decreased by the local heating for Gr > 0 and increased by the

local cooling for $Gr < 0$. This latter relatively subtle effect can be seen in the drag coefficient and Nusselt number plots. For weak local heating ($Gr > 0$), the increase in either C_d or Nu is decreased for the same increase in Ri as Gr is increased from zero. On the other hand, for $Gr < 0$, the increase in C_d or Nu is actually increased at first for the same increase in Ri as Gr is decreased from zero.

Finally, let us consider the effects of ambient stratification for $|Gr|$ moderate to large. In this case it may be seen from either Figure 11 or 12 that the dominant buoyancy effect is due to the natural convection associated with the local heating or cooling of fluid by the plate. For $Gr > 0$, the presence of an ambient temperature (density) gradient causes two competing changes in flow structure: firstly, a reduction of the streamline displacement (an accelerating effect), and secondly, a decrease in the streamwise temperature (or density) gradient (a decelerating effect). The net result is a relatively small change in the local flow structure as can be seen from the streamline plots of Figure 7 for $Gr/Re^2 = 5$ or the C_d and Nu plots of Figures 11 and 12 for $Gr/Re^2 \gtrsim \sim 5$. For $Gr < 0$, the changes in flow structure with Ri are more dramatic. In this case, the added ambient temperature gradient yields both an increased adverse streamwise pressure gradient, and a stronger degree of upstream influence, at least near the plate. Hence, for $Gr < 0$ and moderate in magnitude, the degree of deceleration is increased with increasing Ri, the drag coefficient and Nusselt numbers are decreased, and flow separation occurs for less negative values of Gr, and yields larger regions of recirculating flow for a given Grashof number. Following the lead of our earlier investigation (I), we shall now examine the physical dimensions of this recirculating flow regime in more detail. In particular, we consider three geometric features of the reverse

flow region: the dimensionless overall length between its leading and trailing edges measured at $y = 0$, which we shall label ℓ^*, the dimensionless maximum vertical height, δ^*, and the dimensionless position of the leading edge, x^*, again measured at $y = 0$. In Figures 13 and 14 we have plotted x^*, δ^*, and ℓ^* as functions of Gr/Re^2. For $Ri \gtrsim 0$, x^*, δ^*, and ℓ^* all exhibit similar behavior, increasing as the plate is cooled to lower temperatures, with the recirculating region eventually extending upstream beyond the leading edge of the plate (i.e. $x = -0.5$). Our results appear to suggest the following explanation for the occurrence and properties of the steady-state recirculating eddy. The fluid directly above the plate is stably stratified as a result of the local heat transfer from the cold plate and the ambient stable stratification. Initially, the streamwise variations in the density profile produce only an adverse pressure distribution and the flow separates somewhere on the plate surface. This separation leads to a reverse flow region of finite vertical extent over which the boundary flow must pass. However, the flow upstream of the initial separation point is stably stratified and tends to be blocked by the recirculating eddy. This causes the pressure distribution to be modified in such a fashion that the separation process is enhanced and occurs more quickly. Ultimately, the leading edge of the eddy moves beyond the leading edge of the plate, and attains a finite equilibrium position as the effect of the body weakens with increasing upstream distance due to the influence of viscosity. The effect of increasing Ri for fixed Gr in this regime is two-fold. First, induced streamwise (adverse) pressure gradient is enhanced, thereby causing the initiation of separation to occur for less negative values of Gr. Secondly, the local vertical gradients of density are enhanced, thereby also enhancing the blocking mechanism for production

of a recirculating eddy of maximum dimension and upstream extent (i.e. the mechanism for attaining maximum values for x^*, δ^* and ℓ^*). These two features, taken together, provide a rational explanation for the numerical observations of Figures 8 - 14 for $Gr < 0$ and moderate to large in magnitude.

Finally, we may now return to a more detailed examination of the streamline plots of Figures 8 to 10. In particular, we call attention to the wave structure which exists in the overall flow when $Ri > 0$. It may noted that the amplitudes and wavelengths of these waves decrease as Ri is increased due to the increased stable restoring force (see also Robertson et al., 1975). On the other hand, for fixed $Ri > 0$, the wave structure becomes more evident as Gr/Re^2 is decreased from -4 to -5. As Gr/Re^2 is decreased, the reverse flow eddy is increased in size, thus causing a greater vertical displacement near the plate and a stronger wave structure. In order to verify further that the wave structure in our solutions is induced by the displacement flow near the body, and not as a result of inaccuracies in the outer (ξ_∞) boundary conditions, we have compared the wave structure for various non-integral increments in ξ_∞ (i.e. at $\xi_\infty = 2.58$, 3.27, and 3.45). In each case the wave structure is unchanged and thus shows no explicit dependence of wavelength or magnitude on the position of the outermost mesh points. A hint of the qualitative nature of the flow structure which could be induced by errors in the outer boundary, and especially the dependence of this structure on ξ_∞, was implicit in the second preliminary experiment which we described earlier. A final conclusive exhibition of the inadequacy of free-stream conditions is shown in Figure 15. Here we have plotted the streamlines for $Gr/Re^2 = -5$, $Ri = 1$ and free stream conditions applied at $x_\infty = 6.16$ where the more

accurate Oseen far-field corrections yielded the solution discussed above which was independent of ξ_∞. Clearly, the results of Figure 15 are unrealistic and unacceptable physically.

References

Klemp, J. B. 1972 private communication.

Leal, L. G. 1973 "Combined Forced and Free Convection Heat Transfer from a Horizontal Flat Plate." Z.A.M.P. 24, 20.

Long, R. R. 1959 "The Motions of Fluids with Density Stratification." J. Geophysical Research 64, 2151.

Long, R. R. 1962 "Velocity Concentrations in Stratified Fluids." J. Hydraulics Div. A.S.C.E. 88, 9.

Redekopp, L. G. 1971 "The Boundary Layer on a Flat Plate Moving Transversely in a Rotating, Stratified Fluid." J. Fluid Mech. 46, 769.

Robertson, G. E., Seinfeld, J. H., and Leal, L. G. 1973 "Combined Forced and Free Convection Flow Past a Horizontal Flat Plate." A.I.Ch.E. J. 19, 998.

Robertson, G. E., Seinfeld, J. H., and Leal, L. G. 1975 "Wakes in Stratified Flow Past a Hot or Cold Two-Dimensional Body." submitted for publication to J. Fluid Mech.

Sparrow, E. M. and Minkowycz, W. J. 1962 "Buoyancy Effects on Horizontal Boundary-Layer Flow and Heat Transfer." Int. J. Heat Mass Transfer 5, 505.

Yih, C.-S. 1965 Dynamics of Nonhomogeneous Fluids. MacMillan Co., New York.

Table 1: Numerical Parameters for Re = 40, Pr = 0.7, and h = $\pi/50$

Gr/Re^2	Ri	x_∞	a_ψ	a_ω	a_θ
+8	0	3.08	1.1	0.4	0.4
+8	1	3.08 (6.16)	1.1	0.4	0.4
+8	6.325	3.08 (6.16)	0.8	0.05	0.05
+5	0	3.08	1.1	0.4	0.4
+5	1	3.08 (6.16)	1.1	0.4	0.4
+5	6.325	3.08 (6.16)	1.1	0.4	0.4
+1	0	3.08	1.0	0.2	0.2
+1	1	3.08	1.0	0.2	0.2
0	0	3.08 (6.16)	1.1	0.4	0.4
0	1	3.08 (6.16)	0.8	0.05	0.05
0	6.325	3.08 (6.16)	0.8	0.05	0.05
-3	1	6.16	1.0	0.2	0.2
-4	1	6.16 (3.08)	1.0	0.2	0.2
-4	6.325	6.16 (3.08)	0.6	0.01	0.01
-5	0	6.16 (3.08)	1.0	0.2	0.2
-5	1	6.16 (9.24)	1.0	0.2	0.2
-5	6.325	6.16 (9.24)	0.6	0.01	0.01
-8	0	9.24 (12.32)	0.9	0.1	0.1
-8	1	9.24 (6.16)	0.6	0.01	0.01
-11	0	9.24 (12.32)	0.9	0.1	0.1
-11	1	9.24 (6.16)	0.6	0.01	0.01

FIGURE CAPTIONS

Figure 1: The Physical System

Figure 2: Decay of the Vorticity Disturbance for Re = 40, Pr = 0.7, Ri = 1.0, h = $\pi/50$, x_∞ = 3.08, and no plate being present

(a) initial conditions: ω = -0.5 disturbance everywhere in the interior of the indicated region

(b) iteration 20

(c) iteration 40

(d) iteration 80

(e) iteration 120

(f) iteration 180

Figure 3: Decay of the Streamfunction Disturbance for Re = 40, Pr = 0.7, Ri = 1.0, h = $\pi/50$, x_∞ = 3.08, and no plate being present; ψ = 1.25, 1.0, 0.85, 0.6, 0.3, and 0.1 with 1.25 corresponding to the outermost streamline

(a) initial conditions with disturbance

(b) iteration 10

(c) iteration 20

(d) iteration 40

(e) iteration 80

(f) iteration 120

Figure 4: Decay of $||\omega||^2$, $||\psi - y||^2$, and $||\hat{\theta} - Riy||^2$ for Re = 40, Pr = 0.7, Ri = 1.0, h = $\pi/50$, x_∞ = 3.08, and no plate being present

Figure 5: Steady-state Solution for the Propagation of the Stream-function Error on the Outer Boundary for Re = 40, Pr = 0.7, Ri = 1.0, h = $\pi/50$, x_∞ = 3.08 and no plate being present; $\hat{\psi} = \psi - y$ = - 0.10, -0.08, -0.06, -0.05, -0.04 and -0.03 with -0.03 corresponding to the innermost streamline

Figure 6: Streamlines for Re = 40, Pr = 0.7, and Gr/Re^2 = 0; ψ = 2, 1, 0.5, 0.3, 0.1, and 0.05 with 2 corresponding to the outermost streamline (a) Ri = 0 (b) Ri = 6.325

Figure 7: Streamlines for Re = 40, Pr = 0.7, and Gr/Re^2 = 5; ψ = 2, 1, 0.5, 0.3, 0.1, and 0.05 with 2 corresponding to the outermost streamline (a) Ri = 0 (b) Ri = 6.325

Figure 8: Streamlines for Re = 40, Pr = 0.7, and Gr/Re^2 = -5; ψ = 2, 1, 0.5, 0.3, 0.1, 0.05, and 0 with 2 corresponding to the outermost streamline (a) Ri = 0 (b) Ri = 1

Figure 9: Streamlines for Re = 40, Pr = 0.7, and Gr/Re^2 = -5; ψ = 3, 2, 1, 0.5, 0.3, 0.1, and 0 with 3 corresponding to the outermost streamline (a) Ri = 0 (b) Ri = 1 (c) Ri = 6.325

Figure 10: Streamlines for Re = 40, Pr = 0.7, and Gr/Re^2 = -4; ψ = 3, 2, 1, 0.5, 0.3, 0.1, and 0 with 3 corresponding to the outermost streamline (a) Ri = 1 (b) Ri = 6.325

Figure 11: The Overall Drag Coefficient C_d as a Function of Gr/Re^2 when Re = 40 and Pr = 0.7; Ri = 0, 1, 6.325

Figure 12: The Overall Nusselt Number Nu as a Function of Gr/Re^2 when Re = 40 and Pr = 0.7; Ri = 0, 1

Figure 13: x^* as a function of Gr/Re^2 when Re = 40 and Pr = 0.7

—●— Ri = 0

—×— Ri = 1

o Ri = 6.325

Figure 14: δ^* and ℓ^* as a function of Gr/Re^2 when Re = 40 and Pr = 0.7

—●— Ri = 0

—×— Ri = 1

o Ri = 6.325

Figure 15: Streamlines for Re = 40, Pr = 0.7, Gr/Re^2 = -5, Ri = 1, x_∞ = 6.16, and iteration 575 when the free stream outer boundary conditions are employed; ψ = 2, 1, 0.5, 0.3, and 0.1 with 2 corresponding to the outermost streamline

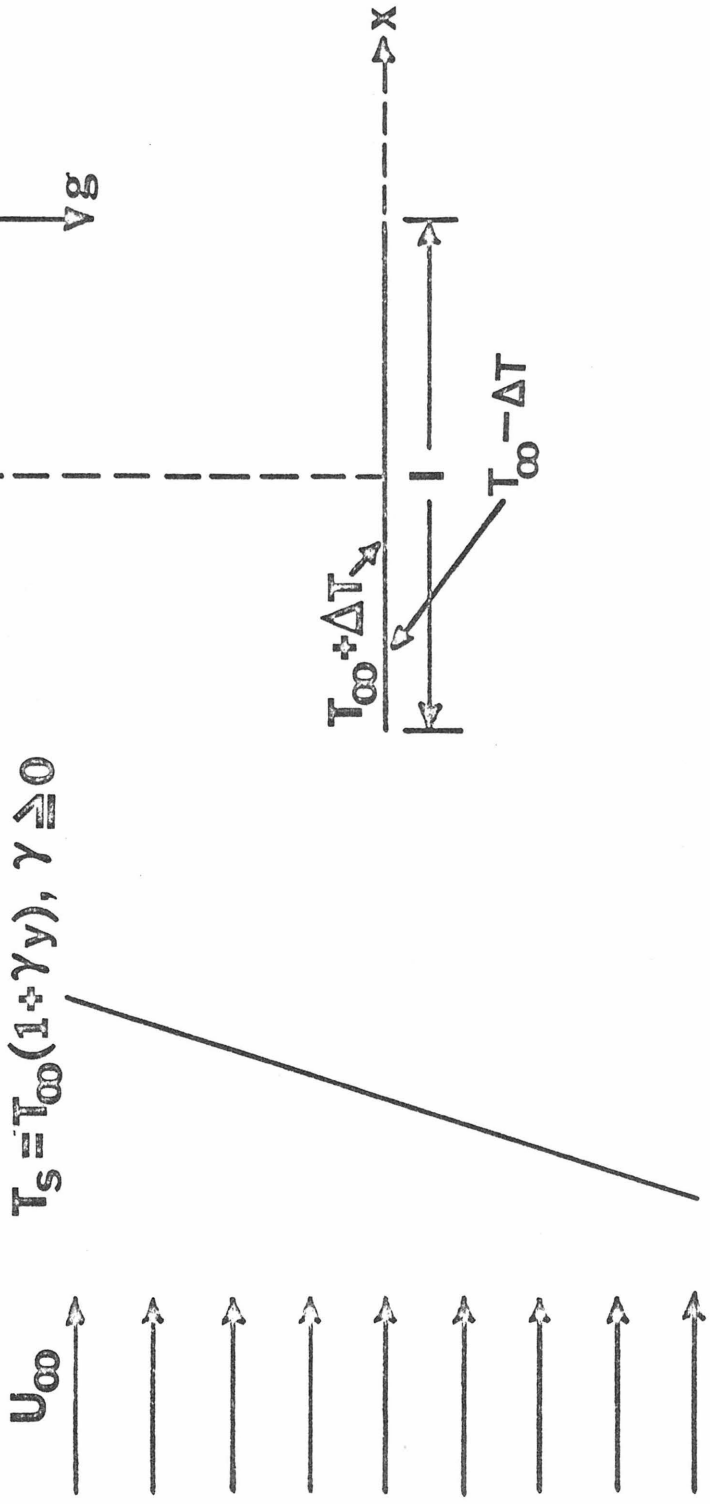
x
g
y
$T_\infty + \Delta T$
$T_\infty - \Delta T$
$T_s = T_\infty(1 + \gamma y)$, $\gamma \geq 0$
U_∞

Figure 1

Figure 2

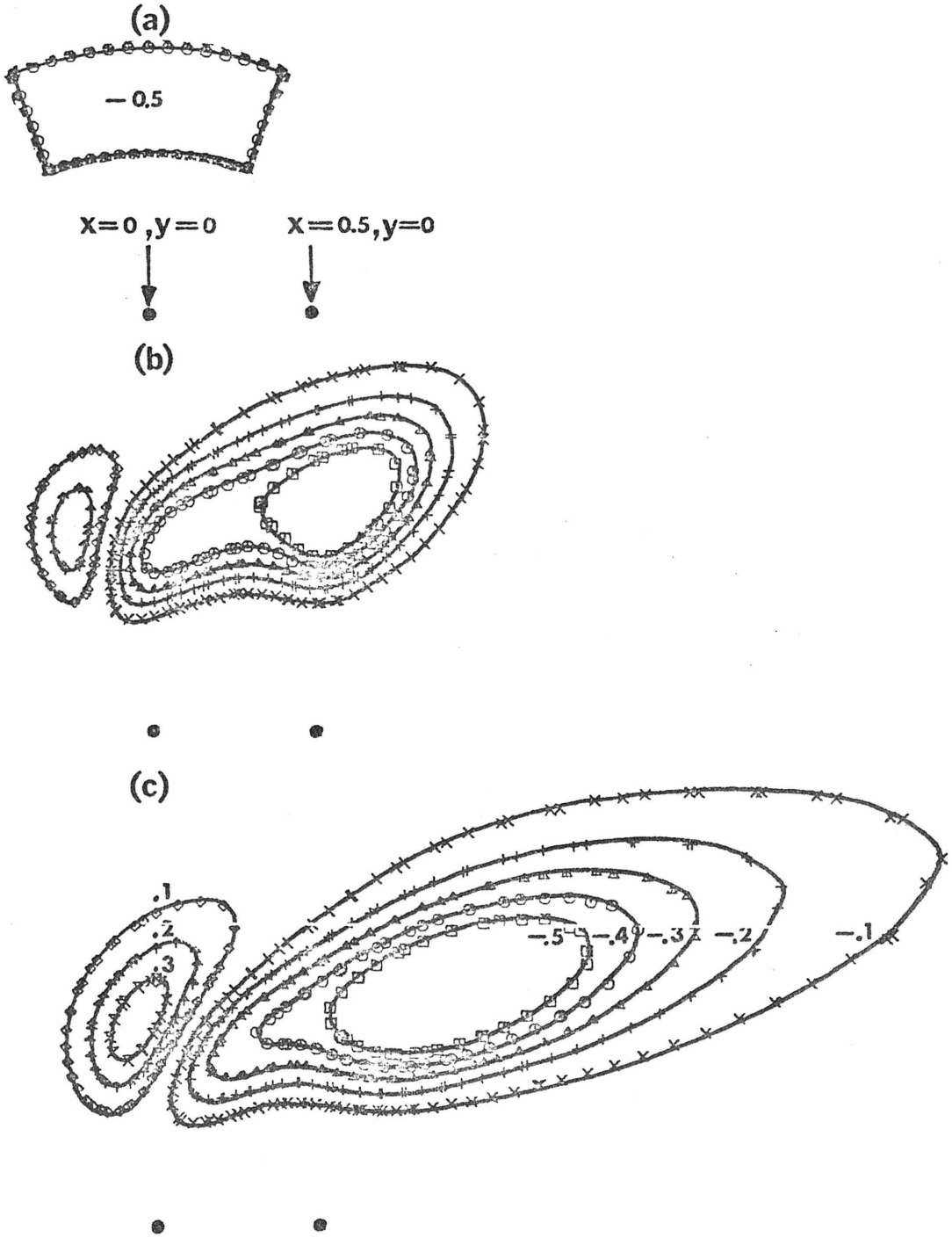

Figure 2

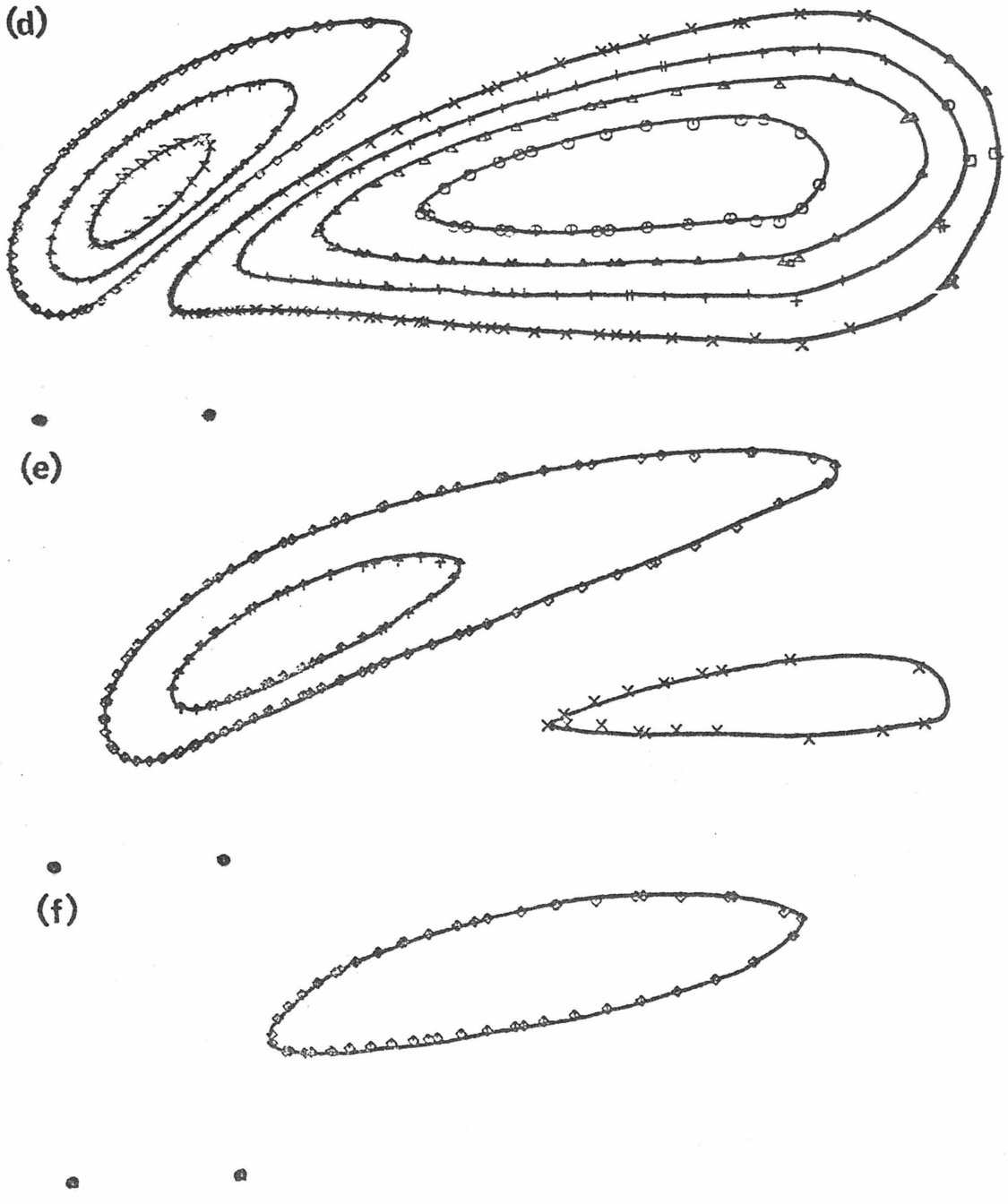

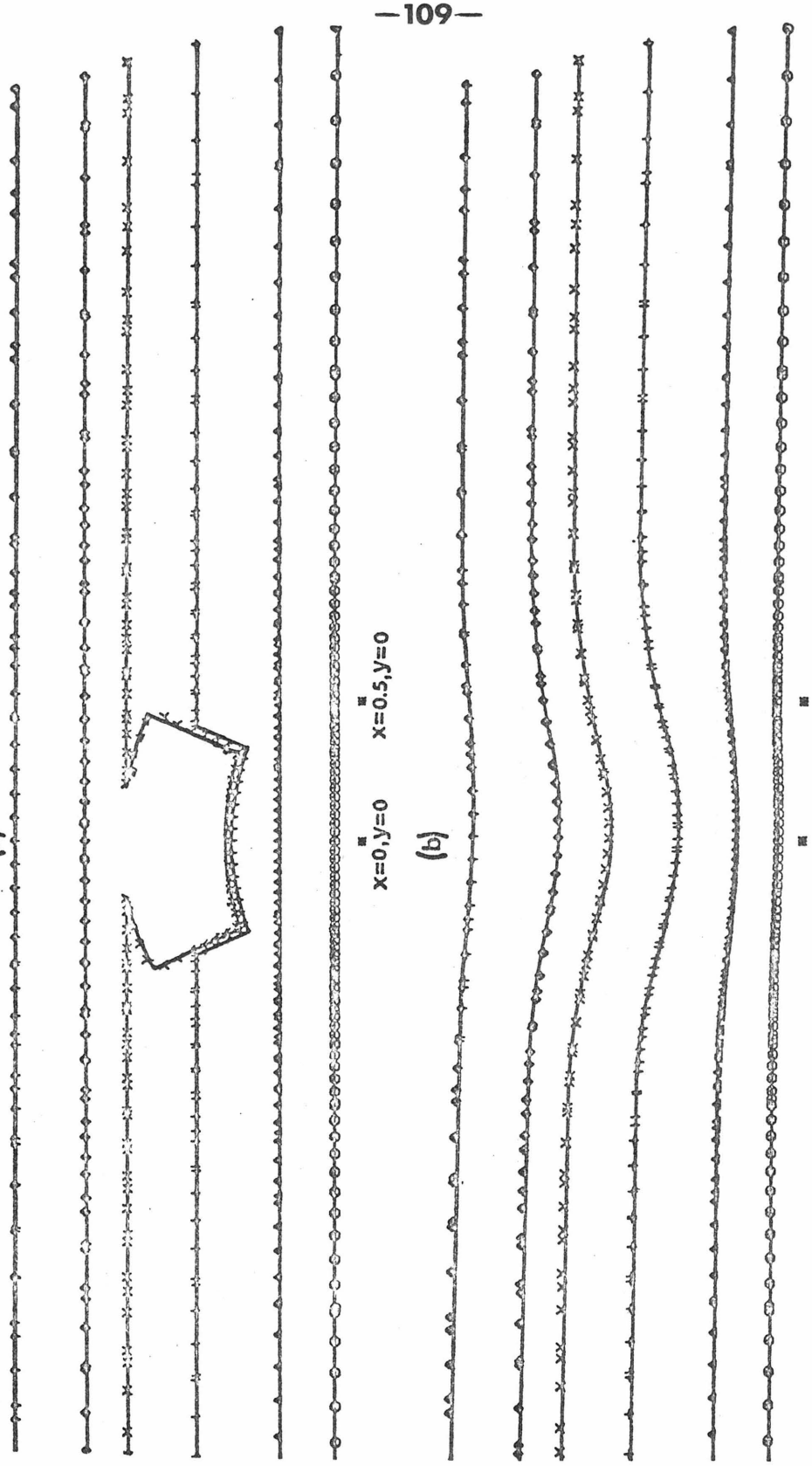

Figure 3

Figure 3

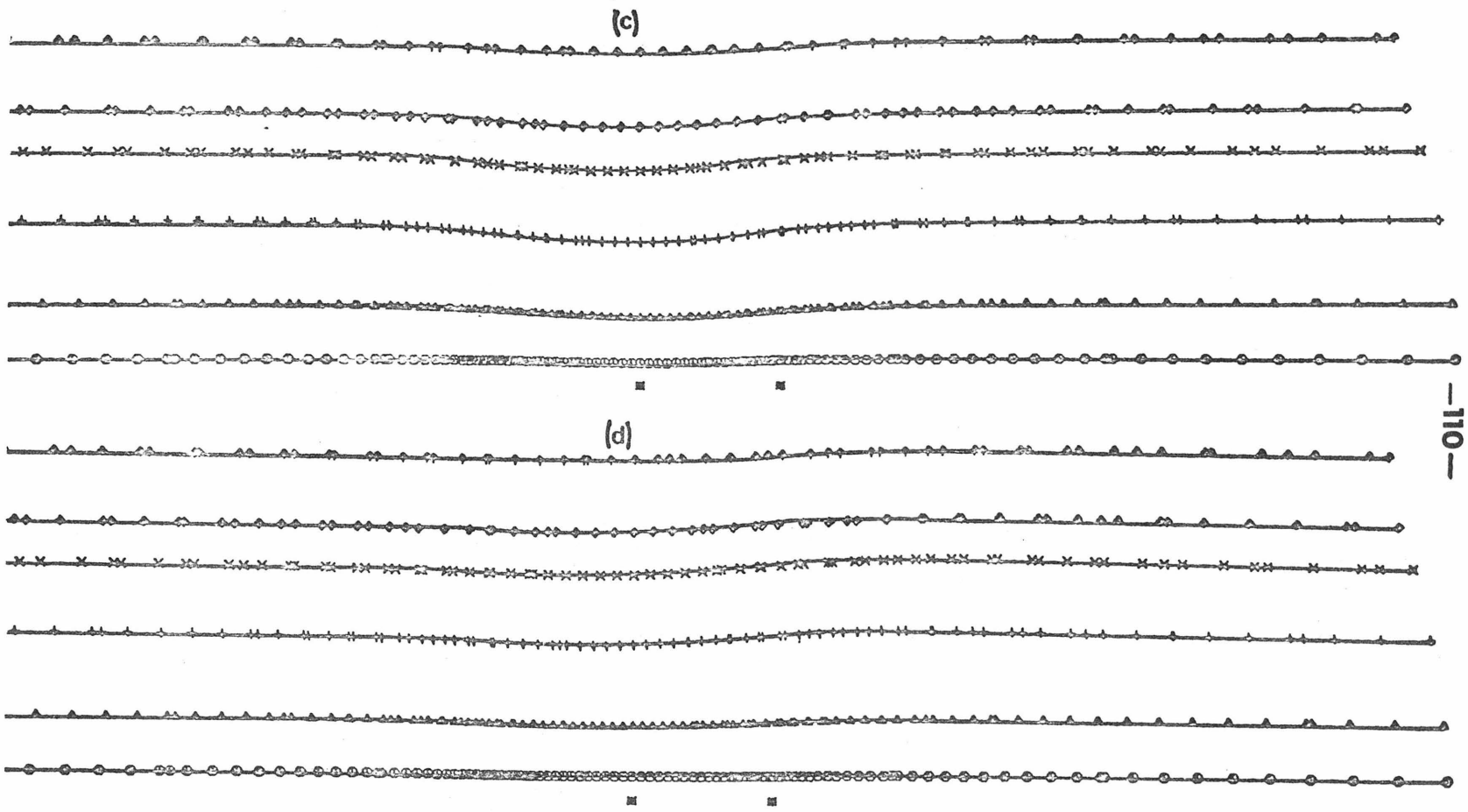

Figure 3

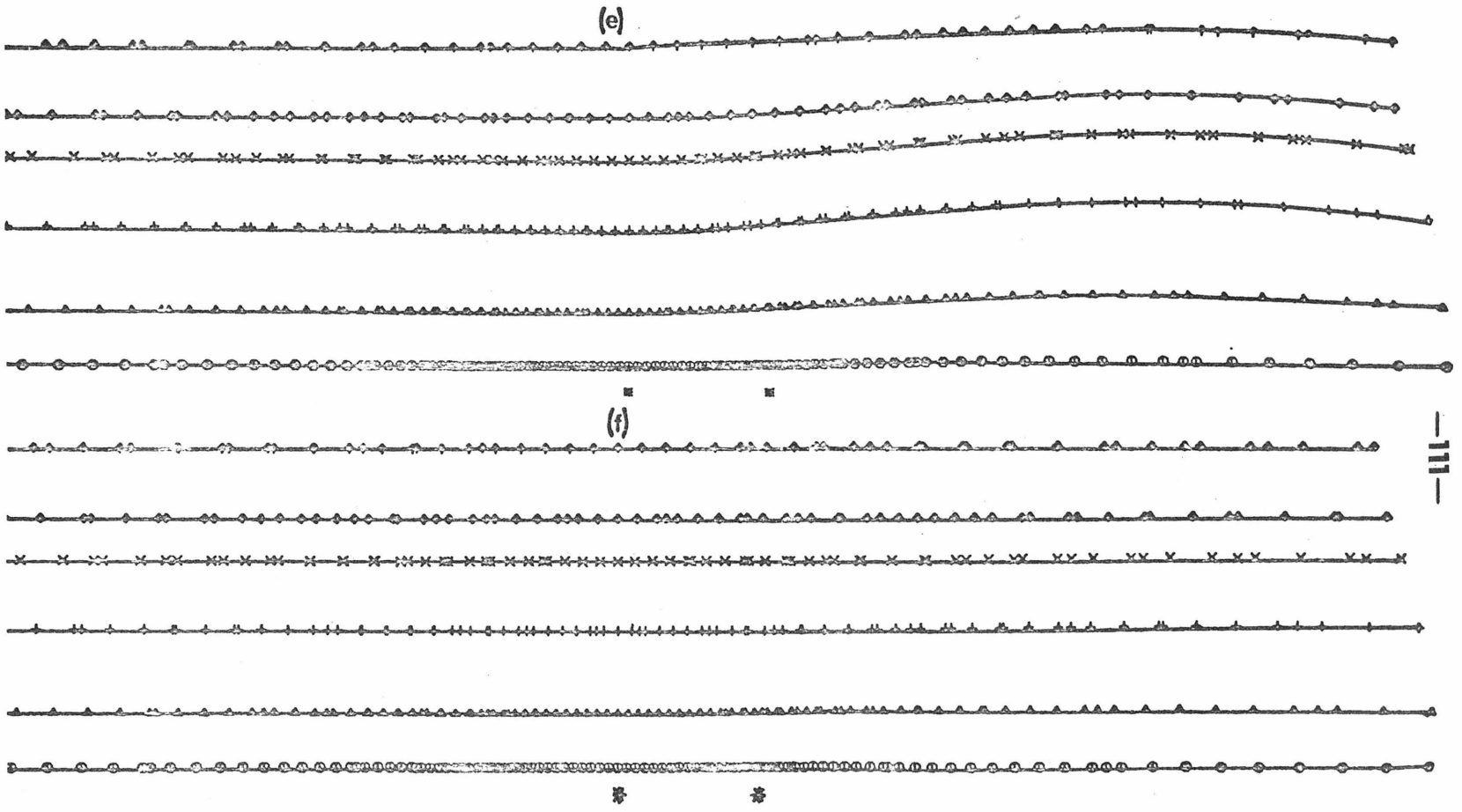

Figure 4

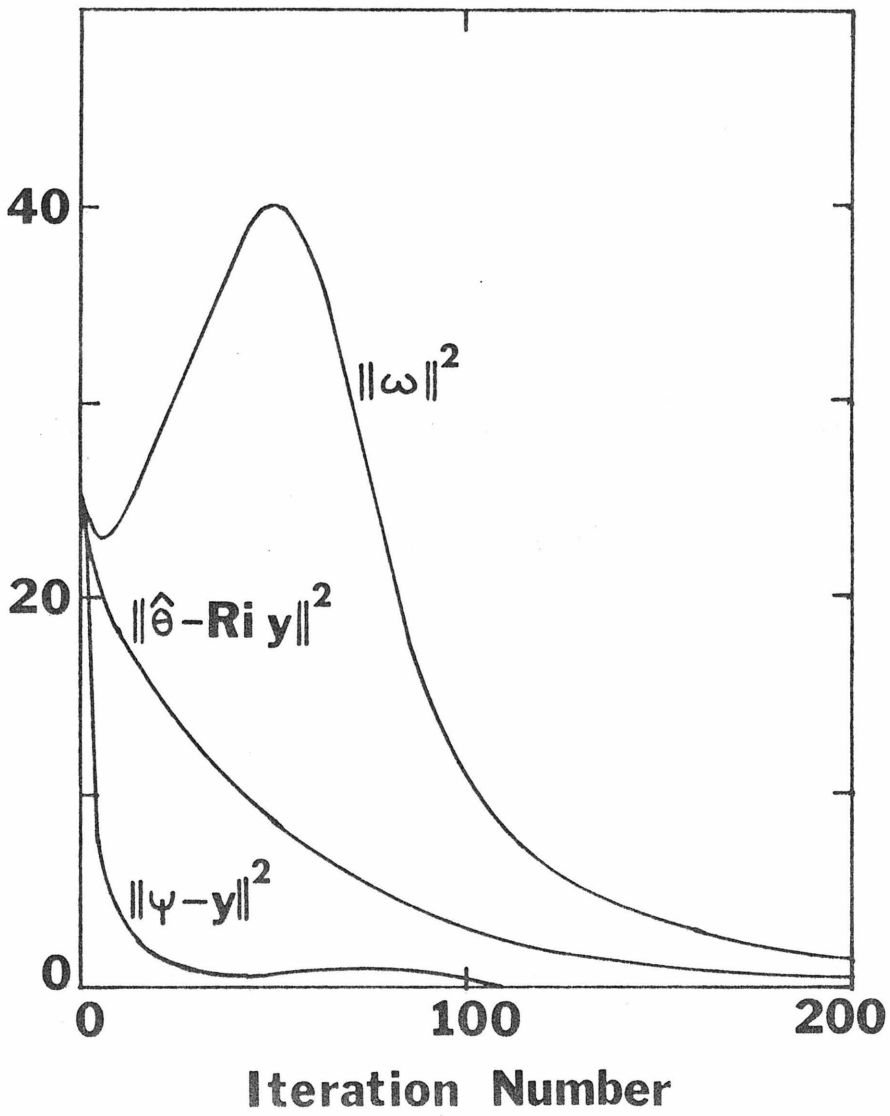
40
20
0
0
100
200
$\|\omega\|^2$
$\|\hat{\theta}-Ri\,y\|^2$
$\|\psi-y\|^2$
Iteration Number

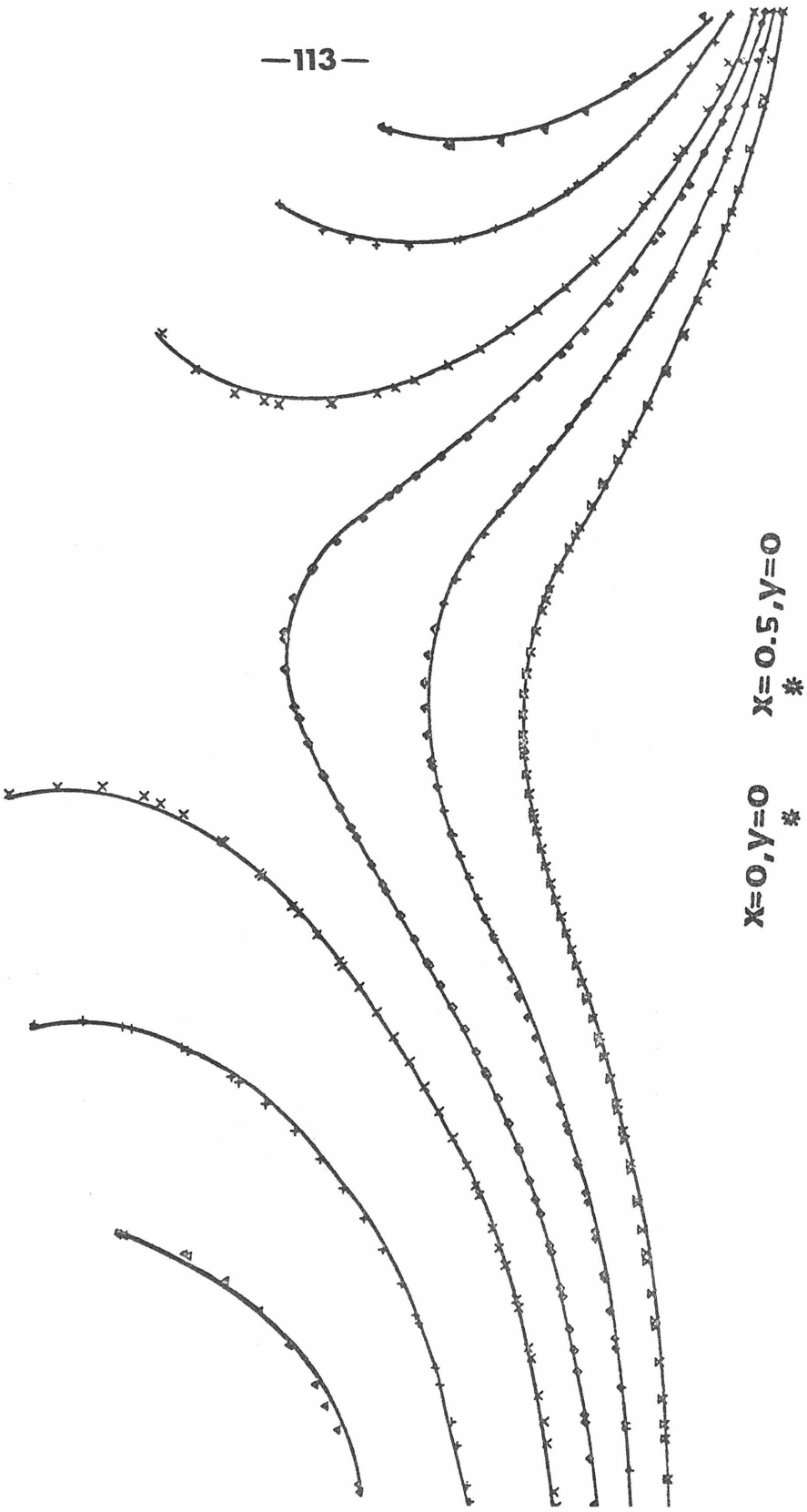

Figure 5

Figure 6

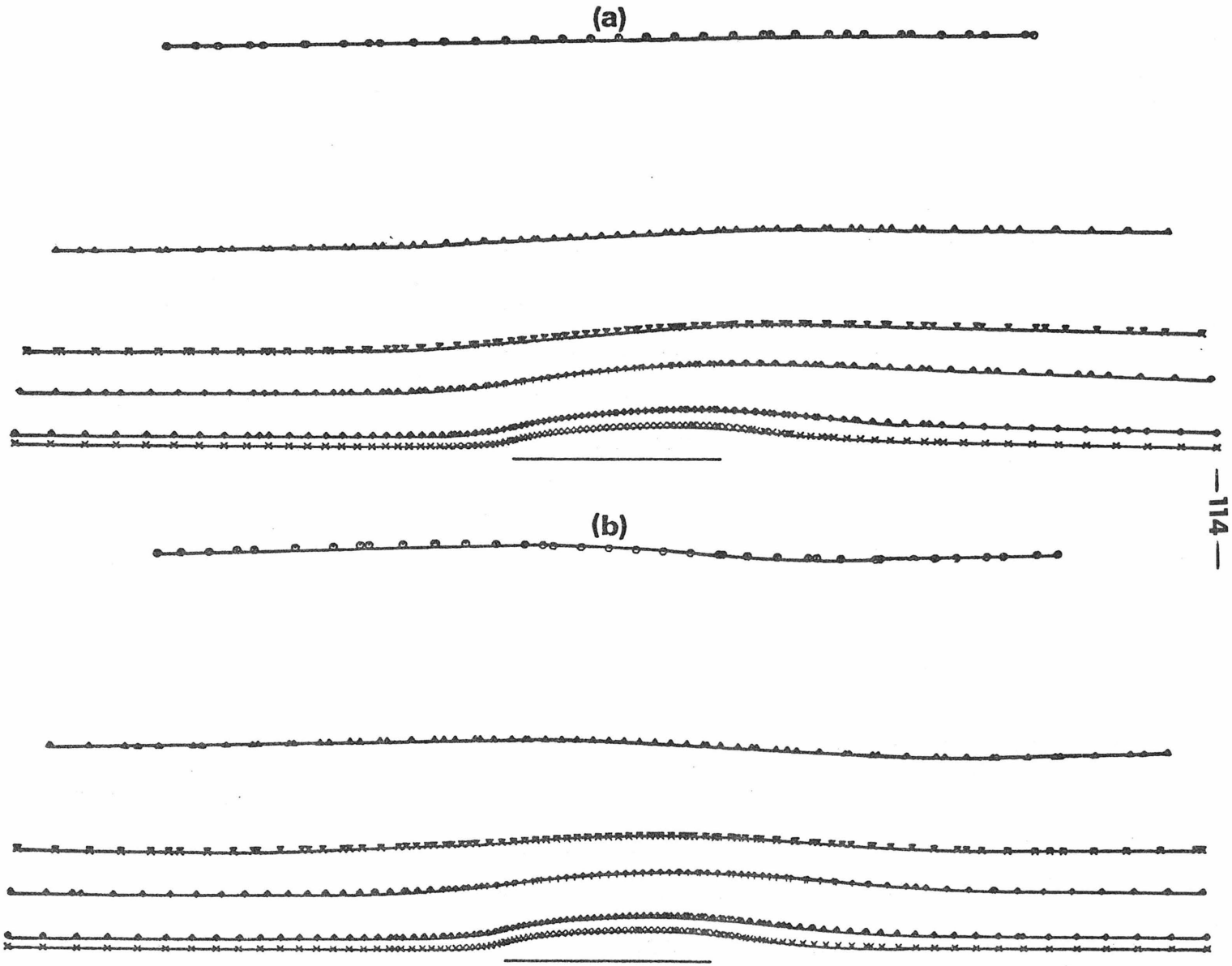

Figure 7

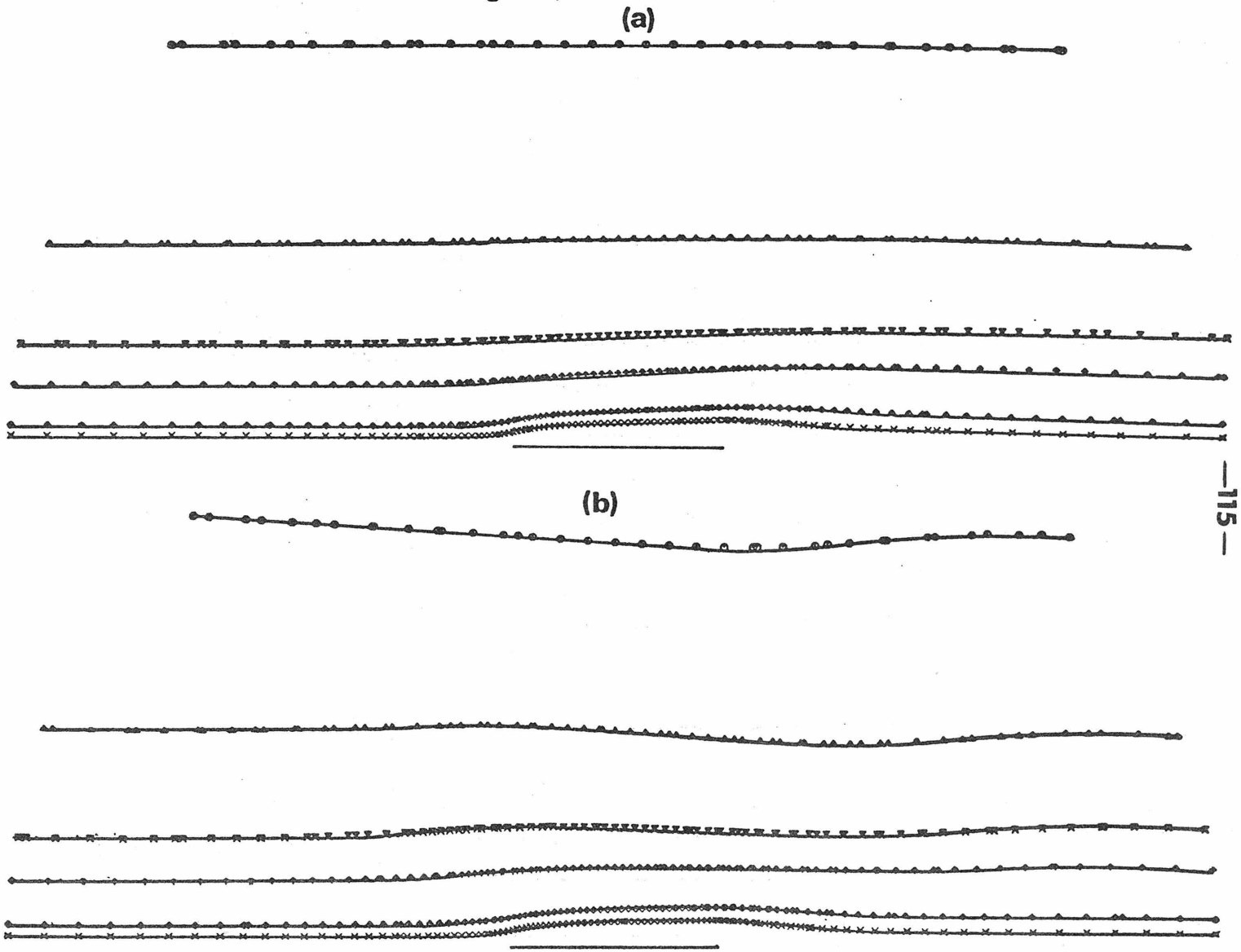

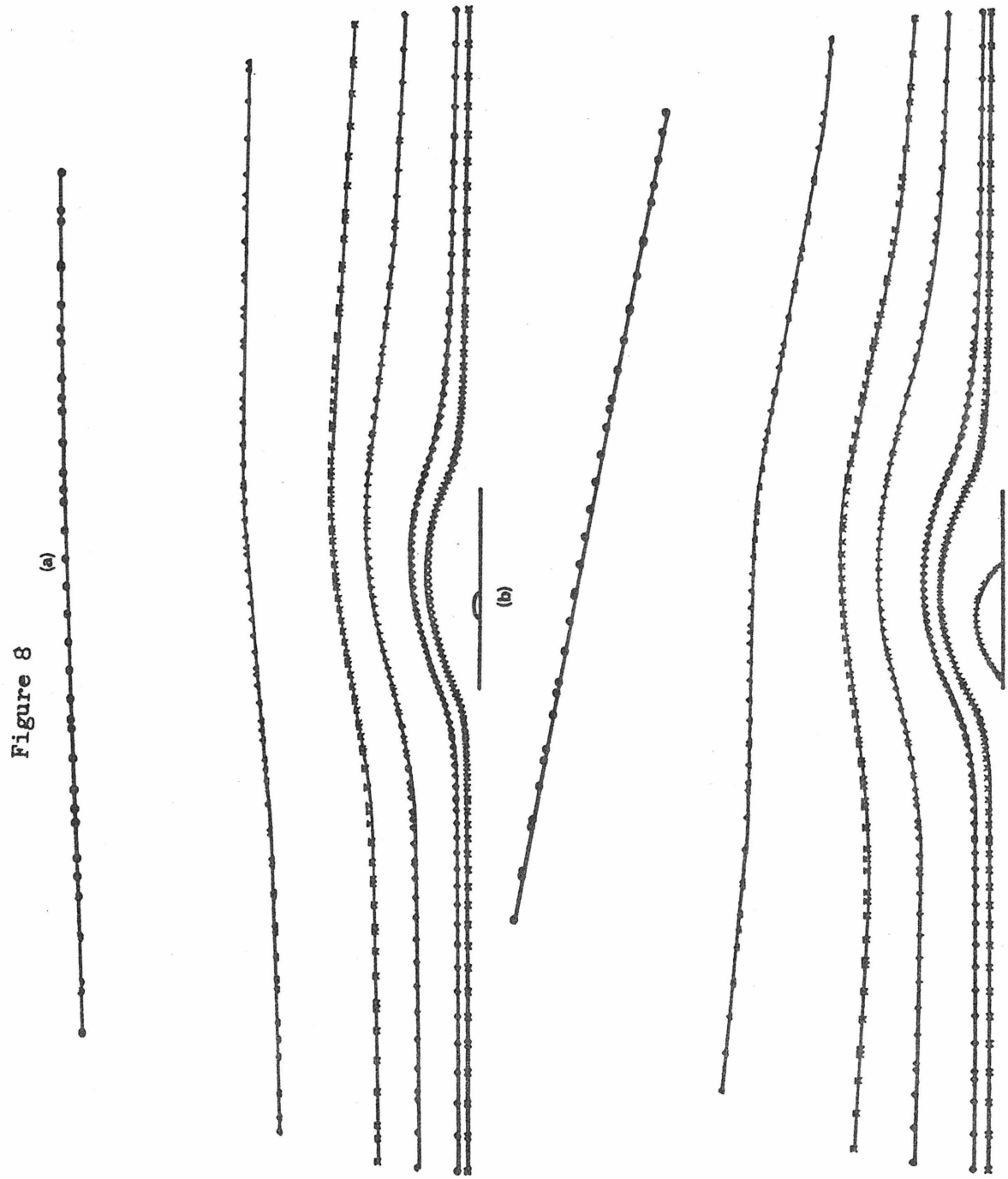

Figure 8

Figure 9

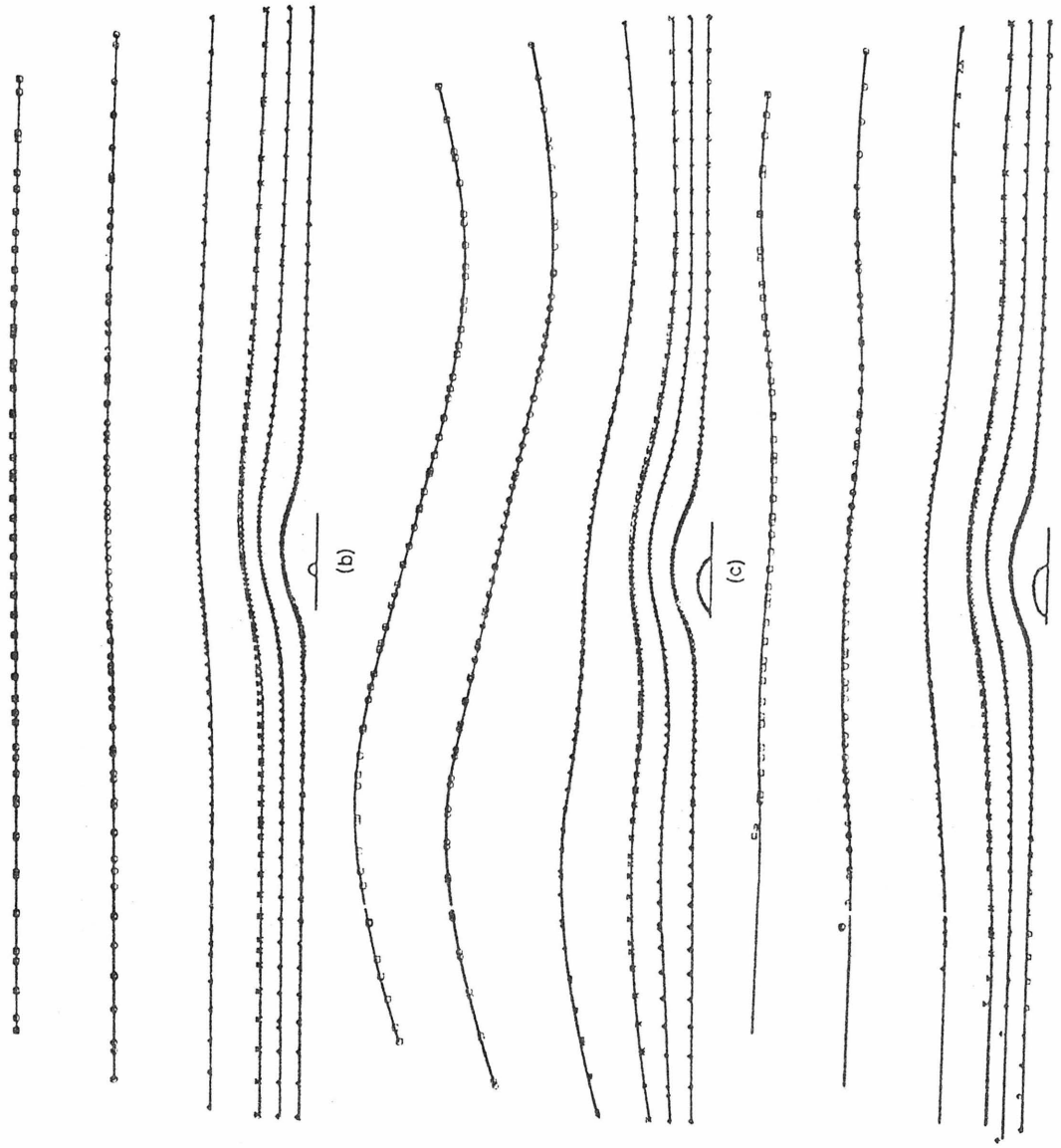

Figure 10

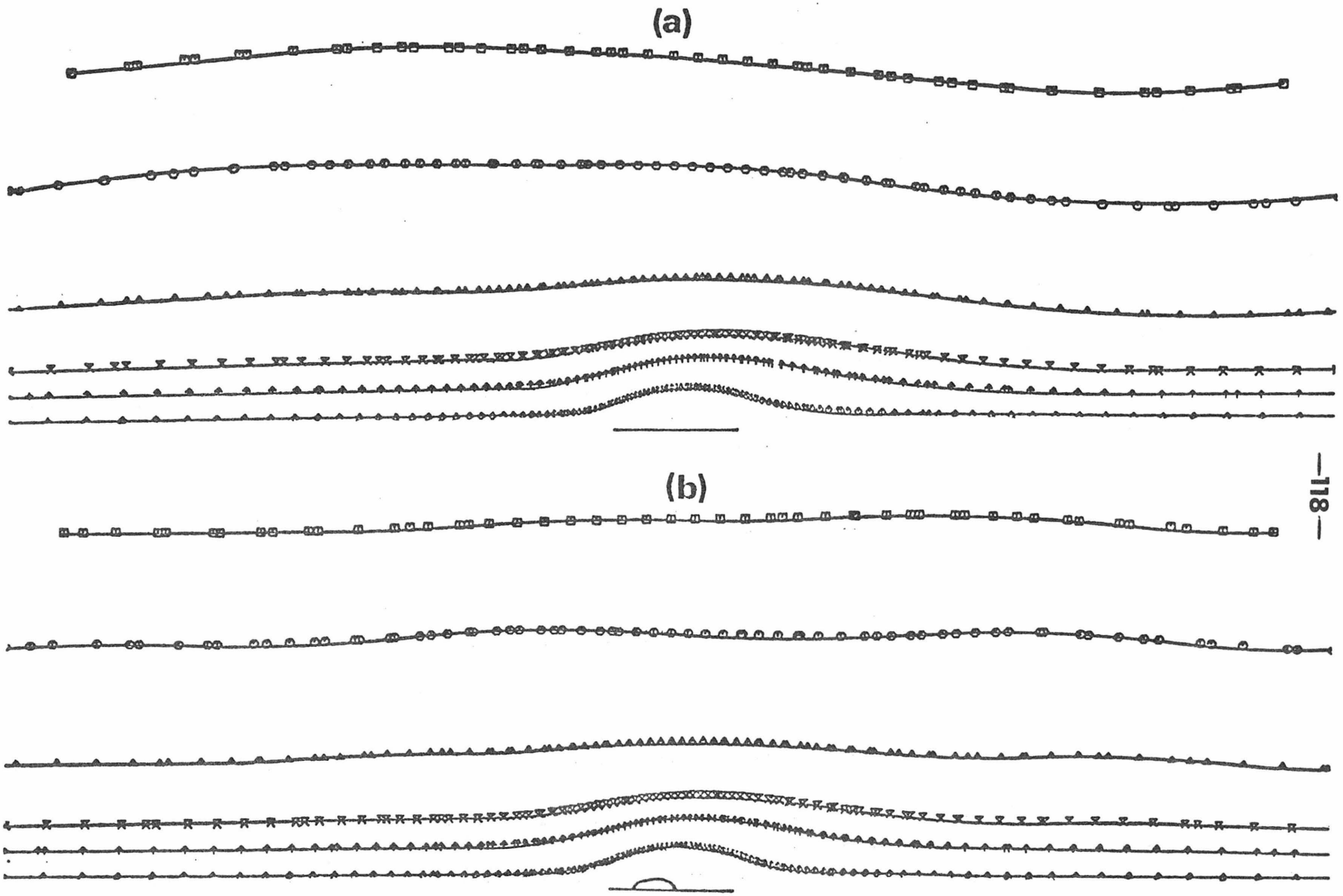

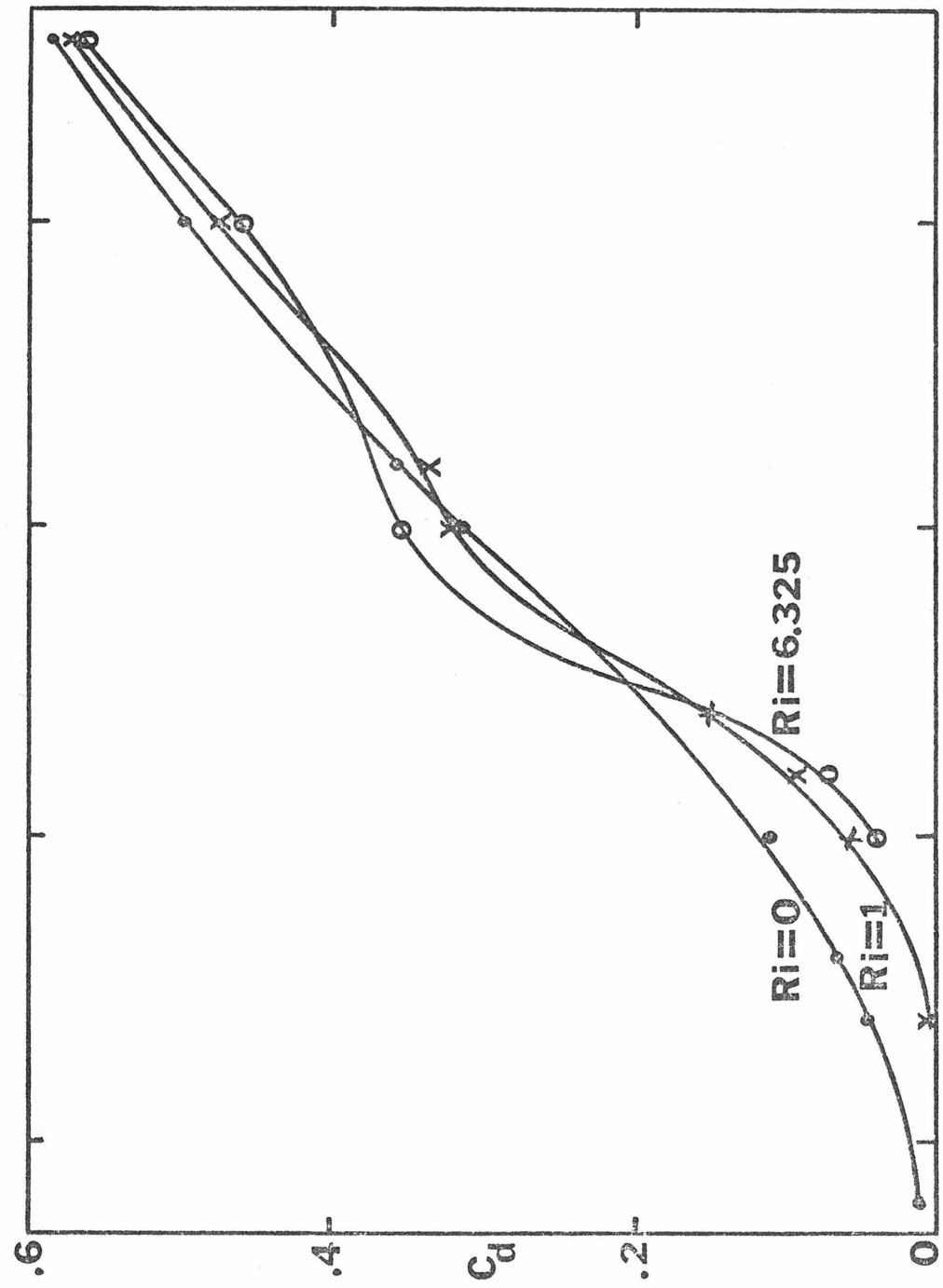

Figure 11

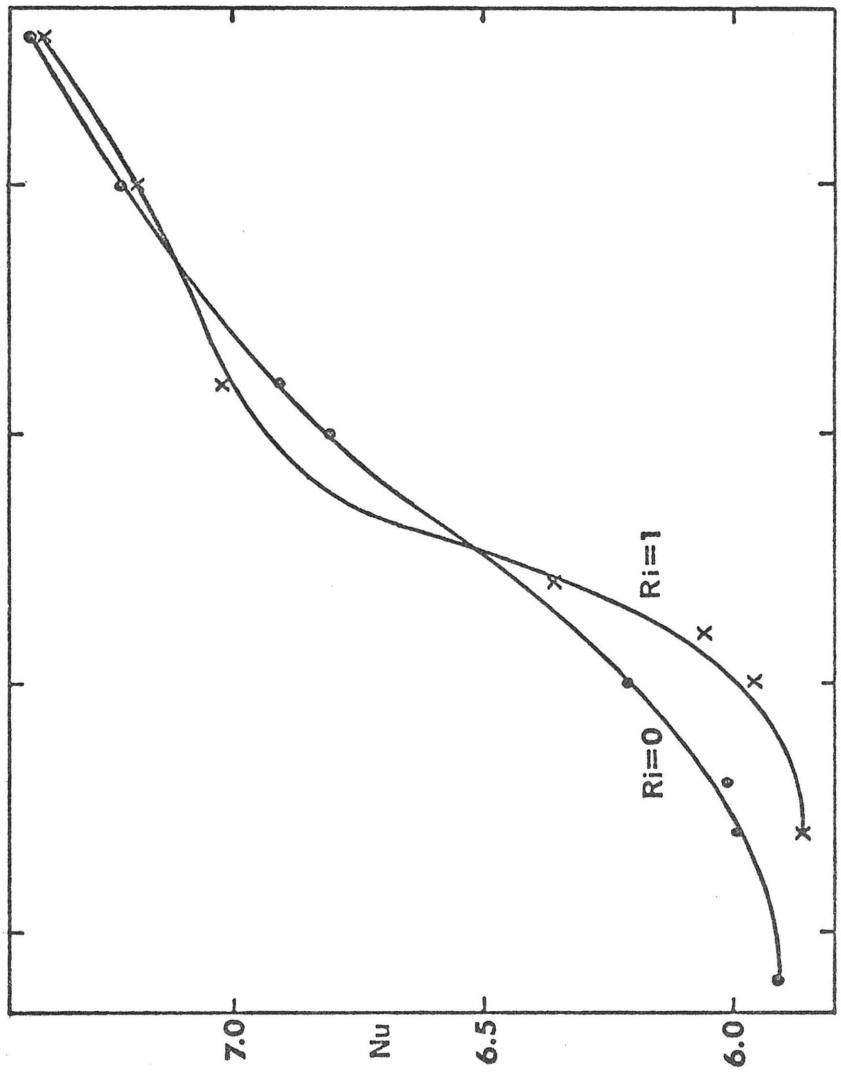

Figure 12

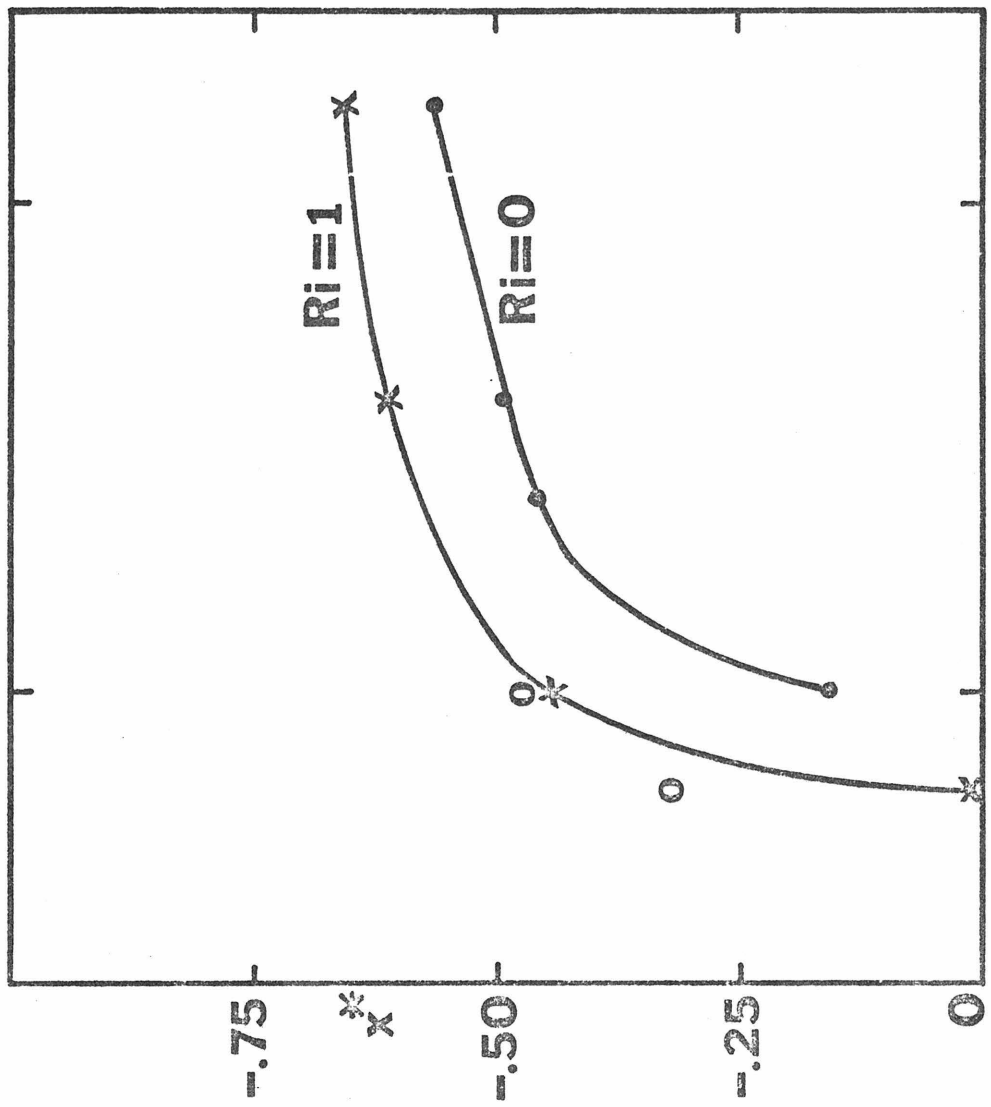

Figure 13

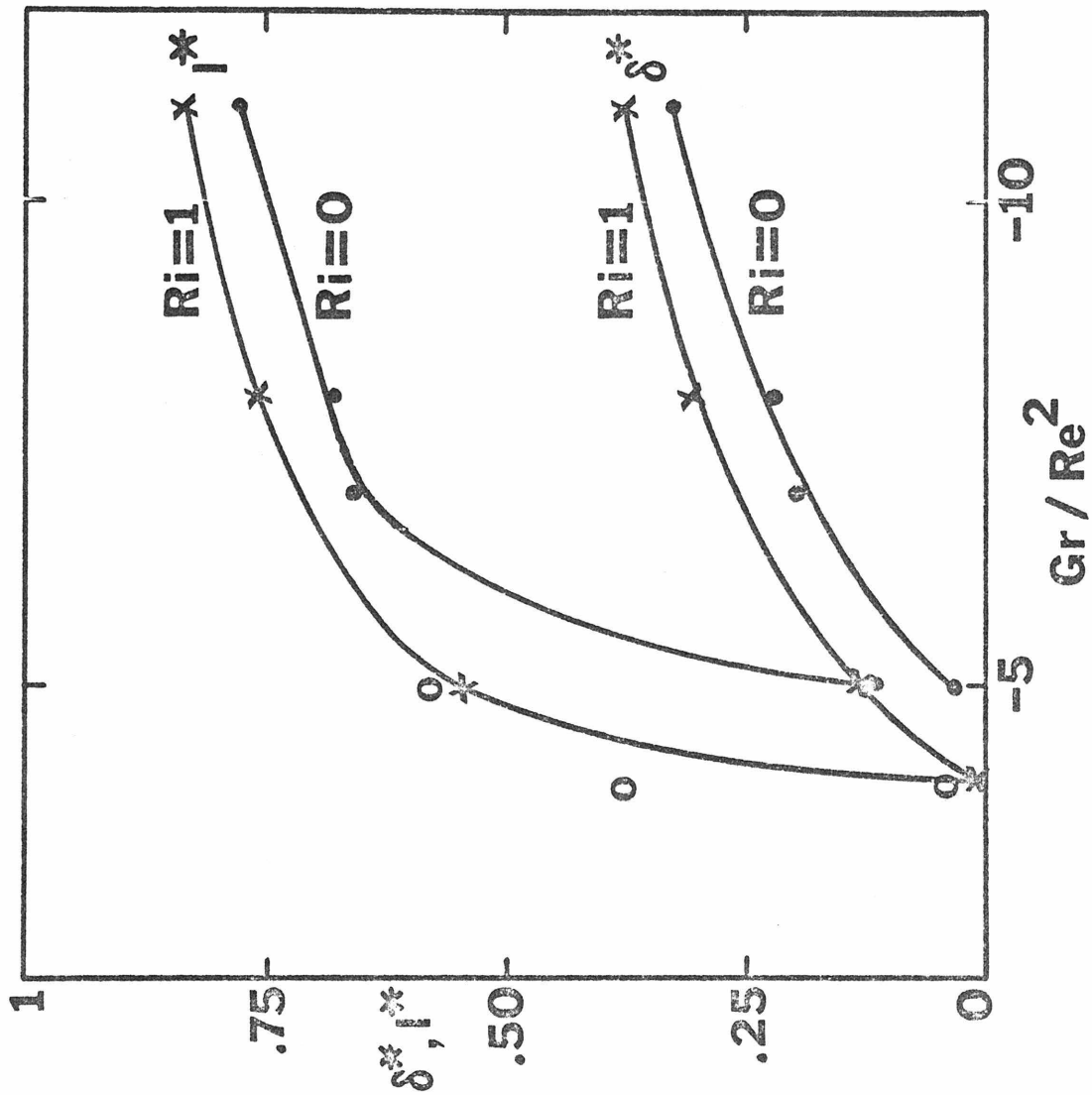
1
.75
.50
.25
0
$\delta^{**}_{\perp}$, δ^{**}
-5
-10
Gr / Re^2
Ri=1
Ri=0
Ri=1
Ri=0
$\delta^{**}_{\perp}$
δ^{**}

Figure 14

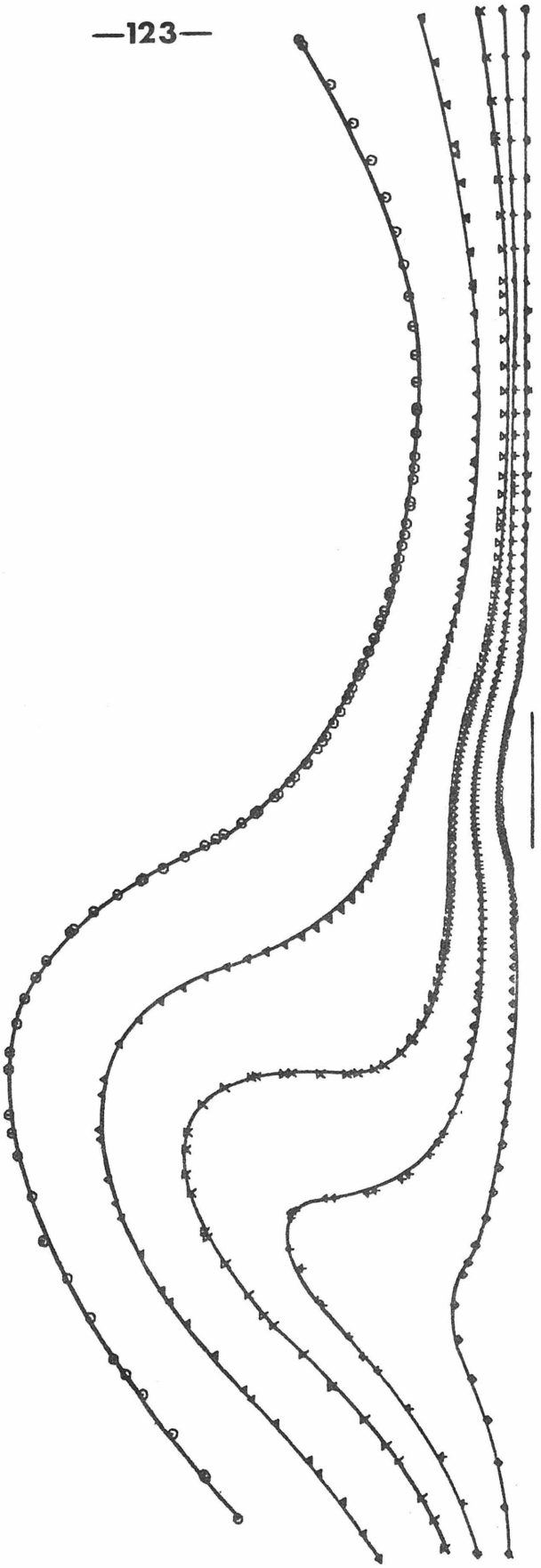

Figure 15

Appendix 3-BB: Additional Figures for Appendix 3-B

This appendix presents the Figures omitted from Appendix 3-B for brevity.

FIGURE CAPTIONS

Figure 1: Decay of the Streamfunction Disturbance for Re = 40, Pr = 0.7, Ri = 0.1, h = $\pi/50$, x_∞ = 3.08, and no plate being present; ψ = 1.25, 1.0, 0.85, 0.6, 0.3, and 0.1 with 1.25 corresponding to the outermost streamline
(a) initial conditions with disturbance
(b) iteration 10
(c) iteration 20
(d) iteration 40
(e) iteration 80

Figure 2: Steady-State Solution for the Propagation of the Streamfunction Error on the Outer Boundary for Re = 40, Pr = 0.7, Ri = 1.0, h = $\pi/50$, x_∞ = 6.16 and no plate being present; $\hat{\psi} = \psi - y$ = -0.04, -0.03, and -0.01 with -0.01 corresponding to the innermost streamline

Figure 3: Steady-State Solution for the Propagation of the Vorticity Error on the Outer Boundary for Re = 40, Pr = 0.7, Ri = 1.0, h = $\pi/50$, and no plate being present
(a) x_∞ = 3.08
(b) x_∞ = 6.16

Figure 4: Streamlines for Re = 40, Pr = 0.7, and Gr/Re^2 = -8; ψ = 3, 2, 1, 0.5, 0.3, 0.1, and 0 with 3 corresponding to the outermost streamline (a) Ri = 0 (b) Ri = 1

Figure 5: Streamlines for Re = 40, Pr = 0.7, and Gr/Re^2 = -8; ψ = 2, 1, 0.5, 0.3, 0.1, 0.05, and 0 with 2 corresponding to the outermost streamline (a) Ri=0 (b) Ri=1

Figure 6: Equivorticity Lines for Re = 40, Pr = 0.7, and $Gr/Re^2 = 0$ (a) Ri = 0 (b) Ri = 6.325

Figure 7: Equivorticity Lines for Re = 40, Pr = 0.7, and $Gr/Re^2 = 5$ (a) Ri = 0 (b) Ri = 6.325

Figure 8: Equivorticity Lines for Re = 40, Pr = 0.7, and $Gr/Re^2 = -5$ (a) Ri = 0 (b) Ri = 1

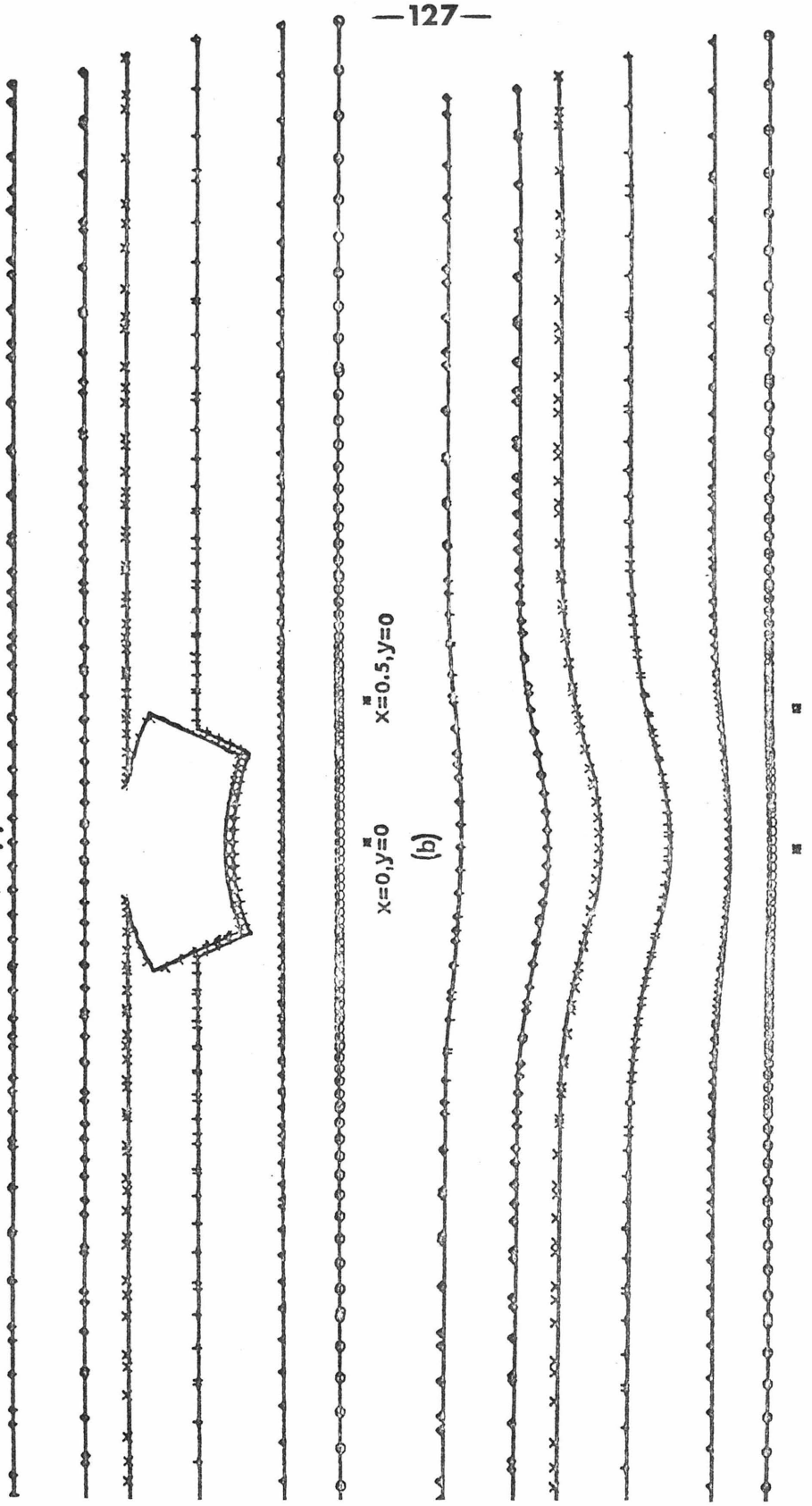

Figure 1

Figure 1

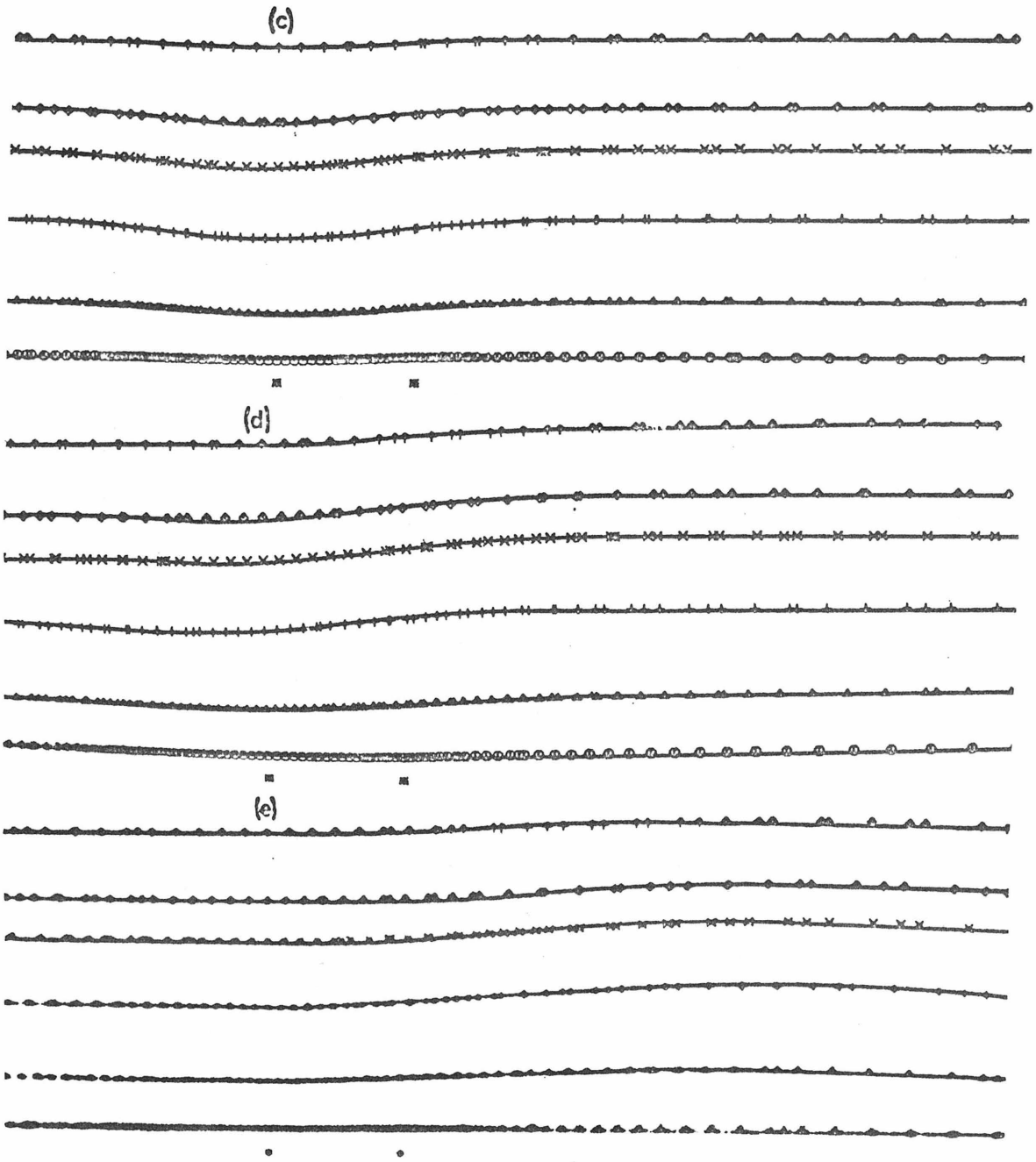

Figure 2

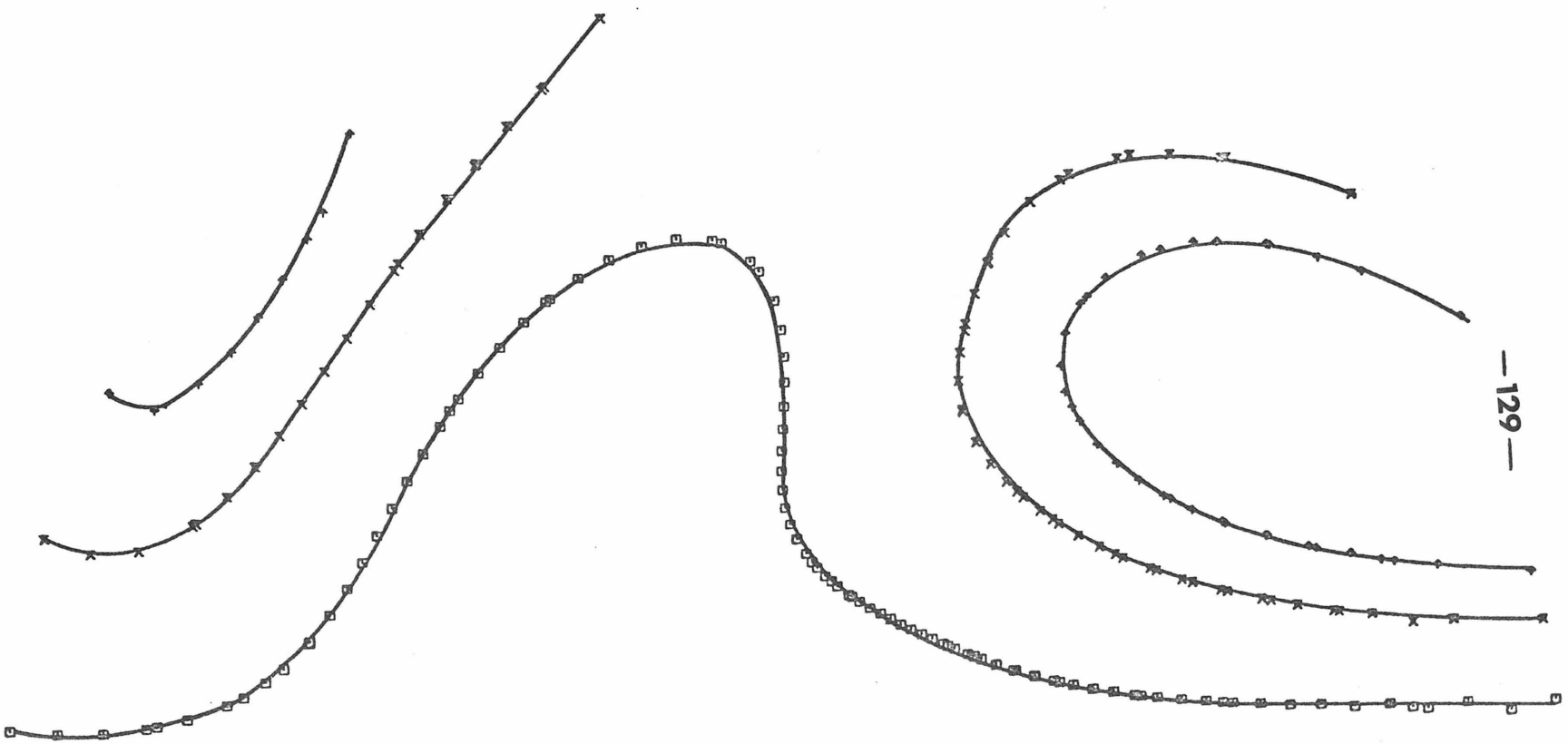

Figure 3

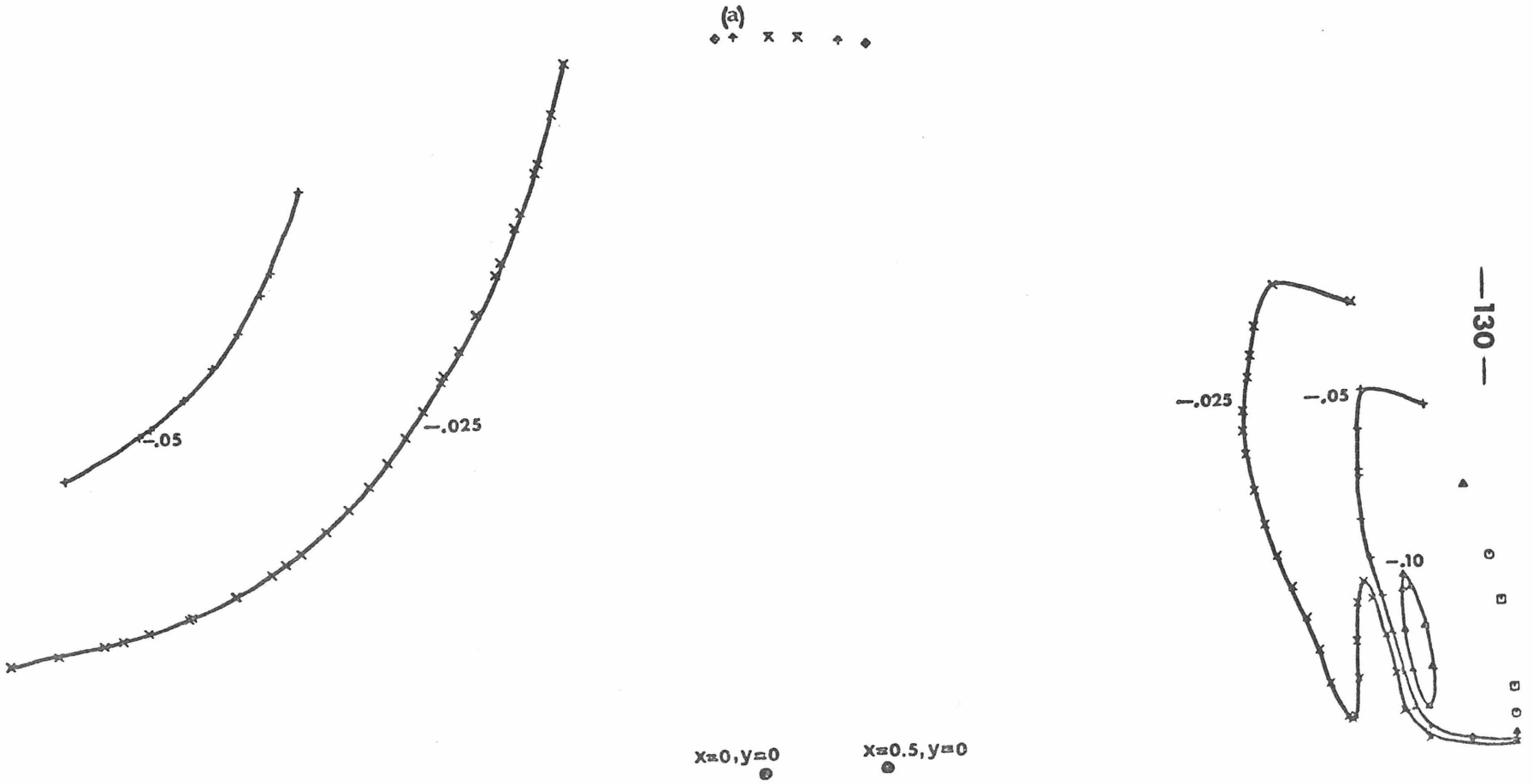

Figure 3

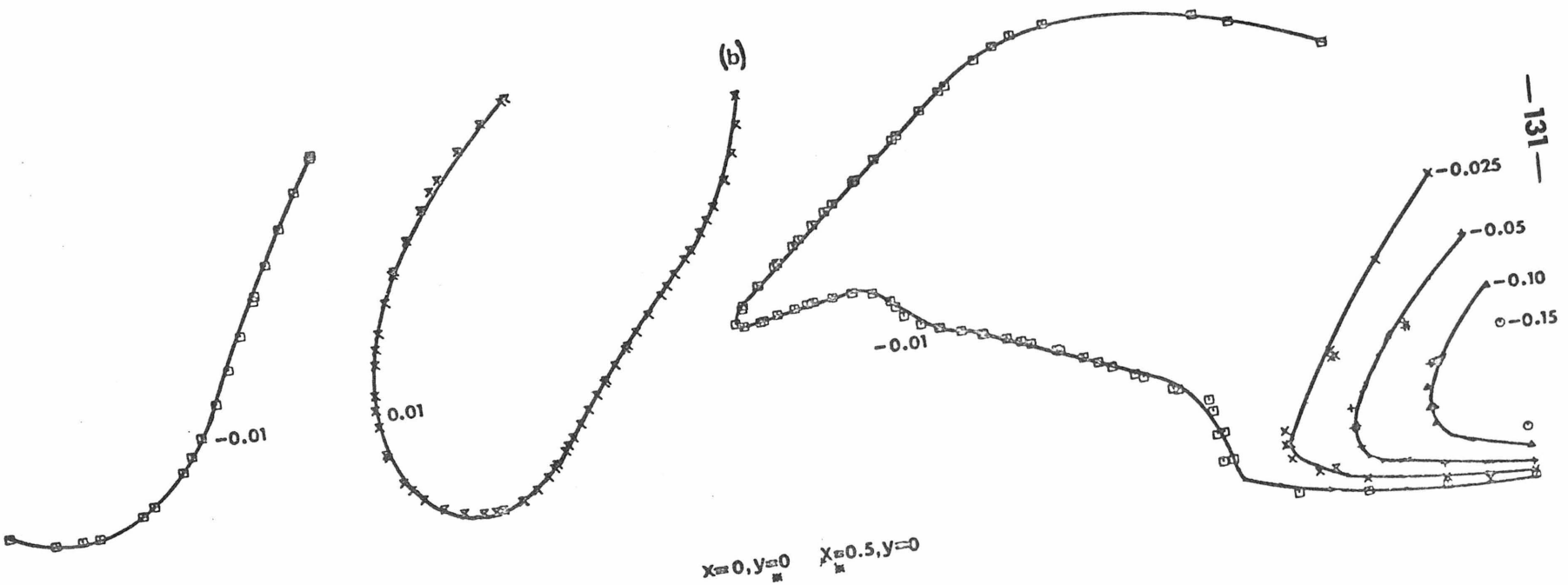

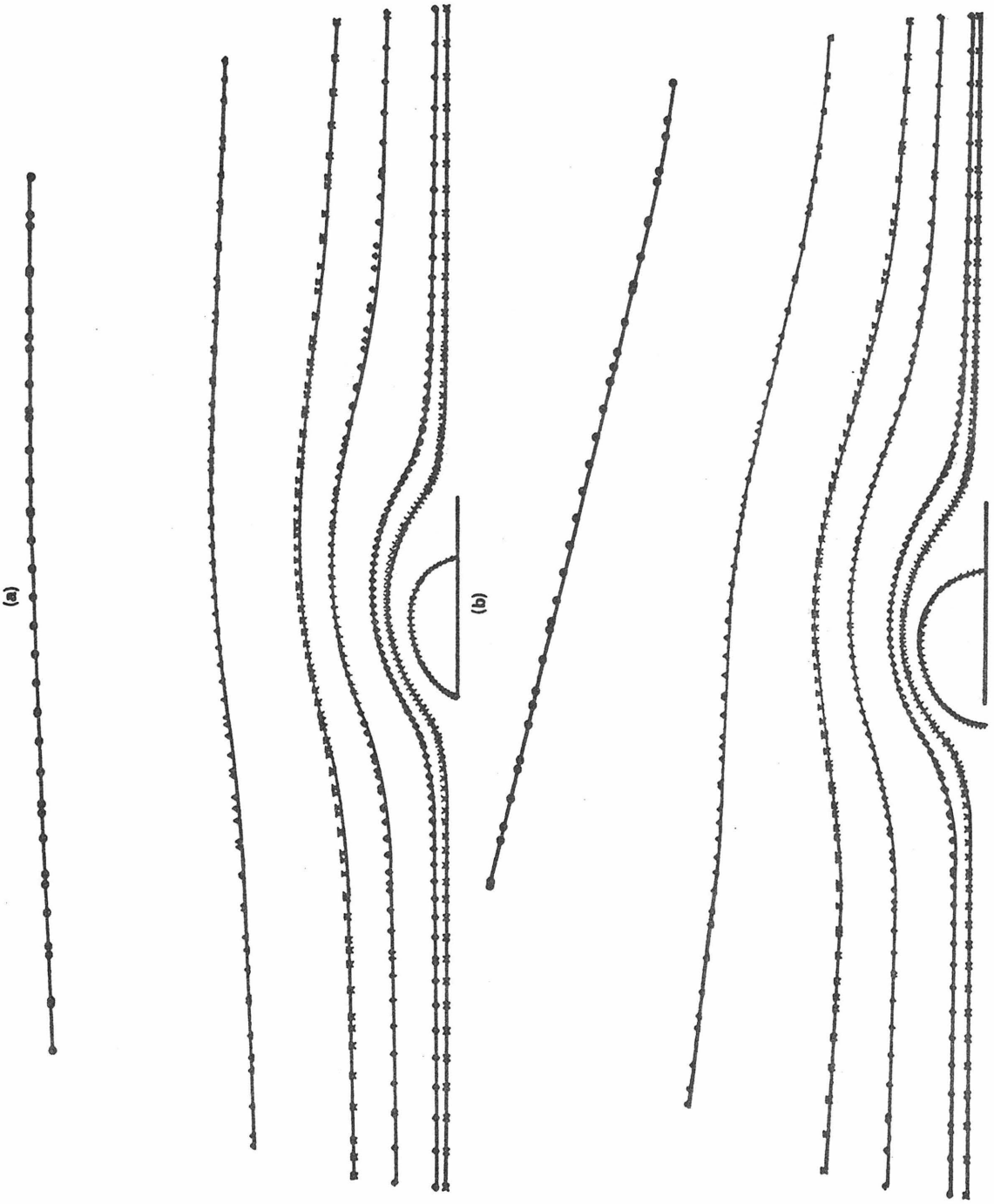

Figure 4

Figure 5

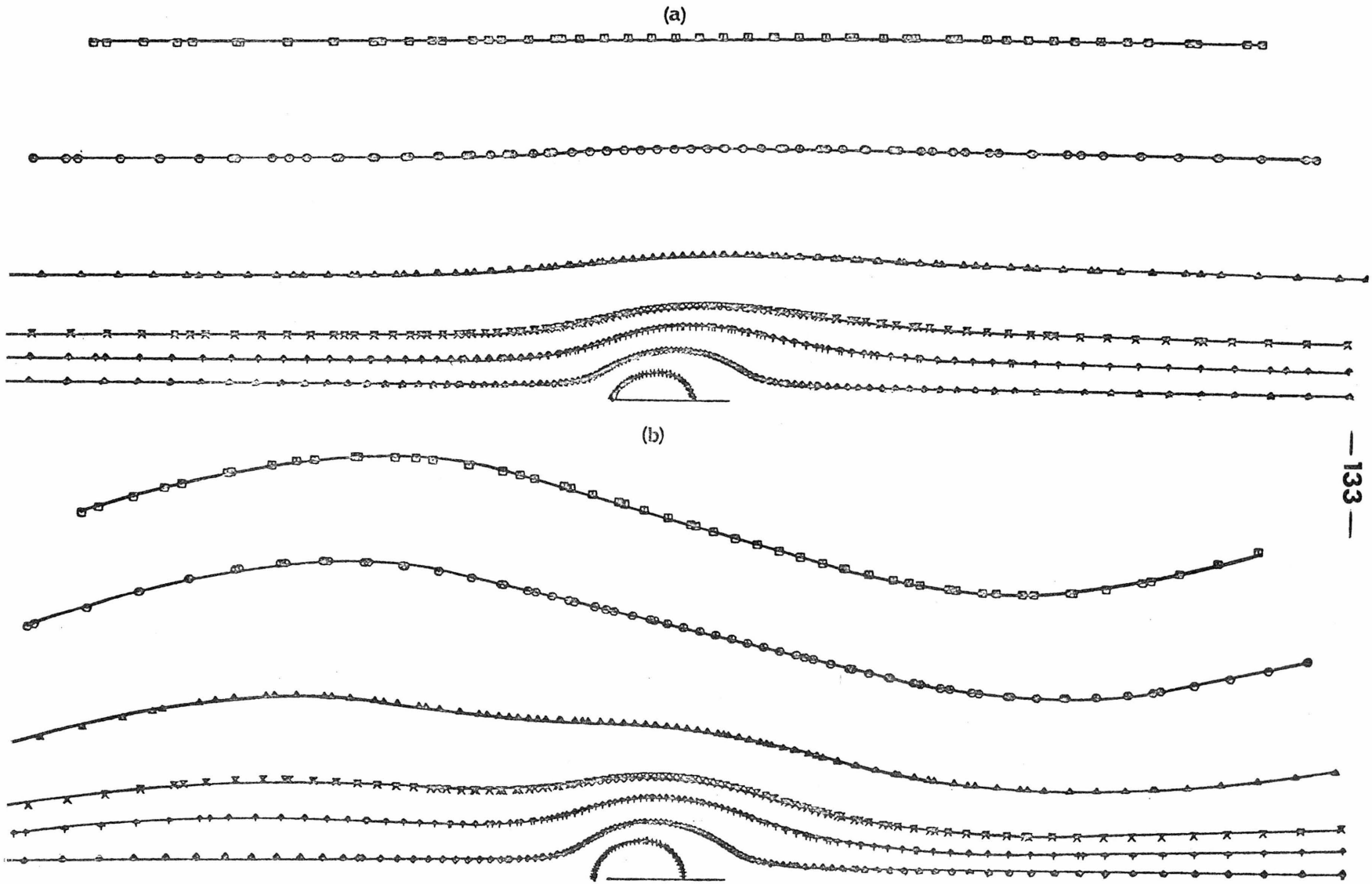

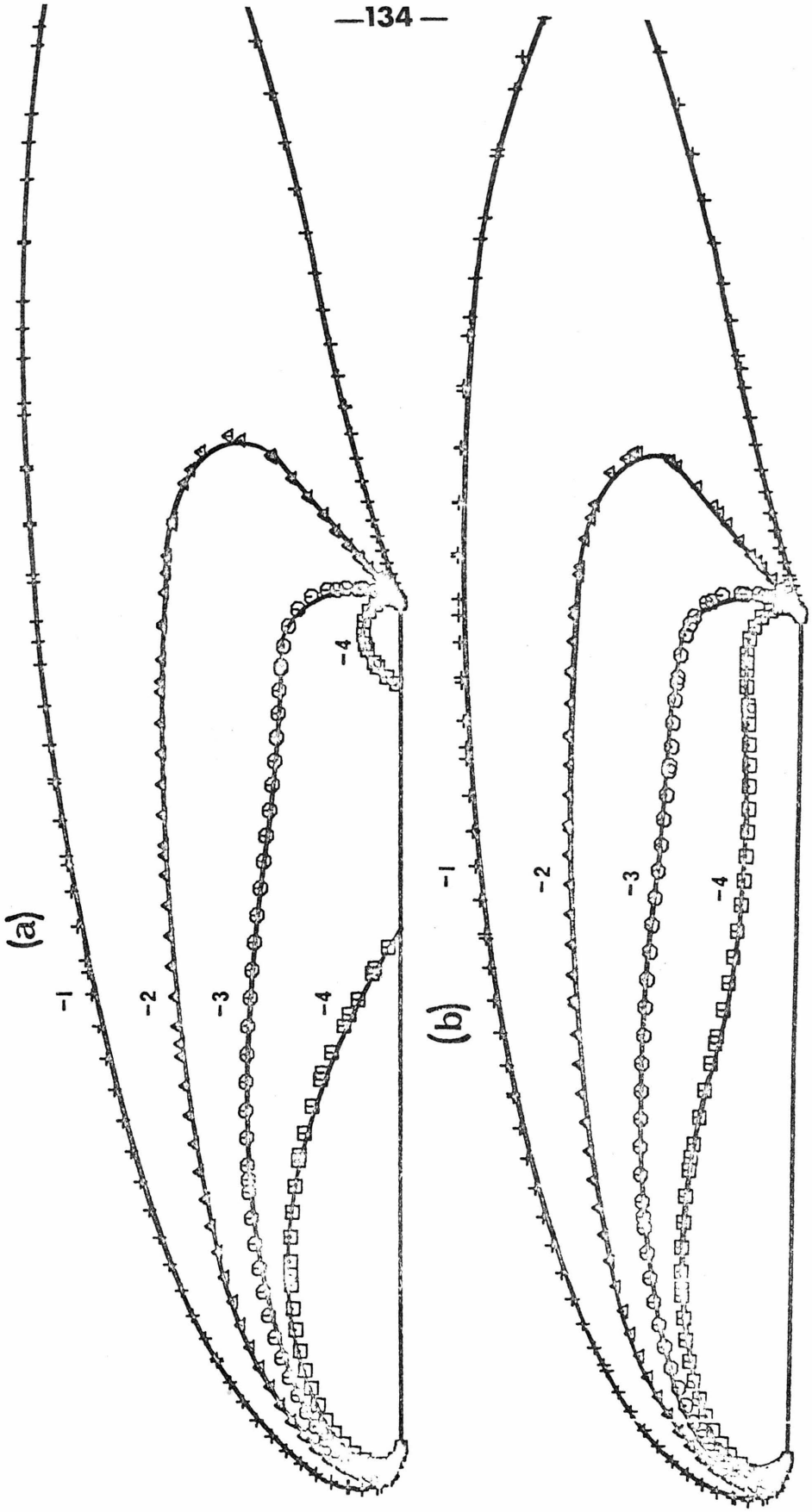

Figure 6

Figure 7

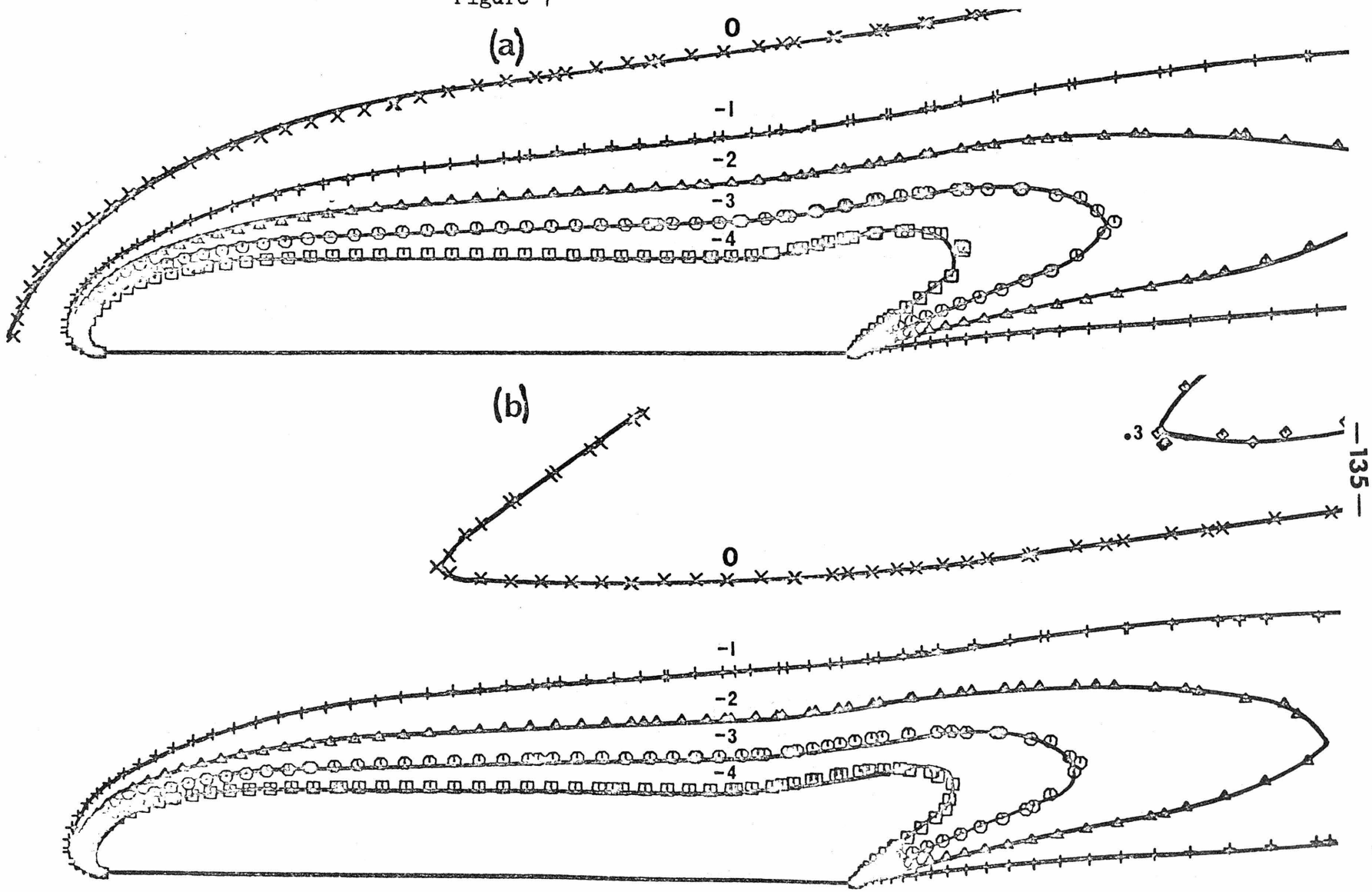

Figure 8

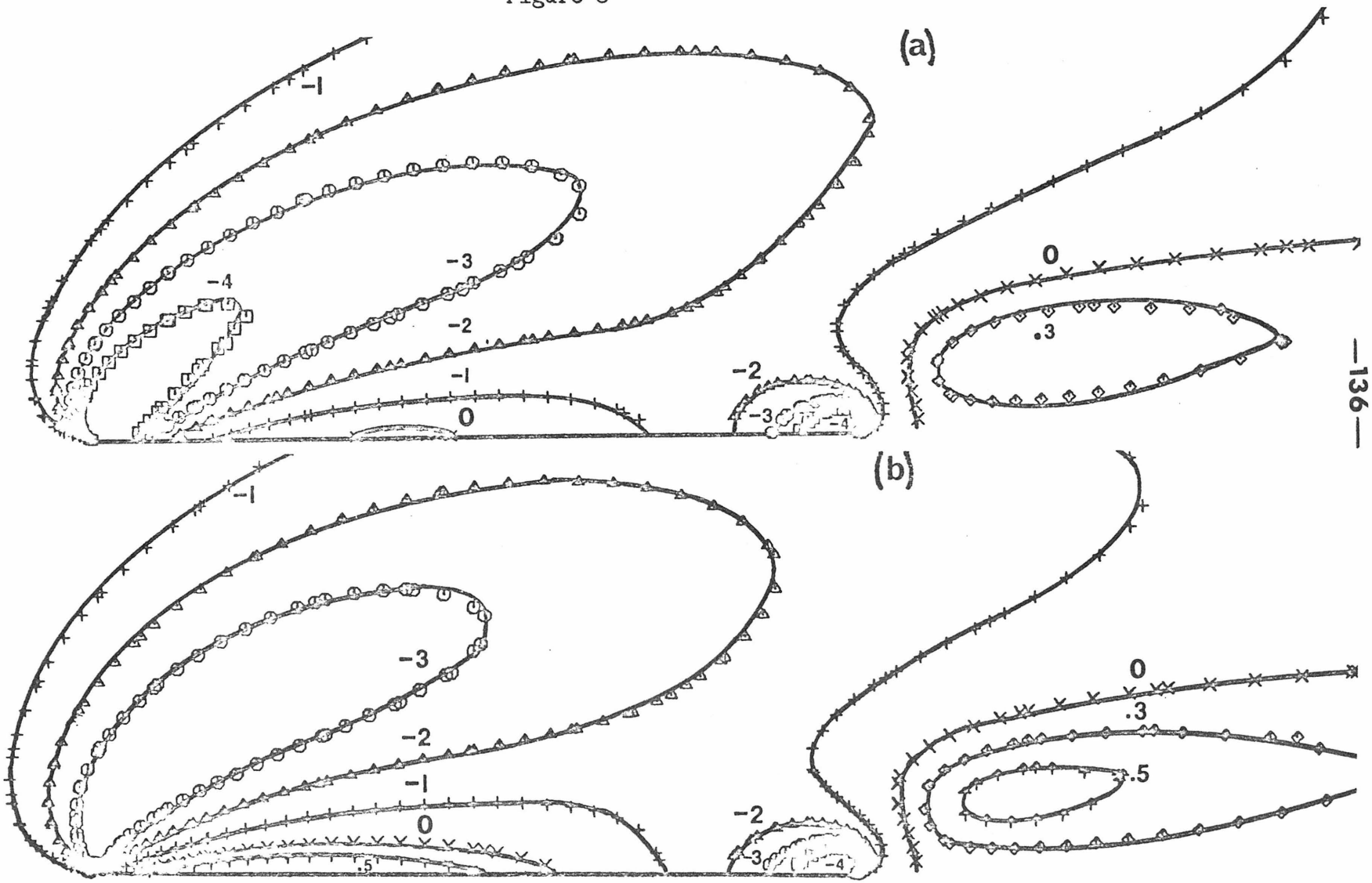

Appendix 3-C: Finite-Difference Equations for the Near-Field Numerical Solutions

The finite-difference equations used in the numerical solution of the steady-state and time-dependent governing nonlinear near-field equations will be given. We shall discuss equations (1) to (3) of Appendix 3-B which are valid for all values of Ri and Gr/Re^2, except $Gr/Re^2 = 0$ with $Ri > 0$. For this latter case, analogous finite-difference representations of the valid formulation of the differential equations in terms of $\hat{\theta} = \frac{Gr}{Re^2}\theta + Ri\, y$ were employed and hence will not be reported here for brevity. We obtain the three dependent variables $\hat{\psi}(= \psi - y = \psi - \frac{1}{2}\sinh\xi \sin\eta)$, θ, and ω in the elliptical cylindrical coordinate system (ξ,η) by solving the following basic governing differential equations:

$$\frac{\partial^2\hat{\psi}}{\partial\xi^2} + \frac{\partial^2\hat{\psi}}{\partial\eta^2} + \frac{1}{4}M^2(\xi,\eta)\omega = 0 \tag{1}$$

$$\frac{1}{4}M^2(\xi,\eta)\frac{\partial\theta}{\partial t} + J(\theta,\hat{\psi}) + \frac{1}{2}\sinh\xi\cos\eta\left(\frac{\partial\theta}{\partial\xi} - \frac{Ri}{Gr/Re^2}\frac{\partial\hat{\psi}}{\partial\xi}\right)$$

$$-\frac{1}{2}\cosh\xi\sin\eta\left(\frac{\partial\theta}{\partial\eta} - \frac{Ri}{Gr/Re^2}\frac{\partial\hat{\psi}}{\partial\eta}\right) = \frac{1}{PrRe}\left(\frac{\partial^2\theta}{\partial\xi^2} + \frac{\partial^2\theta}{\partial\eta^2}\right) \tag{2}$$

$$\frac{1}{4}M^2(\xi,\eta)\frac{\partial\omega}{\partial t} + J(\omega,\hat{\psi}) + \frac{1}{2}\sinh\xi\cos\eta\frac{\partial\omega}{\partial\xi} - \frac{1}{2}\cosh\xi\sin\eta\frac{\partial\omega}{\partial\eta}$$

$$= \frac{1}{Re}\left(\frac{\partial^2\omega}{\partial\xi^2} + \frac{\partial^2\omega}{\partial\eta^2}\right) + \frac{1}{2}\frac{Gr}{Re^2}\left(\sinh\xi\cos\eta\frac{\partial\theta}{\partial\xi} - \cosh\xi\sin\eta\frac{\partial\theta}{\partial\eta}\right) \tag{3}$$

where $M^2(\xi,\eta) = \frac{1}{2}(\cosh 2\xi - \cos 2\eta)$ and the nonlinear, two-dimensional Jacobian is given by:

$$J(\alpha,\phi) = \frac{\partial\alpha}{\partial\xi}\frac{\partial\phi}{\partial\eta} - \frac{\partial\alpha}{\partial\eta}\frac{\partial\phi}{\partial\xi}$$

Let the subscripts i and j be the finite difference coordinates for ξ and η respectively, h be the size of the square mesh, and Δt be the time step. Two alternative representations for the Jacobians $J(\theta,\hat{\psi})$ and $J(\omega,\hat{\psi})$ were used: the four-point scheme using simple two-point central differences for the spatial first derivatives:

$$4h^2 J_{i,j}(\theta,\hat{\psi}) = (\theta_{i+1,j} - \theta_{i-1,j})(\hat{\psi}_{i,j+1} - \hat{\psi}_{i,j-1}) - (\theta_{i,j+1} - \theta_{i,j-1})(\hat{\psi}_{i+1,j} - \hat{\psi}_{i-1,j})$$

and Arakawa's eight-point scheme (Arakawa, 1966; Molenkamp, 1968):

$$\begin{aligned}
-12h^2 J_{i,j}(\theta,\hat{\psi}) &= \theta_{i-1,j-1}(\hat{\psi}_{i-1,j} - \hat{\psi}_{i,j-1}) \\
&+ \theta_{i-1,j}(\hat{\psi}_{i,j+1} + \hat{\psi}_{i-1,j+1} - \hat{\psi}_{i,j-1} - \hat{\psi}_{i-1,j-1}) \\
&+ \theta_{i-1,j+1}(\hat{\psi}_{i,j+1} - \hat{\psi}_{i-1,j}) \\
&+ \theta_{i,j-1}(\hat{\psi}_{i-1,j} + \hat{\psi}_{i-1,j-1} - \hat{\psi}_{i+1,j} - \hat{\psi}_{i+1,j-1}) \\
&+ \theta_{i,j+1}(\hat{\psi}_{i+1,j} + \hat{\psi}_{i+1,j+1} - \hat{\psi}_{i-1,j} - \hat{\psi}_{i-1,j+1}) \\
&+ \theta_{i+1,j-1}(\hat{\psi}_{i,j-1} - \hat{\psi}_{i+1,j}) \\
&+ \theta_{i+1,j}(\hat{\psi}_{i,j-1} + \hat{\psi}_{i+1,j-1} - \hat{\psi}_{i,j+1} - \hat{\psi}_{i+1,j+1}) \\
&+ \theta_{i+1,j+1}(\hat{\psi}_{i+1,j} - \hat{\psi}_{i,j+1})
\end{aligned}$$

Note that Arakawa's expression for $J_{i,j}(\omega,\hat{\psi})$ cannot be used when it

would require the value of ω at either of the two singular end points (where $\omega \to \infty$) of the horizontal flat plate of finite length; the four-point expression for $J_{i,j}(\omega,\hat{\psi})$ which avoids these singular points in such cases must be used.

(1) The Steady-State Equations

Equations (1) to (3), with $\partial\theta/\partial t = 0$ and $\partial\omega/\partial t = 0$, are recast in finite-difference form using the simple two-point central difference formula for a spatial first derivative, the familiar five-point approximation for the Laplacian, and one of the two above representations for the Jacobians.

For $\omega_{i,j}$ known throughout the field, new values of $\hat{\psi}_{i,j}$ are calculated by explicit Gauss-Seidel pointwise iteration from the following finite-difference formulation of equation (1):

$$\hat{\psi}_{i,j} = \frac{1}{4}\left(\hat{\psi}_{i+1,j} + \hat{\psi}_{i-1,j} + \hat{\psi}_{i,j+1} + \hat{\psi}_{i,j-1}\right) + \frac{1}{16} h^2 M^2_{i,j}(\xi,\eta)\, \omega_{i,j}$$

For $\hat{\psi}_{i,j}$ known throughout the field, new values of $\theta_{i,j}$ are calculated by explicit Gauss-Seidel pointwise iteration from the following finite-difference representation of equation (2):

$$\theta_{i,j} = \frac{1}{4}\left(\theta_{i+1,j} + \theta_{i-1,j} + \theta_{i,j+1} + \theta_{i,j-1}\right) - \frac{1}{4}\,\mathrm{PrRe}\, h^2 J_{i,j}(\theta,\hat{\psi}) - \frac{1}{16}\,\mathrm{PrRe}\, h\{\sinh \xi_i \cos \eta_j [(\theta_{i+1,j} - \theta_{i-1,j}) - \frac{Ri}{Gr/Re^2}(\hat{\psi}_{i+1,j} - \hat{\psi}_{i-1,j})] - \cosh \xi_i \sin \eta_j [(\theta_{i,j+1} - \theta_{i,j-1}) -$$

$$\frac{Ri}{Gr/Re^2}\,(\hat{\psi}_{i,j+1} - \hat{\psi}_{i,j-1})]\}$$

For $\hat{\psi}_{i,j}$ and $\theta_{i,j}$ known throughout the field, new values of $\omega_{i,j}$ are calculated by explicit Gauss-Seidel pointwise iteration from the following finite-difference formulation of equation (3):

$$\begin{aligned}\omega_{i,j} = {} & \frac{1}{4}\,(\omega_{i+1,j} + \omega_{i-1,j} + \omega_{i,j+1} + \omega_{i,j-1}) \\ & - \frac{1}{4}\,Re\,h^2\,J_{i,j}(\omega,\hat{\psi}) \\ & - \frac{1}{16}\,Re\,h\{\sinh\xi_i\cos\eta_j(\omega_{i+1,j} - \omega_{i-1,j}) \\ & \qquad - \cosh\xi_i\sin\eta_j(\omega_{i,j+1} - \omega_{i,j-1})\} \\ & + \frac{1}{16}\,\frac{Gr}{Re}\,h\,\{\sinh\xi_i\cos\eta_j(\theta_{i+1,j} - \theta_{i-1,j}) \\ & \qquad - \cosh\xi_i\sin\eta_j(\theta_{i,j+1} - \theta_{i,j-1})\}\end{aligned}$$

(2) The Time-Dependent Equations

Since the elliptic equation (1) is time-independent, values of $\hat{\psi}_{i,j}$ at any time t are calculated by the same method as used for the steady-state scheme described above, knowing $\omega_{i,j}$ at that particular time t.

In solving the time-dependent parabolic equations (2) and (3) for the values of $\theta_{i,j}$ and $\omega_{i,j}$ respectively at time $t = (n+1)\Delta t$, having calculated the corresponding values at $t = n\Delta t$ and $t = (n-1)\Delta t$, we use central-time differencing on the first time derivatives in conjunction with the DuFort-Frankel (1953) expression for the Laplacians,

central-space differencing at $t = n\Delta t$ for the first spatial derivatives, and Arakawa's (1966) expression at $t = n\Delta t$ for the Jacobians. Indicating the time step number (e.g., n) by a superscript, the resulting explicit numerical formulae for $\theta_{i,j}^{n+1}$ and $\omega_{i,j}^{n+1}$ are:

$$\theta_{i,j}^{n+1} = \left(1 + \frac{16\Delta t}{h^2 M_{i,j}^2(\xi,\eta)\,PrRe}\right)^{-1} \left\{ \theta_{i,j}^{n-1} + \frac{8\Delta t}{h^2 M_{i,j}^2(\xi,\eta)} \left[-h^2 J_{i,j}^{n}(\theta,\hat{\psi}) \right.\right.$$

$$- \frac{1}{4} h \sinh \xi_i \cos \eta_j \left\{ (\theta_{i+1,j}^{n} - \theta_{i-1,j}^{n}) - \frac{Ri}{Gr/Re^2} (\hat{\psi}_{i+1,j}^{n} - \hat{\psi}_{i-1,j}^{n}) \right\}$$

$$+ \frac{1}{4} h \cosh \xi_i \sin \eta_j \left\{ (\theta_{i,j+1}^{n} - \theta_{i,j-1}^{n}) - \frac{Ri}{Gr/Re^2} (\hat{\psi}_{i,j+1}^{n} - \hat{\psi}_{i,j-1}^{n}) \right\}$$

$$\left.\left. + \frac{1}{PrRe} (\theta_{i+1,j}^{n} + \theta_{i-1,j}^{n} + \theta_{i,j+1}^{n} + \theta_{i,j-1}^{n} - 2\theta_{i,j}^{n-1}) \right] \right\}$$

$$\omega_{i,j}^{n+1} = \left(1 + \frac{16\Delta t}{h^2 M_{i,j}^2(\xi,\eta)\,Re}\right)^{-1} \left\{ \omega_{i,j}^{n-1} + \frac{8\Delta t}{h^2 M_{i,j}^2(\xi,\eta)} \right. \left[-h^2 J_{i,j}^{n}(\omega,\hat{\psi}) \right.$$

$$- \frac{1}{4} h \sinh \xi_i \cos \eta_j (\omega_{i+1,j}^{n} - \omega_{i-1,j}^{n})$$

$$+ \frac{1}{4} h \cosh \xi_i \sin \eta_j (\omega_{i,j+1}^{n} - \omega_{i,j-1}^{n})$$

$$+ \frac{1}{Re} (\omega_{i+1,j}^{n} + \omega_{i-1,j}^{n} + \omega_{i,j+1}^{n} + \omega_{i,j-1}^{n} - 2\omega_{i,j}^{n-1})$$

$$+ \frac{Gr}{Re^2} \left\{ \frac{1}{4} h \sinh \xi_i \cos \eta_j (\theta_{i+1,j}^{n} - \theta_{i-1,j}^{n}) \right.$$

$$\left.\left. \left. - \frac{1}{4} h \cosh \xi_i \sin \eta_j (\theta_{i,j+1}^{n} - \theta_{i,j-1}^{n}) \right\} \right] \right\}$$

Of course, since central-time differencing is used for the first time derivatives, this scheme cannot be used for the first time step after the initial conditions or a change in Δt . In such cases where we are

advancing from $t = n\Delta t$ to $t = (n+1)\Delta t$, the first time derivatives are approximated by forward-time differences, the Laplacians by the standard five-point formula at $t = n\Delta t$, the first spatial derivatives by central-space differences at $t = n\Delta t$, and the Jacobians by Arakawa's (1966) formula at $t = n\Delta t$. The resulting explicit numerical formulae for $\theta^{n+1}_{i,j}$ and $\omega^{n+1}_{i,j}$ are:

$$\theta^{n+1}_{i,j} = \theta^{n}_{i,j} + \frac{4\Delta t}{h^2 M^2_{i,j}(\xi,\eta)} \left[-h^2 J^n_{i,j}(\theta,\hat{\psi})\right.$$

$$- \frac{1}{4} h \sinh \xi_i \cos \eta_j \left\{(\theta^n_{i+1,j} - \theta^n_{i-1,j}) - \frac{Ri}{Gr/Re^2}(\hat{\psi}^n_{i+1,j} - \hat{\psi}^n_{i-1,j})\right\}$$

$$+ \frac{1}{4} h \cosh \xi_i \sin \eta_j \left\{(\theta^n_{i,j+1} - \theta^n_{i,j-1}) - \frac{Ri}{Gr/Re^2}(\hat{\psi}^n_{i,j+1} - \hat{\psi}^n_{i,j-1})\right\}$$

$$\left. + \frac{1}{PrRe} (\theta^n_{i+1,j} + \theta^n_{i-1,j} + \theta^n_{i,j+1} + \theta^n_{i,j-1} - 4\theta^n_{i,j})\right]$$

$$\omega^{n+1}_{i,j} = \omega^{n}_{i,j} + \frac{4\Delta t}{h^2 M^2_{i,j}(\xi,\eta)} \left[-h^2 J^n_{i,j}(\omega,\hat{\psi})\right.$$

$$- \frac{1}{4} h \sinh \xi_i \cos \eta_j (\omega^n_{i+1,j} - \omega^n_{i-1,j})$$

$$+ \frac{1}{4} h \cosh \xi_i \sin \eta_j (\omega^n_{i,j+1} - \omega^n_{i,j-1})$$

$$+ \frac{1}{Re} (\omega^n_{i+1,j} + \omega^n_{i-1,j} + \omega^n_{i,j+1} + \omega^n_{i,j-1} - 4\omega^n_{i,j})$$

$$+ \frac{Gr}{Re^2} \left\{\frac{1}{4} h \sinh \xi_i \cos \eta_j (\theta^n_{i+1,j} - \theta^n_{i-1,j})\right.$$

$$\left.\left. - \frac{1}{4} h \cosh \xi_i \sin \eta_j (\theta^n_{i,j+1} - \theta^n_{i,j-1})\right\}\right]$$

REFERENCES

Arakawa, A. 1966, "Computational Design for Long-Term Numerical Integration of the Equations of Fluid Motion: Two-Dimensional Incompressible Flow, Part I", J. Comp. Phys. 1, 119.

DuFort, E. C. and Frankel, S. P. 1953, "Stability Conditions in the Numerical Treatment of Parabolic Differential Equations", Math. Tables and Other Aids to Computation 7, 135.

Molenkamp, C. R. 1968, "Accuracy of Finite-Difference Methods Applied to the Advection Equation", J. Appl. Met. 7, 160.

Appendix 3-D: Far-Field Solutions by Chang's Linear Similarity Theory for Neutrally-Stratified Free Stream Flow Past a Symmetric Body Acting as a Heat Dipole

In determining the flow and temperature fields at large distances upstream and downstream from a body symmetric about $y = 0$ and acting as a heat dipole (doublet) in the presence of significant buoyancy, we solve the following basic governing steady-state differential equations, which are equations (1) to (3) of Appendix 3-A, for neutrally-stratified uniform free stream flow:

$$u \frac{\partial u}{\partial x} + v \frac{\partial u}{\partial y} = - \frac{\partial p}{\partial x} + \frac{1}{Re}\left(\frac{\partial^2 u}{\partial x^2} + \frac{\partial^2 u}{\partial y^2}\right) \tag{1a}$$

$$u \frac{\partial v}{\partial x} + v \frac{\partial v}{\partial y} = - \frac{\partial p}{\partial y} + \frac{1}{Re}\left(\frac{\partial^2 v}{\partial x^2} + \frac{\partial^2 v}{\partial y^2}\right) + \frac{Gr}{Re^2}\theta \tag{1b}$$

$$\frac{\partial u}{\partial x} + \frac{\partial v}{\partial y} = 0 \tag{2}$$

$$u \frac{\partial \theta}{\partial x} + v \frac{\partial \theta}{\partial y} = \frac{1}{PrRe}\left(\frac{\partial^2 \theta}{\partial x^2} + \frac{\partial^2 \theta}{\partial y^2}\right) \tag{3}$$

by a similarity theory, after first linearizing the equations by following the procedure documented by Chang (1961) for the momentum transfer problem alone (i.e., $Gr \equiv 0$). Coordinate expansions at large distances are replaced by expansions in the small artificial parameter ε introduced for convenience. The flow field at large distances is divided into two regions: an outer region where the variables are described by outer expansions (denoted by an underbar) and an inner viscous wake region where the variables are described by inner expansions (denoted by an overbar). Of course, the relations for the dependent variables must match in the common region of overlap of the two regions.

In the outer region, let us make the transformation $\underline{x} = \varepsilon x$ such that for small ε and large x, $\underline{x}$ is neither small nor large. All

transformations in both the inner and outer regions are defined such that the new variables are neither small nor large. We can also define $\underline{y} = \varepsilon^n y$, $n \geq 0$; the outer limit is defined as the limit as $\varepsilon \to 0$ for $\underline{x}$ and $\underline{y}$ fixed. Let us also define $v = \varepsilon^q \underline{v}$, $q \geq 0$; note that u is not "stretched" as it is $0(1)$. Substituting these transformations into equation (2) yields $n+q = 1$, and into equation (3), while assuming the convection of heat is more important than its diffusion in the outer region, gives $\underline{\theta} \equiv 0$. Hence, in the outer limit, the outer equations reduce simply to those describing the potential flow outer region studied by Chang (1961) with $\underline{y} = \varepsilon y$, and the following solution expansions that converge asymptotically at large distances:

$$u = 1 + \varepsilon \underline{u}_1 + \cdots \tag{4a}$$

$$v = \varepsilon \underline{v}_1 + \cdots \tag{4b}$$

$$p = \varepsilon \underline{p}_1 + \cdots \tag{4c}$$

where

$$\underline{u}_1 = \frac{m\underline{x}}{2\pi(\underline{x}^2 + \underline{y}^2)} \tag{5a}$$

$$\underline{v}_1 = \frac{m\underline{y}}{2\pi(\underline{x}^2 + \underline{y}^2)} \tag{5b}$$

$$\underline{p}_1 = - \underline{u}_1 \tag{5c}$$

and m is to be determined later from a matching condition.

In the inner region, we make the transformations $\overline{x} = \varepsilon x$, $\overline{y} = \varepsilon^r y$, $0 \leq r < n = 1$; the inner limit is defined as the limit as $\varepsilon \to 0$ for $\overline{x}$ and $\overline{y}$ fixed. Let us also define $v = \varepsilon^a \overline{v}$, $a \geq 0$; $\overline{p} = \varepsilon^d p$; $\theta = \varepsilon^c \overline{\theta}$, $c \geq 0$. Substituting these transformations into equation (2), and into

equation (3) while assuming that the diffusion of heat in the inner region is as important as its convection, yields $r = a = 1/2$. Note that the outer limit implies $|x| \to \infty$ and $|y| \to \infty$ along $y/x =$ constant, whereas the inner limit implies $|x| \to \infty$ and $|y| \to \infty$ along $y^2/x =$ constant. Substituting the transformations into equation (1a) and retaining the horizontal pressure gradient term yields $d = 0$. After a similar substitution into equation (1b), assuming that the buoyancy contribution is as important as the transverse pressure gradient gives $c = 1/2$. In order to solve the inner equations, let us first expand u, $\bar{v}$, $\bar{p}$, and $\bar{\theta}$ in infinite series expansions that converge asymptotically at large distances. Let the expansion for u be

$$u = 1 + \varepsilon^{s}\bar{u}_1 + \cdots, \quad s > 0 \tag{6a}$$

Since ε is an artificial parameter, it must be eliminable from the solution; it will be shown later that $\bar{u}_1$ is of the similarity form $\bar{u}_1 = \bar{x}^{-s} f(\bar{y}^2/\bar{x})$. As will be seen below, the integral $\int_0^\infty \bar{u}_1 d\bar{y}$ is to be independent of $\bar{x}$ giving $s = 1/2$. Similarly, it can be shown that the other expansions are:

$$\bar{v} = \varepsilon^{1/2}\bar{v}_1 + \cdots \tag{6b}$$

$$\bar{p} = \varepsilon^{1/2}\bar{p}_1 + \cdots \tag{6c}$$

$$\bar{\theta} = \varepsilon^{1/2}\bar{\theta}_1 + \cdots \tag{6d}$$

Substituting the transformations and expansions into equations (1) to (3) yields the following equations to be solved for the first correction

terms to the uniform flow conditions:

$$\frac{\partial \bar{u}_1}{\partial \bar{x}} = -\frac{\partial \bar{p}_1}{\partial \bar{x}} + \frac{1}{Re}\frac{\partial^2 \bar{u}_1}{\partial \bar{y}^2} \tag{7a}$$

$$\frac{\partial \bar{p}_1}{\partial \bar{y}} = \frac{Gr}{Re^2}\bar{\theta}_1 \tag{7b}$$

$$\frac{\partial \bar{u}_1}{\partial \bar{x}} + \frac{\partial \bar{v}_1}{\partial \bar{y}} = 0 \tag{8}$$

$$\frac{\partial \bar{\theta}_1}{\partial \bar{x}} = \frac{1}{PrRe}\frac{\partial^2 \bar{\theta}_1}{\partial \bar{y}^2} \tag{9}$$

In solving for the flow structure at large distances from the body, we replace the boundary conditions at the body by certain integral conditions. Since the velocity field about a body symmetric around $y = 0$, and acting as a heat dipole, is also symmetric about $y = 0$, we need to consider a control volume only in the upper half plane. A horizontal force balance on the control volume extending from far upstream at $x = -x_o$ where the uniform flow conditions are applicable to downstream at $x = x_o$ gives

$$\int_0^\infty (1 - u)dy - \int_0^\infty p\ dy = \frac{1}{2} C_d \tag{10}$$

where C_d is the overall horizontal drag coefficient for the body. Utilizing the inner and outer expansions for u and p in equation (10) gives in the limit as $\varepsilon \to 0$:

$$-\int_0^\infty \bar{u}_1 \, d\bar{y} - \int_0^\infty \bar{p}_1 \, d\bar{y} = \frac{1}{2} C_d \tag{11}$$

From this integral condition it is seen that both $\int_0^\infty \bar{u}_1 \, d\bar{y}$ and $\int_0^\infty \bar{p}_1 \, d\bar{y}$ are to be independent of $\bar{x}$. For matching of the inner and outer expansions for p at $O(\varepsilon^{1/2})$, $\bar{p}_1 \to 0$ as $\bar{y} \to \infty$. Hence, integrating equation (7b) gives:

$$\bar{p}_1 = -\frac{Gr}{Re^2} \int_{\bar{y}}^\infty \bar{\theta}_1(\bar{x},\bar{y}_1) \, d\bar{y}_1 \tag{12}$$

and hence we can calculate

$$\int_0^\infty \bar{p}_1 \, d\bar{y} = -\frac{Gr}{Re^2} \int_0^\infty d\bar{y} \int_{\bar{y}}^\infty \bar{\theta}_1(\bar{x},\bar{y}_1) \, d\bar{y}_1 \tag{13}$$

The solution of equation (9) such that $\bar{\theta}_1 = 0$ on $\bar{y} = 0$, $\bar{\theta}_1(\bar{x},-\bar{y}) = -\bar{\theta}_1(\bar{x},\bar{y})$, and the integral in equation (13) is independent of $\bar{x}$ is:

$$\bar{\theta}_1 = A\bar{y}\,\bar{x}^{-3/2} \exp(-PrRe\,\bar{y}^2/4\bar{x}) \tag{14}$$

where the constant A is determined from the following energy-rate balance on the control volume:

$$\int_0^\infty \theta \, dy = \frac{1}{PrRe} \left(Nu - \int_{-x_o}^{-1/2} \left.\frac{\partial\theta}{\partial y}\right|_{y=0} dx - \int_{1/2}^{x_o} \left.\frac{\partial\theta}{\partial y}\right|_{y=0} dx \right) \tag{15}$$

where Nu is the overall Nusselt number for the top surface of the body whose leading and trailing edges are at $x = -1/2$ and $x = +1/2$ respectively.

Using only $\bar{\theta}_1$ in the limit as $\varepsilon \to 0$ since $\underline{\theta} \equiv 0$, the evaluation of $\int_0^\infty \theta \, dy$ in equation (15) yields:

$$A = \frac{x_o^{1/2}}{2} \left(Nu - \int_{-x_o}^{-1/2} \left.\frac{\partial \theta}{\partial y}\right|_{y=0} dx - \int_{1/2}^{x_o} \left.\frac{\partial \theta}{\partial y}\right|_{y=0} dx \right) \tag{16}$$

It should be noted that the parameter A vanishes as $x_o \to \infty$. Substituting equation (12) into equation (7a), and utilizing equations (9) and (14) yields:

$$\frac{\partial \bar{u}_1}{\partial \bar{x}} = -\frac{1}{2} K_1 \bar{x}^{-3/2} (1 - 2\bar{\eta}^2) \exp(-\bar{\eta}^2) + \frac{1}{Re} \frac{\partial^2 \bar{u}_1}{\partial \bar{y}^2} \tag{17}$$

where $K_1 = A \frac{Gr}{Re^2} \frac{2}{PrRe}$ and the similarity variable is defined as $\bar{\eta} = \frac{\bar{y}}{2} \sqrt{\frac{PrRe}{\bar{x}}}$. Assuming $\bar{u}_1$ is of the similarity form:

$$\bar{u}_1 = \bar{x}^{-1/2} \, g(\bar{\eta}) \tag{18}$$

equation (17) becomes

$$\frac{d}{d\bar{\eta}} \left(\frac{Pr}{4} \frac{dg}{d\bar{\eta}} + \frac{1}{2} \bar{\eta} \, g \right) = \frac{1}{2} K_1 (1 - 2\bar{\eta}^2) \exp(-\bar{\eta}^2) \tag{19}$$

In solving equation (19), the boundary conditions are provided by the matching condition for u at $0(\varepsilon^{1/2})$, $\bar{u}_1 \to 0$ as $\bar{y} \to \infty$, and by the symmetric flow condition $dg/d\bar{\eta}\big|_{\bar{\eta}=0} = 0$. The integration of equation (19) gives:

$$g(\bar{\eta}) = g(0) \, e^{-\bar{\eta}^2/Pr} + \frac{K_1}{1-Pr} \left(e^{-\bar{\eta}^2} - e^{-\bar{\eta}^2/Pr} \right) \tag{20}$$

where the constant g(0), obtained from equation (11), is:

$$g(0) = -\frac{C_d}{2}\sqrt{\frac{Re}{\pi}} + K_1\left(\frac{1-\sqrt{Pr}}{1-Pr}\right) \tag{21}$$

Integrating equation (8) with the symmetric flow condition $\bar{v}_1 = 0$ for $\bar{y} = 0$, yields

$$\bar{v}_1 = Pr^{-1/2}\, Re^{-1/2}\, \bar{x}^{-1}\, \bar{\eta}\, g(\bar{\eta}) \tag{22}$$

which also satisfies the matching condition for v at $0(\varepsilon)$; i.e., $\bar{v}_1(\bar{x},\bar{y}\to\infty) = \underline{v}_1(\underline{x}=\bar{x},\underline{y}\to 0^+) = 0$. Also, substituting equation (14) into equation (12) gives

$$\bar{p}_1 = -K_1\bar{x}^{-1/2}\, \exp(-PrRe\, \bar{y}^2/4\bar{x}) \tag{23}$$

To complete the specification of the behavior of the flow structure, we must evaluate the constant m found in the solutions for the outer region. In the outer and inner regions, define:

$$\underline{\psi} = \varepsilon\psi = \underline{y} + \varepsilon\underline{\psi}_1 + \cdots, \quad \underline{u}_1 = \partial\underline{\psi}_1/\partial\underline{y}, \quad \underline{v}_1 = -\partial\underline{\psi}_1/\partial\underline{x}, \cdots$$

$$\bar{\psi} = \varepsilon^{1/2}\psi = \bar{y} + \varepsilon^{1/2}\bar{\psi}_1 + \cdots, \quad \bar{u}_1 = \partial\bar{\psi}_1/\partial\bar{y}, \quad \bar{v}_1 = -\partial\bar{\psi}_1/\partial\bar{x}, \cdots$$

The matching of the inner and outer expansions for ψ at $0(\varepsilon^0)$ yields $\bar{\psi}_1(\bar{x},\bar{y}\to\infty) = \underline{\psi}_1(\underline{x}=\bar{x},\underline{y}\to 0^+)$ and $\bar{\psi}_1(\bar{x},\bar{y}\to-\infty) = \underline{\psi}_1(\underline{x}=\bar{x},\underline{y}\to 0^-)$. Since $\underline{\psi}_1(\underline{x}=\bar{x},\underline{y}\to 0^+) - \underline{\psi}_1(\underline{x}=\bar{x},\underline{y}\to 0^-) = -m$ (Chang, 1961), and $\bar{\psi}_1(\bar{x},\bar{y}\to\infty) - \bar{\psi}_1(\bar{x},\bar{y}\to-\infty) = 2\int_0^\infty \bar{u}_1 d\bar{y}$, then

$$m = -2\sqrt{\frac{\pi}{PrRe}}\left[\sqrt{Pr}\, g(0) + K_1\left(\frac{1-\sqrt{Pr}}{1-Pr}\right)\right] \tag{24}$$

By forming composite expansions of the solutions for the inner and outer regions, we obtain the following overall flow and temperature fields at large distances upstream and downstream from a body symmetric about $y = 0$ and acting as a heat dipole in the presence of significant buoyancy:

$$u = 1 + \frac{mx}{2\pi(x^2+ y^2)} + x^{-1/2}\, g\left(\frac{y}{2}\sqrt{\frac{PrRe}{x}}\right) + \cdots, \quad x > 0 \tag{25a}$$

$$u = 1 + \frac{mx}{2\pi(x^2+ y^2)} + \cdots, \quad x < 0 \tag{25b}$$

$$v = \frac{my}{2\pi(x^2+ y^2)} + \frac{1}{2}\, yx^{-3/2}\, g\left(\frac{y}{2}\sqrt{\frac{PrRe}{x}}\right) + \cdots, \quad x > 0 \tag{26a}$$

$$v = \frac{my}{2\pi(x^2+ y^2)} + \cdots, \quad x < 0 \tag{26b}$$

$$p = \frac{-mx}{2\pi(x^2+ y^2)} - K_1\, x^{-1/2} \exp\left(-\frac{PrRe}{4}\frac{y^2}{x}\right) + \cdots, \quad x > 0 \tag{27a}$$

$$p = \frac{-mx}{2\pi(x^2+ y^2)} + \cdots, \quad x < 0 \tag{27b}$$

$$\theta = Ayx^{-3/2} \exp\left(-\frac{PrRe}{4}\frac{y^2}{x}\right) + \cdots, \quad x > 0 \tag{28a}$$

$$\theta = 0, \quad x < 0 \tag{28b}$$

The corresponding overall stream function and vorticity fields are given in equations (15) and (16) of Appendix 3-A. As expected, for the momentum transfer problem alone, our results reduce to those of Chang (1961) and Imai (1951) by setting $Gr = K_1 = 0$.

REFERENCES

Chang, I.-D. 1961, "Navier-Stokes Solutions at Large Distances from a Finite Body", J. Math. Mech. 10, 811.

Imai, I. 1951, "On the Asymptotic Behavior of Viscous Fluid Flow at a Great Distance from a Cylindrical Body, with Special Reference to Filon's Paradox", Proc. Roy. Soc. London A208, 487.

Appendix 3-E: Near-Field Solutions for Neutrally-Stratified Free Stream Flow Past a Horizontal Flat Plate of Finite Length when $\partial\theta/\partial y = 0$ on $y = 0$, $|x| > 1/2$

Dennis and Smith (1966) studied the forced convection case (i.e., $Gr = 0$) when the boundary condition for θ on $y = 0$, $|x| > 1/2$ was $\partial\theta/\partial y = 0$, rather than $\theta = 0$ which is discussed in Appendix 3-A. Two physical situations in which we can study the flow in the upper half plane with $\partial\theta/\partial y = 0$ on $y = 0$, $|x| > 1/2$, while the other boundary conditions (in particular, $\partial u/\partial y = v = 0$ for $y = 0$, $|x| > 1/2$ and $u = v = 0$, $\theta = 1$ for $y = 0$, $|x| \leq 1/2$) remain the same as in Appendix 3-A are:

(a) a system of two fluids whose interface is at $y = 0$. The less dense fluid on top is moving at free stream velocity U_∞ and has a neutrally-stratified free stream temperature T_∞ and density ρ_∞, and constant physical properties μ_∞ and k_∞. The more dense fluid on the bottom is stationary and has a neutrally-stratified free stream temperature, T_∞ and density ρ_∞, and constant physical properties (denoted by a superscript prime) $\mu'_\infty << \mu_\infty$ and $k'_\infty << k_\infty$. The top surface of the plate is at temperature $T_\infty + \Delta T$, whereas the bottom surface is at temperature T_∞.

(b) a fluid flowing over a wall stretching from $x = -\infty$ to $x = +\infty$ at $y = 0$. For $|x| > 1/2$, the wall is considered insulated and acting as a no shear stress surface, whereas the hot spot on the wall for $|x| \leq 1/2$ is considered at temperature $T_\infty + \Delta T$ and acting as a no slip surface.

We considered combined forced and free convection by solving the governing nonlinear equations, including significant buoyancy,

numerically in the manner detailed in Appendix 3-A. We studied hot plates (i.e., $Gr \geq 0$) for which the uniform flow outer boundary conditions are satisfactory numerically, as indicated in Appendix 3-A. The cases investigated with the corresponding values obtained for the overall drag coefficient, C_d, and the overall Nussett number, Nu, are given in Table 1. For $Gr = 0$, the forced convection heat transfer results compare very well with those of Dennis and Smith (1966). For $Gr > 0$, the results given here for $\partial\theta/\partial y = 0$ on $y = 0$, $|x| > 1/2$ exhibit qualitatively the same behavior as those calculated in Appendix 3-A for $\theta = 0$ on $y = 0$, $|x| > 1/2$. For example, when $Gr > 0$, the boundary flow near the plate surface is accelerated relative to the corresponding forced convection flow, with a resulting increase in skin friction and heat transfer.

REFERENCES

Dennis, S.C.R. and Smith, N. 1966, "Forced Convection from a Heated Flat Plate", J. Fluid Mech. 24, 509.

Table 1: $C_d Re^{1/2}$ and $NuRe^{-1/2}$ for $\partial\theta/\partial y = 0$ on $y = 0$, $|x| > 1/2$ when $\gamma' = 0$ and $Pr = 0.7$

Re	$Gr/Re^{5/2}$	$C_d Re^{1/2}$	$NuRe^{-1/2}$
10	0	2.40	0.76
10	1.58	4.63	0.86
10	3.16	6.29	0.93
40	0	2.07	0.68
40	0.79	3.28	0.76
40	1.58	4.29	0.81
100	0	1.88	0.66
100	0.50	2.76	0.72
100	1.00	3.46	0.77

Appendix 3-F: Boundary-Layer Theories for the Uniform Flow Past a Hot or Cold Horizontal Flat Plate: Reduction of Redekopp's Stably-Stratified Fluid Analysis for the Diffusive, Inertia-Viscous Balance Region with $1 < Ri < Re^{1/2}$ and $|\gamma/\Delta|$ of $0(1)$ to Sparrow and Minkowycz' Neutrally-Stratified Fluid Analysis

This appendix shows that Redekopp's (1971) stably-stratified fluid analysis for the diffusive, inertia-viscous boundary-layer balance with $1 < Ri < Re^{1/2}$ and $|\gamma/\Delta|$ of 0(1) for the uniform flow past a hot or cold horizontal flat plate reduces exactly to Sparrow and Minkowycz' (1962) boundary-layer analysis for a neutrally-stratified fluid (i.e., Ri = 0). The nomenclature of Chapter 3 will be used here, as well as the subscripts R and SM to denote expressions employed strictly in Redekopp's and Sparrow and Minkowycz' papers respectively. For Ri = 0, Sparrow and Minkowycz found that the local skin friction and heat transfer coefficients, including the small corrections to the Blasius and Polhausen solutions, respectively, due to the effect of the plate being hot or cold, are given by

$$c_{f_R} Re^{1/2} = \frac{0.332}{x^{1/2}} + \frac{Gr}{Re^{5/2}} f''_{1_{SM}}(0) \tag{1}$$

$$- c_{h_R} PrRe^{1/2} + \frac{\gamma}{\Delta} Re^{-1/2} = - \frac{h'_1(0)}{x^{1/2}} + \frac{Gr}{Re^{5/2}} (-\theta'_{1_{SM}}(0)) \tag{2}$$

respectively, where $-h'_1(0)$ is the Polhausen solution and $f''_{1_{SM}}(0)$ and $(-\theta'_{1_{SM}}(0))$ are functions only of Pr and have been tabulated by Sparrow and Minkowycz. For $1 < Ri < Re^{1/2}$ and $|\gamma/\Delta|$ of 0(1), Redekopp found that:

$$c_{f_R} Re^{1/2} = \frac{0.332}{x^{1/2}} + \frac{Gr}{Re^{5/2}} \frac{\gamma}{\Delta} f''_{b_R}(0) \tag{3}$$

$$- c_{h_R} PrRe^{1/2} + \frac{\gamma}{\Delta} Re^{-1/2} = - \frac{h'_1(0)}{x^{1/2}} + \frac{Gr}{Re^{5/2}} \frac{\gamma}{\Delta} (-h'_{b_R}(0)) \tag{4}$$

For a particular value of Pr, Redekopp calculated $f''_{b_R}(0)$ and $-h'_{b_R}(0)$ for various values of γ/Δ by solving equations and boundary conditions (3.19a-c) given in his paper, and has plotted these values for Pr = 1 in Figure 3 of his paper. However, by multiplying equations and boundary conditions (3.19a-c) by γ/Δ, the resulting equations with $1 < Ri < Re^{1/2}$, and therefore the solutions for the new functions $\tilde{f}_{b_R}$, $\tilde{g}_{b_R}$, and $\tilde{h}_{b_R}$ given by

$$\tilde{f}_{b_R} = \frac{\gamma}{\Delta} f_{b_R}$$

$$\tilde{g}_{b_R} = \frac{\gamma}{\Delta} g_{b_R}$$

$$\tilde{h}_{b_R} = \frac{\gamma}{\Delta} h_{b_R}$$

are independent of the value of γ/Δ and depend only on Pr. Consequently, the correction terms $\frac{\gamma}{\Delta} f''_{b_R}(0) = \tilde{f}''_{b_R}(0)$ and $\frac{\gamma}{\Delta}(-h'_{b_R}(0)) = -\tilde{h}'_{b_R}(0)$ of equations (3) and (4) are independent of γ/Δ and depend only on Pr. Hence, plotting $f''_{b_R}(0)$ and $-h'_{b_R}(0)$ for various values of γ/Δ is superfluous, as the correction terms $\frac{\gamma}{\Delta} f''_{b_R}(0)$ and $\frac{\gamma}{\Delta}(-h'_{b_R}(0))$ are independent of γ/Δ and given by $f''_{1_{SM}}(0)$ and $-\theta'_{1_{SM}}(0)$ respectively for each value of Pr .

REFERENCES

Redekopp, L. G. 1971, "The boundary layer on a flat plate moving transversely in a rotating, stratified fluid", J. Fluid Mech. 46, 769.

Sparrow, E. M. and Minkowycz, W. J. 1962, "Buoyancy Effects on Horizontal Boundary-Layer Flow and Heat Transfer", Int. J. Heat Mass Transfer 5, 505.

Chapter 4. Conclusions

We have developed accurate analytical and numerical techniques to calculate velocity and temperature distributions for stratified laminar flows past hot or cold two-dimensional bodies. The resulting solutions have been used to explain some of the physical phenomena which can result due to ambient stable temperature (or density) stratification and/or buoyancy-induced convection. It was found convenient to consider separately two aspects of the full problem: the "near- and far-field" regions. The "near-field" solution, which is calculated by solving numerically the governing nonlinear equations, considers the effects of ambient stratification and locally produced buoyancy contributions very close to the body, and depends on the precise body geometry and surface temperature distribution. The "far-field" solution, which is obtained by linear analysis, regards the body as a line disturbance for both momentum and thermal energy, and is independent of the details of the body shape and surface temperature distributions. In the near-field numerical solutions, the accuracy of the outer boundary conditions was found to be critical in obtaining correct results. The far-field solutions were found to provide these proper conditions.

For stable stratifications, the Oseen flow fields at large distances from a line sink of horizontal or vertical momentum, or a line heat source or heat dipole, exhibit the common feature of multiple recirculating rotors of finite thicknesses. The rotors produce an alternating jet structure, both upstream and downstream, for the horizontal velocity components and lee-waves in the overall flow. For each singularity type and increasing amounts of stratification, the rotors

increase in number and decrease in strength and size due to the increasing buoyancy restoring force, thereby causing the Oseen horizontal velocity profiles, both upstream and downstream, to decrease in magnitude and to be compressed more vertically. At very large distances upstream and downstream, the velocity, temperature, and pressure fields become self-similar.

For the "near-field" solutions, we consider the flow past a horizontal flat plate of finite length and constant surface temperature. For all stratifications, the gravitationally induced streamwise pressure gradient produces either an acceleration or deceleration of the boundary flow compared with the corresponding forced convection case, depending on whether the plate is hot or cold. For sufficiently cold plates, the buoyancy-induced adverse streamwise pressure gradient actually causes the flow to separate, and this phenomenon is enhanced by further cooling or increasing the amount of ambient stratification. A wave-structure exists only for stably-stratified fluids, with the amplitudes and wavelengths of the waves being decreased for increasing amounts of ambient stratification.

The solution procedures developed in this dissertation may be useful in analyzing other flow situations. Three-dimensional body geometries may produce different physical phenomena than two-dimensional bodies, as the fluid has the ability in the former case to flow past the obstacle in the third direction. These techniques may also yield more quantitative results and assist engineering predictions in the study of various geophysical turbulent flows.